OAK RIDGE
NATIONAL LABORATORY
MANAGED BY UT-BATTELLE
FOR THE DEPARTMENT OF ENERGY

ORNL/TM-2012/230

Manufacturing Process Modeling of 100-400 kW_e Combined Heat and Power Stationary Fuel Cell Systems

July 2012

Prepared by
Joshua Warren
Oak Ridge National Laboratory

Sujit Das
Oak Ridge National Laboratory

Wei Zhang
Oak Ridge National Laboratory

UT-BATTELLE
ORNL-27 (4-00)

ORNL/TM-2012/230

Energy and Transportation Science Division

MANUFACTURING PROCESS MODELING OF 100-400 kW_e COMBINED HEAT AND POWER STATIONARY FUEL CELL SYSTEMS

Joshua Warren
Sujit Das
Wei Zhang

Date Published: July 2012

Prepared by
OAK RIDGE NATIONAL LABORATORY
Oak Ridge, Tennessee 37831-6283
managed by
UT-BATTELLE, LLC
for the
U.S. DEPARTMENT OF ENERGY
under contract DE-AC05-00OR22725

CONTENTS

Page

LIST OF FIGURES

Figure **Page**

LIST OF TABLES

Table **Page**

LIST OF ACRONYMS AND ABBREVIATIONS

A	Amp
AC	Alternating Current
BOL	Beginning of Life
BOP	Balance of Plant
C	Celsius
CHP	Combined Heat and Power
cm	Centimeter
CNC	Computer Numeric Controlled
CTE	Coefficient of Thermal Expansion
DC	Direct Current
DFMA	Design for Manufacture and Assembly
ERP	Electrolyte Reservoir Plate
EVD	Electrochemical Vapor Deposition
F	Fahrenheit
FCE	FuelCell Energy
ft	Foot
GDC	Gadolinium-doped Ceria
Hex	Heat Exchanger
hr	Hour
HVAC	Heating Ventilation and Air Conditioning
kW	Kilowatt
kWe	Kilowatt Electrical
kWh	Kilowatt hour
LHV	Lower Heating Value
LSCF	Lanthanum Strontium Cobalt Ferrite
m	Meter
MCFC	Molten Carbonate Fuel Cell
mg	Milligram
mm	Millimeter
MMBTU	Million British Thermal Units
MW	Megawatt
MWe	Megawatt Electrical
NG	Natural Gas
nm	Nanometer
O&M	Operations and Maintenance
ORNL	Oak Ridge National Laboratory
PAFC	Phosphoric Acid Fuel Cell
PBCM	Process Based Cost Model
PEMFC	Polymer Electrolyte Membrane Fuel Cell
PTFE	Polytetrafluoroethylene

R&D	Research and Development
SMT	Surface Mount Technology
SOFC	Solid Oxide Fuel Cell
TGO	Thermally Grown Oxide
US	United States
UTC	United Technologies Corporation
V	Volt
W	Watt
wt%	Weight percent
yr	Year
YSZ	Yttria Stabilized Zirconia

ACKNOWLEDGMENTS

The authors would like to acknowledge the DOE Fuel Cells Technology Program for its support, in particular Nancy Garland and Pete Devlin. In addition, the authors would like to thank our industry partners at UTC Power, HydroGen, FuelCell Energy, Versa Power, NexTech Materials, Acumentrics, and Rolls Royce whose willingness to share information made this research possible.

0. EXECUTIVE SUMMARY

0.1 INTRODUCTION AND OBJECTIVE

A one year project to examine the processes employed in the manufacture of combined heat and power stationary fuel cells operating in the 100-400kWe range was commissioned in June 2010. The results of this project would be used to inform decision makers in charge of allocating R&D resources by highlighting the most expensive steps in the manufacturing process where processing alternatives might have the greatest potential for high impact cost reduction.

Three fuel cell technologies were examined: phosphoric acid (PAFC), molten carbonate (MCFC), and solid oxide (SOFC) fuel cells. Two fuel cell technologies, PAFC and MCFC, are represented by commercially available products within the study boundaries. United Technologies Corporation (UTC) offers the PureCell 400®, a 400 kWe combined heat and power PAFC system. FuelCell Energy (FCE) offers the DFC-300®, a 375 kWe combined heat and power MCFC. A combined heat and power SOFC within the study boundaries is not available in the marketplace at the time of this study.

Process based cost models using 2010 dollars were developed for each fuel cell technology. For all three technologies, model boundaries encompassed all direct and indirect materials; direct and indirect labor; capital, maintenance, tooling, floor space, and energy costs associated with the manufacturing process. Cost estimates were developed with academic and patent literature, industry partners, supplier quotations, Monte Carlo simulation software, and DFMA software. Life cycle and non-manufacturing costs such as sales, administration, R&D, office floor space, and profit were not quantified. Results presented are for assumed annual production volumes of 5, 20, 50, and 500 MWe/yr, and expressed in terms of dollars per kilowatt of electrical energy. A model baseline production volume of 20 MWe/yr (similar to recent production volumes experienced by UTC and FCE) was assumed for all three technologies.

0.2 PAFC RESULTS SUMMARY

The manufacturing costs of a 400 kWe PAFC system that is 42% electrical, 48% thermal, and 90% system efficient (LHV NG, BOL, hot water CHP) were modeled for production volumes of 5, 20, 50, and 500 MWe/yr. For the baseline annual production volume of 20 MWe/yr (roughly equivalent to UTC's recent production volume), PAFC manufacturing cost was estimated to be $3049/kWe.

- An 11% cost reduction may be expected by increasing production volume from the baseline of 20 MWe/yr to 500 MWe/yr through economies of scale.
- PAFC manufacturing costs are driven by items sourced from suppliers (cell materials, stack materials and components, and BOP components and subsystems), which range from 67% to 78% of total manufacturing cost for production volumes of 5 and 500 MWe/yr, respectively.

- Pt catalyzed carbon is both the largest cost item (16% of total manufacturing cost) and the largest contributor to cost variance (71%). Reducing Pt loadings from 0.75-1.00 mg/cm^2 for PAFC to a level comparable with PEM (0.15 mg/cm^2) may significantly reduce total system cost. Reducing platinum surface area loss and anion absorption are important R&D needs which much be addressed to allow cells to be manufactured with significantly reduced platinum loadings.
- 24% of total system cost is attributable to fuel processing BOP components (desulfurizer, reformer, integrated low temperature shift converter, ammonia scrubber and all piping and heat exchangers associated with these). The reformer cost is the second largest cost item after Pt catalyzed carbon. A noble metal (rather than Ni) based reformer may have the potential to reduce fuel processing BOP costs as such a reformer can be significantly smaller in volume and mass, and the ammonia scrubber may no longer be required.
- Carbon paper substrates are the third highest cost component, exceeded only by Pt catalyzed carbon and the reformer. Process improvements for substrate manufacturing (e.g. continuous paper making, step elimination, reduced carbonization and graphitization cycle times) are needed.
- Bipolar plate flow field machining is capital, labor, energy, and floor space intensive. Near net shape molding of flow field channels which require little to no subsequent machining could result in substantial cost savings. Materials which do not adhere to molds are needed. Non-contact sensing methods are also needed for flow field channel inspection.
- Separator plate carbonization and graphitization must proceed very slowly to minimize disruptive outgassing which would result in undesirable porosity. State of the art separator plate manufacturing may require carbonization and graphitization cycle times in excess of two weeks with temperatures of approximately 4000 ^0F. Acceleration of carbonization and graphitization cycle times reduces capital and energy costs associated with these processes.
- Hot press molding steps used in separator plate, bipolar plate, and cooling unit manufacturing are capital, labor, and floor space intensive. Reducing hot pressing cycle times for these components could result in significant cost savings.
- Alternatives which streamline electrode manufacturing by eliminating inefficient steps such as catalyst pelletizing and dual matrix printing are needed.
- A means for bypassing bad cells identified in stack testing and conditioning would reduce cycle times for this process bottleneck.

0.3 MCFC RESULTS SUMMARY

The manufacturing costs of a 375 kWe MCFC system that is 56% electrical, 33% thermal, and 89% system efficient (LHV NG, BOL, hot water CHP) were modeled for production volumes of 5, 20, 50, and 500 MWe/yr. For MCFC specifically, limited discussion of manufacturing processes and model results is given due to the proprietary nature of information disclosed to ORNL by FCE.

- The baseline production volume of 20 MWe/yr (roughly equivalent to FCE's recent production volume) was assigned a relative value of 1.0. A 19% cost reduction may be expected by increasing production volume from the baseline of 20 MWe/yr to 500 MWe/yr through economies of scale.
- MCFC manufacturing costs are driven by items sourced from suppliers (cell materials, stack materials and components, and BOP components and subsystems), which range from 65% to 80% of total manufacturing cost for production volumes of 5 and 500 MWe/yr, respectively.
- The most important MCFC cell materials in terms of quantity used and total costs are nickel (cathodes, anodes, and anode supports), lithium aluminate (matrix), and alkali carbonates (electrolyte). While nickel is an exchange traded commodity with relatively wide commercial availability, suppliers for matrix and electrolyte materials are comparably few. Vertical integration of matrix and/or electrolyte material production affords MCFC manufacturers the potential for lower costs, more control over product quality, and better response to supply constraints.
- Many stack components such as current collectors, separator plates, wet seal rails, and reforming units are stainless steel devices manufactured using high cost metal working operations. Additional coatings or claddings of these parts are often required to minimize corrosion by electrolyte. Corrosion protection measures and high cost metalworking contribute significantly to high stack costs, and could be high impact areas for cost reduction.
- The adsorbent based desulfurizer system is on the order of 15-40% of total system cost depending on fuel feedstock quality. Desulfurization is also the highest recurring O&M cost. A manufacturing design incorporating a low cost online sulfur detection system would enable optimal utilization of adsorbent while reducing the likelihood of sulfur breakthrough and concomitant irreversible stack damage.
- High labor cost steps identified in this study include certain process steps associated with anode current collector manufacturing, bipolar plate manufacturing, electrode/current collector/bipolar plate mating, and stack and system assembly. Many of these procedures may be difficult to duplicate with automated machinery because of complex motions. Moreover, high production volume may be required before custom, automated assembly equipment is economically justifiable. Detailed DFMA redesign studies of components

which currently show high labor inputs may lead to designs with a reduced labor requirement or ones conducive to low cost automated assembly.

- The dollar per kilowatt electrical ($/kWe) cost of larger systems is lower than that of smaller systems because BOP costs scale nonlinearly. Thus, while the present study focused on fuel cell systems in the 100-400 kWe range, the greatest economic opportunities for MCFC manufacturers appears to reside with multi-megawatt systems.
- State of the art anode and matrix manufacturing use the well-established technique of tape casting. Of the two, matrix tape casting is less productive due to long drying times. Some matrix tape casting procedures require the lamination of multiple tapes, which further reduces the productivity of this manufacturing station and introduces opportunities for yield diminishing quality control errors. Methods for speeding up and improving the yield of matrix manufacturing should be examined.
- Electrolyte loss and cathode dissolution, the two major life limiting factors in state of the art MCFC operation, are technology R&D challenges to address in order to extend stack life and reduce life cycle cost.

0.4 SOFC RESULTS SUMMARY

The manufacturing costs of a 362 kWe SOFC system that is 55% electrical, 35% thermal, and 90% system efficient (LHV NG, BOL, hot water CHP) were modeled for production volumes of 5, 20, 50, and 500 MWe/yr. At the time of this study, no SOFC manufacturer is producing CHP systems in the range of 100-400 kWe. However, a model baseline of 20 MWe/yr was selected to be congruent with the model baseline assumptions for PAFC and MCFC. For the baseline production volume of 20 MWe/yr, SOFC manufacturing cost was estimated to be $1242/kWe, significantly less than PAFC or MCFC. A major driver for this low cost is the high power density (watt per unit of active cell area) attainable by SOFC, resulting in much less active cell areas needed for achieving a given stack power compared to PAFC and MCFC. It is noted the predicted manufacturing cost for SOFC, though consistent with those published in the literature, is expected to have a higher uncertainty than those for PAFC and MCFC because more assumptions have to be employed as SOFC technology is still evolving.

- A 22% cost reduction may be expected just by increasing production volume from the baseline of 20 MWe/yr to 500 MWe/yr through economies of scale.
- SOFC manufacturing costs are driven by items sourced from suppliers (cell materials, stack materials and components, and BOP components and subsystems), which range from 55% to 88% of total manufacturing cost for production volumes of 5 and 500 MWe/yr, respectively.
- The five highest cost procured items (inverter, desulfurizer, air preheater, waste heat exchanger, and blowers) collectively represent 62% of all material costs and 48% of total system cost. All five are BOP components, underscoring the significance of reducing

BOP costs as a means for reducing total system cost. The relatively large proportion of cost attributable to BOP is again a function of the relatively high power density of SOFC cells as less material is required for a given stack power.

- Stainless steel stack repeat components (interconnects, separator plates, and picture frames) also are significant costs. These may be manufactured with either machining or powder metallurgy techniques. Cathode side stainless steel components have the additional cost burden of high cost coatings to preserve electrical conductivity and slow the rate of cathode poisoning by chromia vapors. Other repeat components such as seals and spacers also contribute significantly to cost.

- Sintering, the bottleneck of cell manufacturing, is a slow, carefully controlled process that is capital, maintenance, floor space, and energy intensive. Reducing the duration and/or number of sintering steps can lead to significant cost savings. Continuous rather than batch furnaces would be preferred in high production volume scenarios, although the former is more capital intensive. Alternatives to traditional resistance furnaces, such as microwave sintering, are being examined by SOFC developers.

- Screen printers allow high automation in cell layer deposition. However, screen printers which have been adopted from and optimized for the electronics industry are not optimized for SOFC manufacturing. SOFC screen printing compared to electronics industry screen printing requires thinner prints and uses an ink whose rheology differs from that of solder paste. A developmental-stage alternative to screen printing is inkjet printing, which allows 3-dimensional control of cell microstructure, a key ingredient for overcoming challenges associated with internal reforming.

- Cell manufacturing uses automated equipment readily available in the marketplace (attrition mills, high shear mixers, tape casters, screen printers, continuous resistance furnaces). However, stack and system assembly, as well as visual quality control steps, are manual and labor intensive and may benefit from automation. High production volume is needed to justify the capital expenditure to automate these processes.

- Sealing and interconnect reliability challenges are among the largest factors inhibiting the mass commercialization of SOFC systems, as numerous cost studies have demonstrated that these systems can be manufactured at relatively competitive costs. A suitable sealing material which is gas tight, chemically non-reactive, and can withstand thermal cycling without embrittlement is needed. Similarly, an interconnect material which remains a good electrical conductor over time without poisoning cathodes will be required.

1. INTRODUCTION

1.1 OBJECTIVE

By offering the promise of both very high efficiencies and low emissions, fuel cells are positioned to become one of the most attractive members in an already diverse suite of power generation technologies. The fuel cell class itself has a very diverse taxonomy. From sub milliwatt systems operating on methanol in handheld electronic devices, to multi-megawatt systems operating on natural gas to power homes and businesses, fuel cells have found numerous applications for providing the clean energy we need. However, despite having been conceived over 170 years ago, fuel cells have to date enjoyed limited commercial success, partly due to cost and reliability challenges. Innovative manufacturing techniques are needed to address these challenges.

A one year project to examine the processes employed in the manufacture of combined heat and power (CHP) stationary fuel cells operating in the 100-400 kWe range was commissioned in June 2010. The objective was to clearly define the processes used and the costs incurred at each of the major manufacturing steps, and to incorporate these findings into fuel cell system cost models. By highlighting the high cost steps, the results of this project would be used to inform decision-makers in prioritizing and allocating R&D resources to processing alternatives with the greatest potential for high impact cost reduction.

In the present study, three combined heat and power technologies were examined: phosphoric acid (PAFC), molten carbonate (MCFC), and solid oxide (SOFC). PAFC is the most mature of the three technologies with systems having been commercially available since 1991 when International Fuel Cells Corporation (now a division of United Technologies Corporation) released the PC-25^{TM}, a 200kWe combined heat and power stationary system whose technology had been under development since the 1960's. FuelCell Energy (FCE) and its predecessor Energy Research Corporation have been the primary developers in the United States of the second most mature technology, MCFC. FCE offers commercially available combined heat and power systems ranging in size from 375kWe to 3MWe. SOFC is the least mature of the three technologies. With the exception of Bloom Energy's 100kWe electrical only system (i.e. no thermal power production) a commercially available SOFC in the 100-400kWe range does not exist at the time of this project.

1.2 MODELING BOUNDARIES

The modeling methodology employed in the present study was process based cost modeling (PBCM). PBCM entails, first, identifying with a process flow diagram all major process steps required in the manufacture of some product. Second, the key technical details of each manufacturing step (examples are part geometry, tolerance, material mass, process temperature, scrap rate, machine cycle time, labor requirement) are used to develop a cost estimate for that step. Costs are classified using major cost component categories such as materials, capital, labor, energy, and floor space. The total cost of a given step is the sum of all cost components present

in that step. Similarly, the sum of all manufacturing cost components for all steps is the estimated total manufacturing cost. PBCMs are especially useful for assessing the cost implications of alternatives in product design (e.g. small versus large planform area cells), processes used (e.g. batch versus continuous sintering), and production volume. An optimal set of manufacturing parameters can be identified by using the PBCM to examine the various manufacturing alternatives under consideration. Moreover, because costs are disaggregated by process steps and cost components, graphical illustrations can be used to efficiently communicate which specific steps and cost components are the primary drivers of total manufacturing cost. In turn, these high cost steps can be targeted for research and development to identify lower cost alternatives.

For this study, manufacturing cost components were defined as follows:

- Materials – A material is defined as any item procured from a supplier which is necessary for the manufacture of the fuel cell system. The materials cost figures presented in this study are inclusive of direct materials and indirect materials. Direct materials are items sourced from suppliers which are present in the final fuel cell product. Example direct materials are platinum catalyst, stainless steel separator plates, and inverters. It should be noted that a direct material for the fuel cell manufacturer is usually a finished good for an upstream supplier. For instance, an inverter, while often thought of as simply a finished good because of its complex nature, is to be treated as a direct material from the perspective of the fuel cell system manufacturer. Indirect materials are items sourced from suppliers which are not present in the final fuel cell product but still necessary for its manufacture. Example indirect materials include gases necessary for maintaining a reducing atmosphere in a furnace, or cleaning supplies for cleaning a screen printer stencil. For modeling purposes, materials have been subclassified as cell, stack, or BOP materials.
- Labor – Labor cost figures presented in this study are inclusive of direct and indirect labor. Direct labor is defined as man-hours directly attributable to fuel cell manufacturing, such as a worker operating a tape caster. Indirect labor is defined as man-hours not directly attributable to fuel cell manufacturing, but still necessary for plant operation. Supervisors, engineers, and janitors are examples of indirect labor staff.
- Capital – Capital cost figures presented in this study are the annualized discounted cost of owning manufacturing assets inclusive of maintenance and tooling.
- Energy – Energy cost figures presented in this study are the energy costs incurred from operating manufacturing assets.
- Plant floor space – Floor space costs presented in this study are inclusive of the rent/depreciation, general utilities, insurance, property taxes, and maintenance costs incurred from owning and operating a manufacturing facility.

PBCMs are less useful for determining costs beyond those which can be easily related to processes. However, this is not a significant limitation as emphasis in the present study was placed on identifying manufacturing improvement opportunities. Costs which were not examined include non-manufacturing, fuel cell installation, and fuel cell operational costs. Non-manufacturing costs include:

- Sales – all costs attributable to marketing and selling the fuel cell product
- Administration – all costs attributable to the general administration of the fuel cell company
- R&D – costs for research and development of improved or new product technology
- Office floor space - rent/depreciation, general utilities, insurance, property taxes, and maintenance costs incurred from owning and operating an office facility
- Profit – cost added to the sum of manufacturing and non-manufacturing costs to enable the company to make a profit

The sum of all manufacturing and non-manufacturing costs is the system cost as realized by a purchaser. The installed cost is system cost plus the installation costs of delivery and civil work at the purchaser's site. Finally, the operational costs of fuel, maintenance, and end-of-life disposal are added to the installed cost giving the total cost of ownership for a fuel cell system. The boundaries of the present study are restricted to manufacturing costs only as depicted in Figure 1-1.

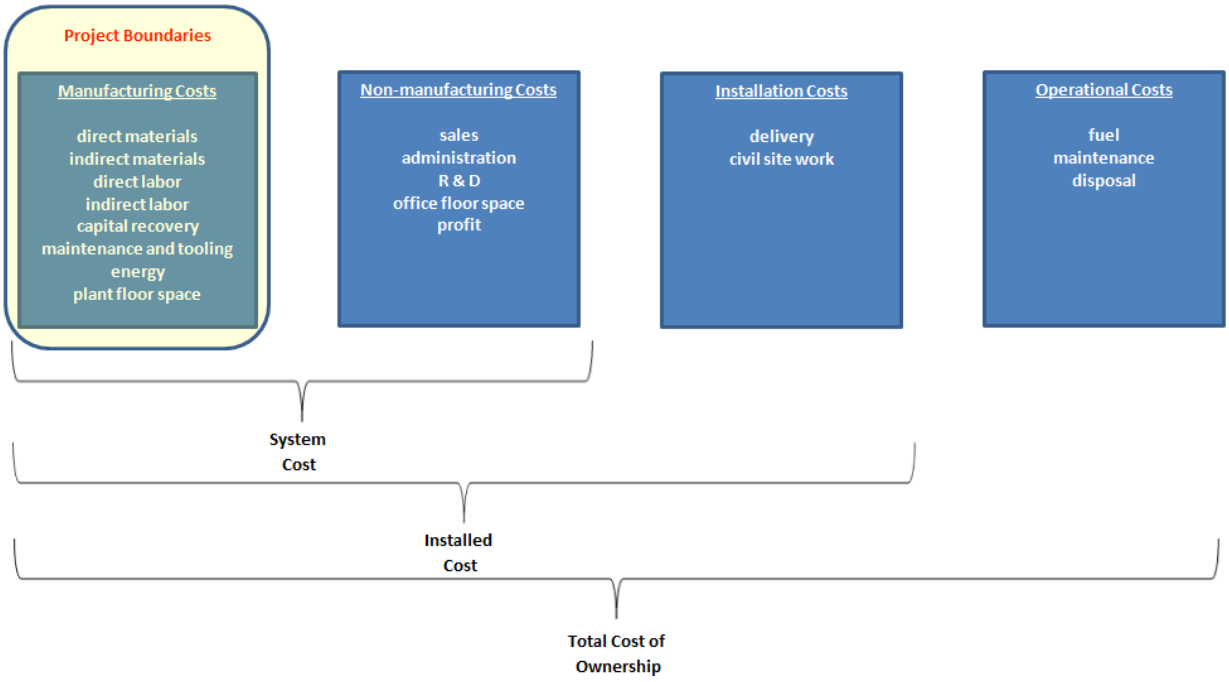

Figure 1-1. Cost Components and Model Boundaries

1.3 MODELING METHODOLOGY

A process based cost model using spreadsheet software was created for each of the three technologies examined. A diverse suite of tools and resources were utilized for gathering inputs for, experimenting with, and validating the models, including:

- Literature review
- Process flow diagrams
- Design for Manufacture and Assembly (DFMA) software
- Monte Carlo simulation software
- Industry and academia partners
- Component specification calculations
- Supplier quotations
- Lean manufacturing principles

The baseline manufacturing scenario for each of the technologies was a production volume equivalent to 20 MWe/year which is representative of the recent demand experienced by both UTC and FCE for their phosphoric acid and molten carbonate systems, respectively. However, cost behavior was studied for production volumes ranging from 5 to 500 MWe/yr. The number of plant shifts per day was made a function of yearly production volume and allowed to rise by integer increments from 1 to 3 as volume increased. Manufacturing facilities were assumed to be available for production activities for 5 days per week and 50 weeks per year implying 2000, 4000, and 6000 maximum available production hours for 1, 2, and 3 shift operations, respectively. A plant efficiency penalty, however, was imposed which reduced available production hours from their maximum. For instance, a two shift operation with an 80% plant efficiency accomplished only 3200 actual hours production for the 4000 hours available to it.

With production volume and available hours defined, a takt time was calculated for each manufacturing station in the production process by dividing the available production hours by the number of parts that must be processed in order to meet required yearly production volume. For instance, if 3200 electrolyte screen printing hours are available per year, during which time 800,000 solid oxide fuel cell electrolyte layers must be printed, then the takt time for the screen printing manufacturing station is 3200/800,000 = 0.004 hours per cell, or 14.4 seconds per cell. The takt time for a given cell was further refined by adjusting for scrap rates downstream of that manufacturing station. Scrap rates were determined based on literature searches and in consultation with industry/academia partners. As an example, if 800,000 SOFC cells are required at the end of the entire production process, and the scrap rate between electrolyte screen printing and the completed fuel cell product is 2%, then 800,000/0.98 = 816,327 cells must pass through the electrolyte screen printing manufacturing station, giving a yield adjusted takt time of 3200/816,327 = 14.11 seconds per cell.

The amount of time for a single machine or worker to perform an operation was defined as the

capacity of that resource. For any given manufacturing station, the number of resources required at a given production volume was defined as the capacity of a single resource divided by the takt time of the manufacturing station. This value was always rounded up to the nearest integer. For instance, if a screen printer requires 20 seconds to print an electrolyte layer on a solid oxide fuel cell, and the takt time of the electrolyte screen printing manufacturing station is 14.11 seconds, then 20/14.11 = 1.42 screen printers are indicated. The model rounds this result to 2 screen printers. Capital equipment costs were determined based on literature searches and in consultation with industry/academia partners. Equipment lifetime was assumed to be ten years and the cost of capital was assumed to be in the range of 8-15%.

The utilization of a manufacturing station was defined as the capacity of a single resource divided by the number of resources required divided by the takt time of the manufacturing station. For instance, 2 screen printers each having a capacity of 20 seconds per electrolyte layer have a combined capacity of 20/2 = 10 seconds per electrolyte layer. If the takt time of this manufacturing station is 14.11 seconds then the screen printers are collectively 10/14.11 = 71% utilized. Thus, the two screen printers are in operation for 0.71*3200 = 2272 hours each or 2272*2 = 4544 hours combined. The number of hours during which a resource is in operation per year times the kilowatt rating of the resource times the cost of grid electricity is defined as the energy cost of resource. So, to further develop the preceding example, two screen printers operating for 2272 hours each at 1.6kW each where grid electricity costs $0.10/kWh have an expected energy cost of 2*2272*1.6*0.10 = $727/yr.

Plant floor space was allocated to each manufacturing station based upon the footprint required for machines and/or assembly operations plus additional space for auxiliary equipment, aisles and storage. A cost per square foot factor encompassing rent/depreciation, general utilities, insurance, property taxes, and maintenance costs was multiplied by the square footage required for a given manufacturing station.

In the short-term direct labor is a fixed cost as workers generally are not added or subtracted as production volume varies from week to week or month to month. However, in modeling scenarios where fuel cell manufacturing volume ranges from 5 to 500 MWe/yr, clearly direct labor must be treated as a variable cost. As such, direct labor requirements were defined using the length of time required to perform an operation. When the length of time required to perform an operation is considered with the number of operations that must be performed in a year, the quantity of labor hours that must be expended per year on a given operation can be determined. As an example, if an assumed yearly production volume requires a tape caster to receive 4 liters of slip (mixture of ceramic particles and solvents to be cast into a tape) per hour for a 2 shift operation having an efficiency adjusted 3200 available production hours per year, then 4*3200 = 12,800 liters of slip must be manufactured per year. If a batch high shear mixer processes slip in batches of 20 liters then 12,800/20 = 640 batches of slip must be processed per year, and the batch takt time is 3200/640 = 5 hours per batch. Further, if each batch requires 1.5 hours labor then 640*1.5 = 960 labor hours are required for slip manufacturing per year. If the assumed cost for direct labor is $25/hr, then the direct labor cost component allocated to slip manufacturing is 960*25 = $24,000/yr. Indirect labor has been modeled as a decreasing percentage of direct labor as production volume increases.

Direct material quantities were estimated by first determining a part's geometrical shape taking into account whether the part was dense or porous. The relative proportions of the part's constituent materials were determined, as well as the densities of those materials. As an example, a typical anode-supported planar solid oxide fuel cell might be 500 μm thick for a cell with planar dimensions of 25cm X 25cm. This anode support thus would occupy a volume of $31.25cm^3$. A typical anode support would be 33.33% porous, 33.33% NiO, and 33.33% 8YSZ before the NiO is reduced to Ni. Thus, $0.3333*31.25 = 10.42cm^3$ would be occupied by NiO and likewise for 8YSZ. Given that the density of NiO is 6.67 g/cm^3, the mass of NiO in one anode support must be 10.42*6.67 = 69.47 g. A similar calculation is possible with 8YSZ. Significant indirect materials were also modeled such as wax paper used as tape casting substrates and nitrogen gas flows used to maintain a reducing atmosphere in a sintering furnace.

Balance of stack and balance of plant estimates were determined through a combination of DFMA software, component specification calculations, supplier quotations, literature searches, scaling factors, and consultation with industry/academia partners. DFMA™ by Boothroyd and Dewhurst is a software package useful in estimating costs in manufacturing and assembly operations. DFMA principles espouse close interaction between design and manufacturing engineers so that products 1) meet design specifications, and 2) are easily manufactured and assembled. Such products both meet customer requirements and are low cost. Part count reduction is central to DFMA methodology. The DFMA™ software package contains extensive machine, material, and operation libraries mostly representative of traditional metalworking operations. Many processes particularly relevant to fuel cell manufacturing such as tape casting and carbon paper manufacturing are not members of these libraries and thus were examined strictly with process based cost modeling. However, BOP and stack components such as stack manifolds and coolant headers which are created through traditional metalworking operations can be accurately estimated with DFMA™. Cost estimates for specific components modeled with DFMA™ software were incorporated into the larger process based cost models.

Many BOP components such as heat exchangers and blowers are off-the-shelf items already manufactured in high volume for diverse industries. By estimating heat and mass balances throughout the fuel cell system, required heat exchanger surface areas can be determined which can then be translated into costs through supplier quotations. Similarly, determining the volume of air that must be moved per unit time in order to meet stoichiometric and cooling requirements indicates what size blower must be used for supplying cathode oxidant. Blower specifications can in turn be translated into a cost with supplier quotations.

Other BOP components such as steam methane reformers and integrated low temperature shift converters are either not common off-the-shelf items or are of a complexity beyond the scope of this project to model with DFMA™. In such cases, component costs were estimated through consultation with industry/academia partners, scaling factors, and literature searches.

Cost estimates at each manufacturing step were summed across all manufacturing steps to determine an estimated total manufacturing cost. Monte Carlo simulations, sensitivity analyses, and graphical analyses were performed to highlight cost sensitive processing steps.

2. PHOSPHORIC ACID FUEL CELLS

2.1 BASIC OPERATION

Having been in development since the 1960s, phosphoric acid fuel cells are the most mature of the three technologies examined in this study. Most PAFC development has occurred in Japan and the United States. Japanese developers include Fuji Electric Corporation, Toshiba IFC, and Mitsubishi Electric Corporation. In the United States PAFC technology has been developed primarily by UTC Power, a division of United Technologies Corporation (UTC). Other United States developers have included Westinghouse Electric Corporation and HydroGen Corporation.

The basic operation of a phosphoric acid fuel cell using reformed natural gas for fuel is depicted in Figure 2-1.

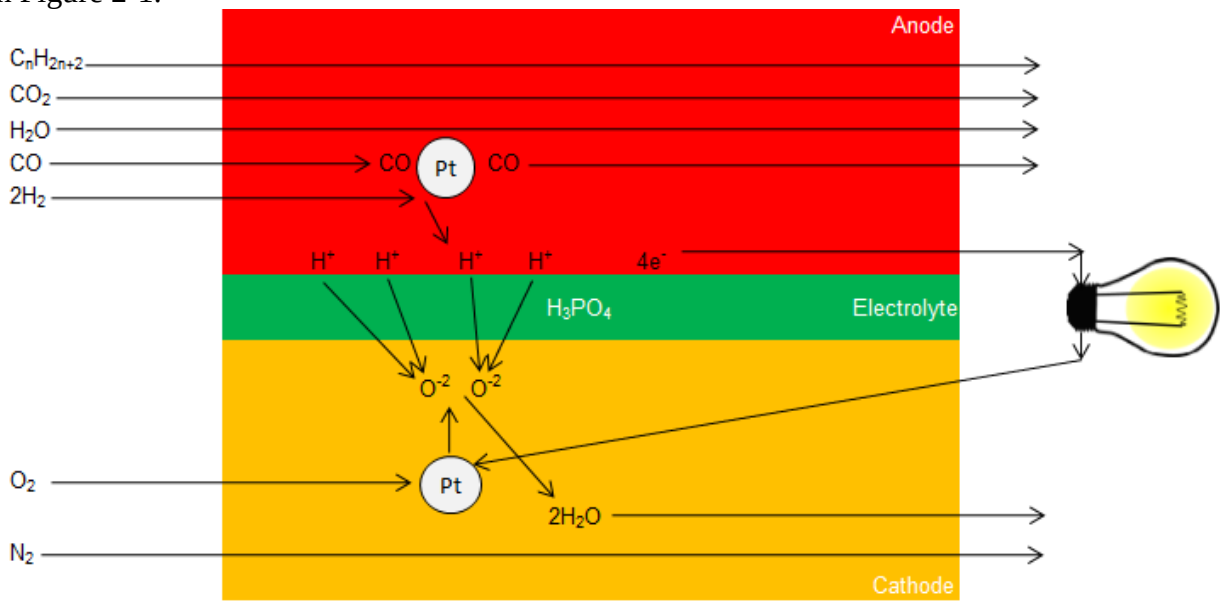

Figure 2-1. Basic Operation of a Phosphoric Acid Fuel Cell

A reformed natural gas mixture consisting of predominantly diatomic hydrogen enters the anode. Inside the anode, two diatomic hydrogen molecules are shown to contact a platinum catalyst where the hydrogen molecules are split into four protons with four electrons liberated. The protons are conducted through the electrolyte consisting of concentrated phosphoric acid contained by capillary forces in a matrix of silicon carbide (SiC). After passing through the electrolyte, the protons enter the cathode. The electrolyte is nonconductive to the electrons liberated during the splitting of diatomic hydrogen in the anode. Thus, the electrons are forced through an external circuit passing through an electrical load and performing work before reaching the cathode. Air consisting of predominantly diatomic nitrogen and diatomic oxygen is introduced into the cathode. Diatomic oxygen contacts a platinum catalyst in the cathode where it is reduced into two oxygen ions by the 4 electrons liberated in the anode reaction. Each oxygen ion reacts with two protons to form one molecule of water which exits the cathode as a vapor. Diatomic nitrogen exits the cathode unreacted.

Other compounds introduced into the anode include carbon monoxide, water vapor, carbon dioxide, and unreformed natural gas. It is desirable to minimize the concentration of these compounds as they are diluents to the hydrogen fuel. Dilution of hydrogen with other compounds results in diminished partial pressure of hydrogen and consequently reduced cell voltage and power. In addition, carbon monoxide in high enough concentration will attach to the catalyst as depicted in Figure 2-1, and thereby diminishes or prevents the catalysis of hydrogen. With higher operating temperatures, the propensity for carbon monoxide to attach to the platinum catalyst diminishes, and thus a higher concentration of carbon monoxide is tolerable. Higher carbon monoxide tolerance is desirable as this eases constraints on the fuel processing system. In addition, higher operating temperatures improve the ionic conductivity of phosphoric acid while diminishing other sources of voltage loss. However, higher operating temperatures also result in an increased rate at which phosphoric acid is volatilized and lost from the cell by becoming entrained in the exhaust streams. System pressurization increases the partial pressures of fuel and oxidant in the fuel cell improving voltage and power. However, pressurization also increases the complexity and cost of the balance of plant and may not result in an improved cost of electricity over the life of the system. Additionally, pressurization increases the partial pressure of phosphoric acid vapor in the fuel cell which results in increased corrosion of cell components. The selection of operating temperature and pressure thus presents an optimization challenge with complex benefits and tradeoffs.

2.2 CELL, STACK, AND SYSTEM DESIGN ASSUMPTIONS

The PAFC manufacturing cost model developed in the present study was developed using inputs gathered from publicly available literature, nonproprietary inputs gathered in consultation with industry partners, supplier quotations, and DFMA™ software. UTC offered the world's first commercially available fuel cell in 1991 with the introduction of the PC-25™, a 200 kWe atmospheric pressure combined heat and power stationary fuel cell system. This system has recently been succeeded by the PureCell 400™, a 400 kWe system made commercially available in late 2009. UTC's website indicates the PureCell 400™ can achieve greater than 40% initial electrical efficiency (LHV natural gas) with greater than 38% average electrical efficiency over the 10 year life of a stack.[1] The system is designed for a 20-year life with a stack replacement overhaul after the first 10 years of operation. Overall efficiency approaches 90%, with non-recovered energy lost to the environment. Thermal energy is available as high grade heat (water at 250^0F) and low grade heat (water at 120^0F) at an average of 1.876 MMBtu/hr over the course of a ten-year stack life assuming cooling water is returned to the fuel cell system's condenser at a temperature of 80^0F.

A patent issued to Breault and Fredley in 2010 describing design considerations which impart long life characteristics to a phosphoric acid fuel cell system served as the guiding template for the system modeled in this cost analysis.[2] In this patent, the authors describe four design parameters leading to an expected stack life of approximately 90,000 hours, twice the expected life of previous designs such as the PC-25™. Among those design considerations imparting long life characteristics is a condensation zone which has been described in previous patents.[3,4] A condensation zone is an uncatalyzed section of the cathode adjacent to the oxidant exhaust

manifold. The absence of catalyst in the condensation zone creates an environment where the fuel cell reaction does not take place. As a consequence, exit temperatures are reduced in the condensation zone, thereby allowing a substantial portion of the volatilized phosphoric acid entrained in the oxidant exhaust to be condensed and returned to the cell. Returning a substantial portion of volatilized acid to the cell greatly diminishes this failure mode and is key to extending the life of the fuel cell. The patent[2] describes a condensation zone that cools reactant exit gases to less than 140^0C which is approximately 25^0C less than previous designs. Such aggressive cooling leads to an 80% reduction in the acid loss rate compared with previous designs. Patent literature indicates that allocating 5-10% of total cell area is sufficient for creating an effective condensation zone.[3] Any cell area allocated to a condensation zone must necessarily deduct from the active cell area. Further reducing active cell area are edge seals, mechanisms which prevent fuel from entering a cathode and oxidant from entering an anode. In this model, edge seals and condensation zones are assumed to collectively require 15% of total cell area. Also, the model assumes a rectangular cell as shown in Figure 2-2 having planform dimensions of 42.60 cm X 69.05 cm, giving a total cell area of 2941.53 cm^2 and an active cell area of approximately 2500 cm^2.

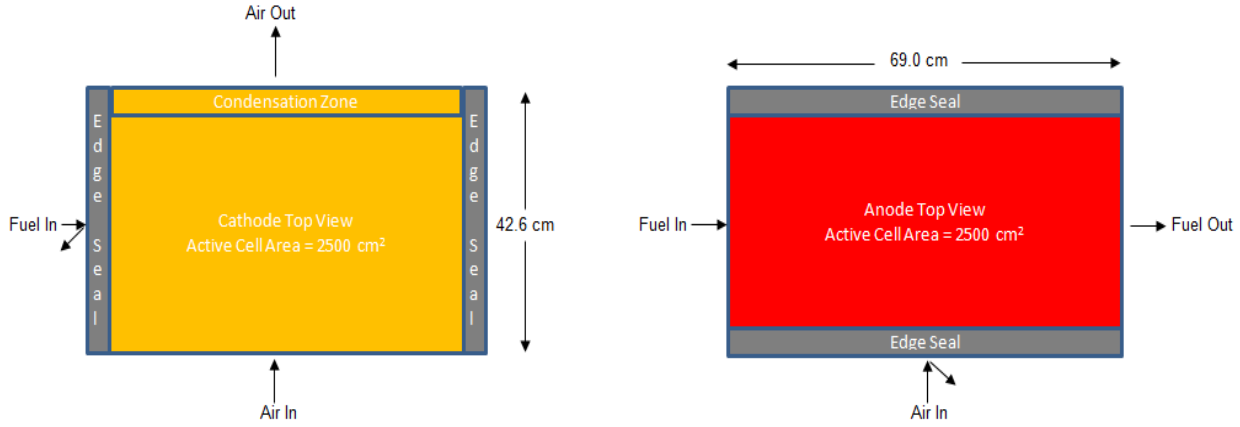

Figure 2-2. PAFC Planform Cell Geometry

UTC indicates 376 cells per stack and 4 stacks per PureCell 400™ system.[5] Incorporating these cell and stack counts with an assumed cell active area of 2500 cm^2 results in a total active area of 376 m^2 per system. Using an assumed current density of approximately 0.1940 A/cm^2 and cell voltage of 0.6014 V, a power density of 0.1167 W/cm^2 is achieved. With an active cell area of 2500 cm^2, each cell is producing DC at a rate of 291.7 W, and the entire system is thus producing 439 kW. It is further assumed that the inverter efficiency is 96%, resulting in 421 kW of gross AC power. Parasitic loads are assumed to deduct an additional 5% from gross AC resulting in 400kW of net AC. A total system efficiency of 90% (LHV NG) is assumed achievable for a CHP hot water application, with 42% electrical efficiency and 48% thermal efficiency. The above assumptions are listed in Table 2-1 below.

Table 2-1. PAFC Cell, Stack, and Power assumptions

Cell area	69.05 x 42.60 = 2941.53 cm^2
Percent cell area used for edge seals and cond. zone	15%
Active cell area	2941.53 cm^2 x 0.85 = 2500 cm^2
Current density	0.1940 A/cm^2
Voltage	0.6014 V
Power density	0.1167 W/cm^2
Single cell power	0.29175 kW
Gross System DC at 0hr	$\frac{0.29175\ kW}{cell} \times \frac{376\ cells}{stack} \times \frac{4\ stacks}{system} = \frac{439kW\ DC}{system}$
Losses:	
Inverter efficiency 96%	439kW DC x 0.96 = 421kW AC
Parasitic Losses 5%	421kW x 0.95 = 400 kWe net AC
Electrical efficiency (LHV natural gas)	42%
Thermal efficiency	48% → 1.56 MMBtu/hr
Total system efficiency	90%

A second design consideration for imparting long life characteristics to a phosphoric acid fuel cell as described by Breault and Fredley is the use of non-wetproofed (i.e. hydrophilic) substrates which function simultaneously as both electrodes and electrolyte reservoir layers for both anodes and cathodes.[2] These substrates are indicated as having suitable thicknesses in the range of 0.25 mm to 0.46 mm with the minimal thickness being preferable. In previous designs, electrolyte reservoir plates (ERP), which were separate entities from electrode substrates themselves, have been used to increase the acid volume present in a cell. Acid lost from the electrolyte during the cell's operation would be replenished by the capillary migration of acid stored in the ERP to the electrolyte. However, in US Patent 4,035,551, Grevstad demonstrated that non-wetproofed carbon papers having a range of pores sizes randomly distributed throughout the carbon paper could function as both electrolyte reservoir layers and as electrode substrates.[6] Smaller pores in the carbon paper store acid while larger pores remain open pathways for gas exchange with the catalyst layer that is deposited on one side of the carbon paper substrate. From a manufacturing standpoint, combining the function of an ERP and an electrode substrate is desirable as doing so reduces part count and cell complexity. Additionally, minimizing the thicknesses of layers reduces material costs. Elimination of wetproofing is also desirable as doing so removes processing and material costs. Wetproofing is a slow and costly process whereby substrates are treated with polytetrafluoroethylene (PTFE), a hydrophobic substance that when applied to a substrate prevents "electrode flooding," manifest by a substrate's pores becoming occluded with phosphoric acid. Pore occlusion prevents reactant gases from reaching the catalyst layer, thereby preventing the fuel cell electrochemical reaction from taking place. Substrates that do not flood even without wetproofing were demonstrated by Grevstad [6] and incorporated into the Breault and Fredley design.[2]

A third design consideration for imparting long life characteristics to a phosphoric acid fuel cell as described by Breault and Fredley is the use of non-porous, hydrophobic flow fields for both anode and cathode with a separator plate sandwiched in between.[2] Non-porous, hydrophobic flow fields are desirable in order to minimize acid absorption which would lead to cell failure as acid is depleted from the electrolyte layer. Previous designs used grooved, porous, hydrophilic ERP/flow fields having the duel tasks of being both acid reservoirs and reactant gas conductors on both the anode and cathode sides of the cell.[7] More recently, as described in US Patent 5,558,955, a grooved, porous, hydrophilic ERP/flow field was used on the anode side of a cell and a non-porous, hydrophobic flow field with no ERP was used on the cathode side of a cell.[8] In their 2010 patent, Breault and Fredley indicate that the findings of US Patent 5,558,955 are applicable for not only cathode but also anode flow field manufacturing with the electrode substrates themselves functioning as the electrolyte reservoir layers.[2] In keeping with Breault and Fredley's 2010 patent, this cost model assumes both anode and cathode flow fields are hydrophobic, non-porous, molded graphite/resin structures each having a thickness of about 1.42 mm. Sandwiched between and chemically bonded to both an anode and cathode flow field is a graphite separator plate that may be manufactured through a variety of methods as has been described in the patent literature, [9,10,11] but is not discussed in the 2010 Breault and Fredley patent.[2] For modeling purposes, separator plates are assumed to be manufactured according to Grasso (the most recent of the three patents cited above) which uses layers of resin and graphite impregnated carbon felts that are laminated together by hot pressing.[11] This procedure results in separator plates having a final thickness of about 0.71 mm after graphitization.

A fourth design consideration for imparting long life characteristics to a phosphoric acid fuel cell as described by Breault and Fredley is the use of a 0.05 mm thick electrolyte retaining matrix comprised of silicon carbide with a mean particle size of 3 microns.[2] Such a matrix imparts long life characteristics to a phosphoric acid fuel cell because of the relatively slow kinetics of silicon carbide's destructive reaction with phosphoric acid whereby acid mass is lost from the electrolyte layer by being converted to silicon phosphate.

The patent literature inputs described in the preceding paragraphs along with others that will be discussed in later sections of this report are the basis for the model cell structure shown in Figure 2-3. A 0.05 mm thick, 50% porous matrix comprised of primarily silicon carbide is saturated with concentrated phosphoric acid and serves as the electrolyte layer. Graphitized carbon papers being 0.25 mm thick, 70% porous and hydrophilic serve as both electrode substrates and electrolyte reservoir layers for both anodes and cathodes. The anode substrate has a 0.10mm thick, 60% porous catalyst layer deposited on the surface facing the electrolyte layer. The anode catalyst is assumed to be 10 wt% Pt supported on carbon black with an areal loading of 0.25 mg Pt/cm^2. Similarly, the cathode substrate also has a 0.10mm thick, 60% porous catalyst layer deposited the surface which faces the electrolyte layer. The cathode catalyst is assumed to be 10 wt% Pt alloyed with cobalt and chromium supported on graphitized carbon black with an areal loading of 0.50 mg Pt/cm^2. Both anode and cathode flow fields are assumed to be 1.42 mm thick, non-porous, and hydrophobic. Sandwiched between the flow fields is a dense, graphitized separator plate having a thickness of 0.71 mm.

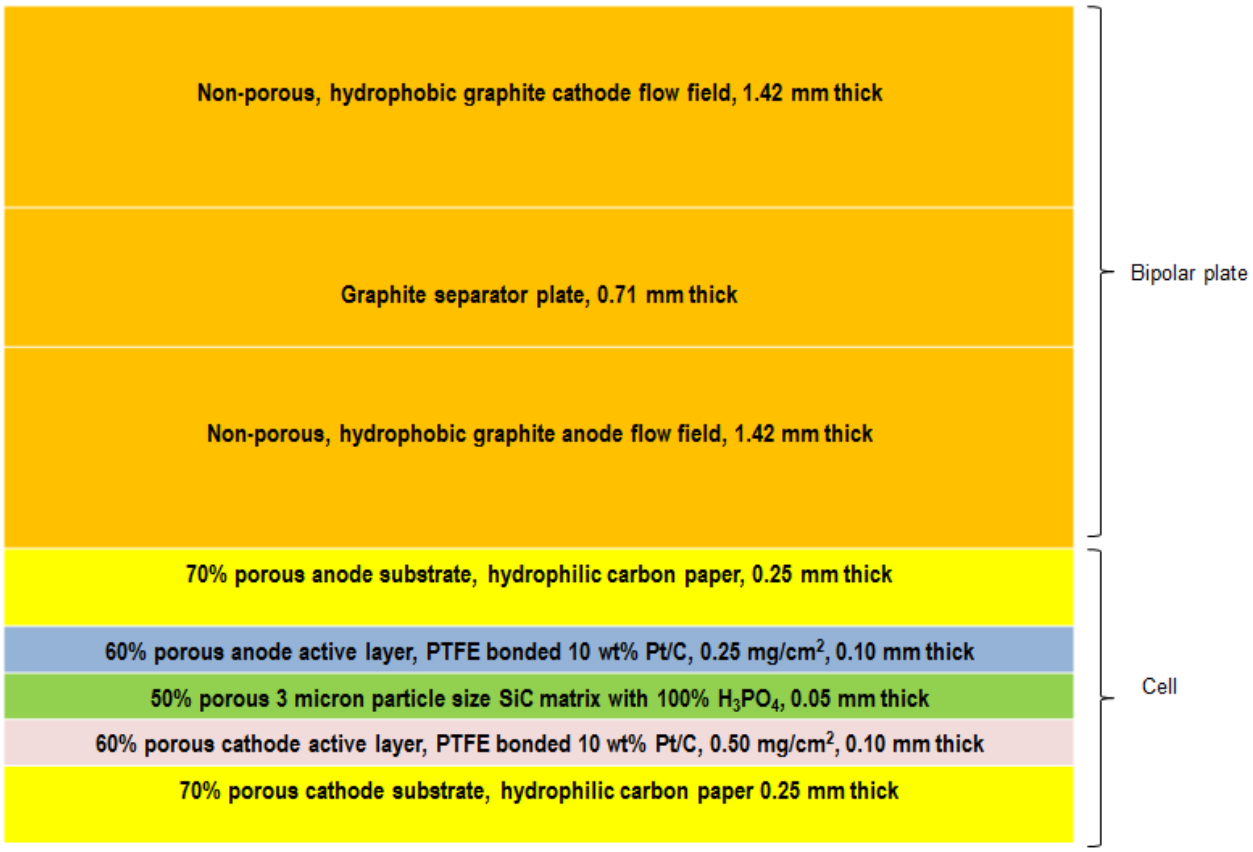

Figure 2-3. PAFC Cell Structure

The system modeled in this study is a water-cooled, atmospheric pressure PAFC with external reactant manifolds. Stack temperature is maintained by passing cooling water through cooling plates intermittently placed between cells. A cooling plate consists of a serpentine stainless steel tube which is embedded in a flat, plate-like graphite housing through which cooling water is conducted. The graphite housing is manufactured with layers of differing coefficients of thermal expansion (CTE), transitioning from high to low CTE to minimize stresses accrued from the different rates of expansion between cooling units and cells/bipolar plates. Each cooling unit also has two flow field layers for conducting reactant gases to adjacent cells. UTC indicates 376 cells per stack with each stack built up from 47 substacks.[5] A substack is itself comprised of one cooling unit and 8 cells with 7 bipolar plates interspersed between the 8 cells. Figure 2-4 below shows the assumed structure of one complete substack used in this study.

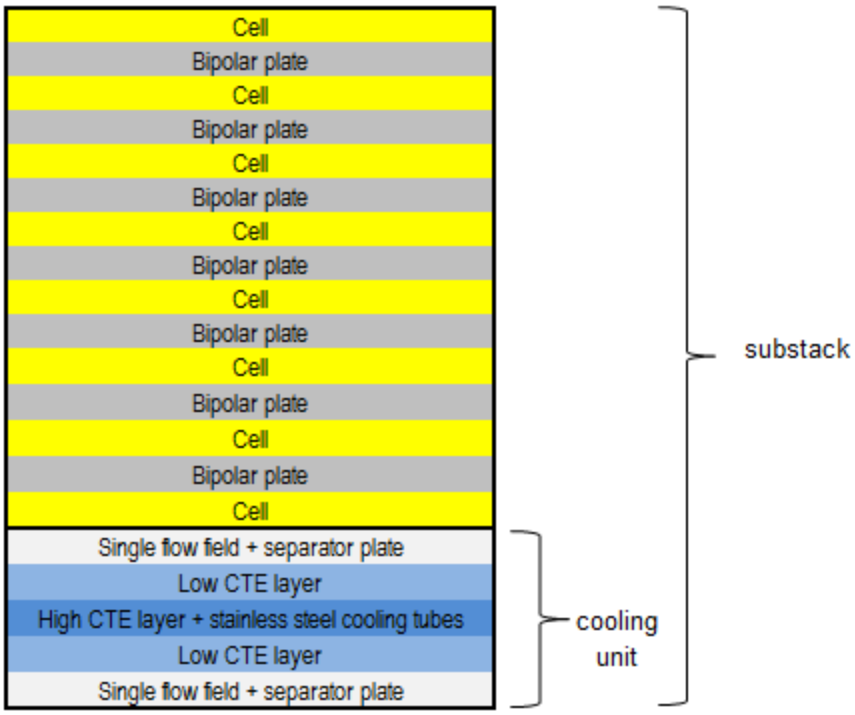

Figure 2-4. PAFC Substack Structure

The integration of 47 substacks with one additional cooling unit and other stack components constitutes a stack in this study. Four stacks are integrated with necessary BOP components to produce a completed fuel cell system. Figure 2-5 is a simplified diagram of the mechanical BOP assumed in this study. Raw natural gas enters the fuel cell system and passes through Hex 1 where it is heated with reformer effluent to warm the natural gas to a temperature suitable for desulfurization. Natural gas then proceeds to the hydrodesulfurizer where it is mixed with a small stream of hydrogen gas harvested from the integrated low temperature shift converter effluent. In the hydrodesulfurizer, hydrogen gas reacts with sulfur compounds in natural gas to form H_2S which in turn reacts with ZnO to form ZnS and H_2O. Zinc sulfide (ZnS) is a solid that remains within the hydrodesulfurizer, thus preventing the introduction of sulfur into the fuel cell. The desulfurized natural gas stream exits the hydrodesulfurizer and is mixed with steam originating from the stack cooling loop. The natural gas/steam mixture then passes through Hex 2 and is warmed once more by reformer effluent before being introduced into the reformer itself. In the reformer, the natural gas/steam mixture undergoes the reforming reaction to produce a mixture of H_2, CO, CO_2, H_2O, and any unreformed hydrocarbons originally present in the natural gas.

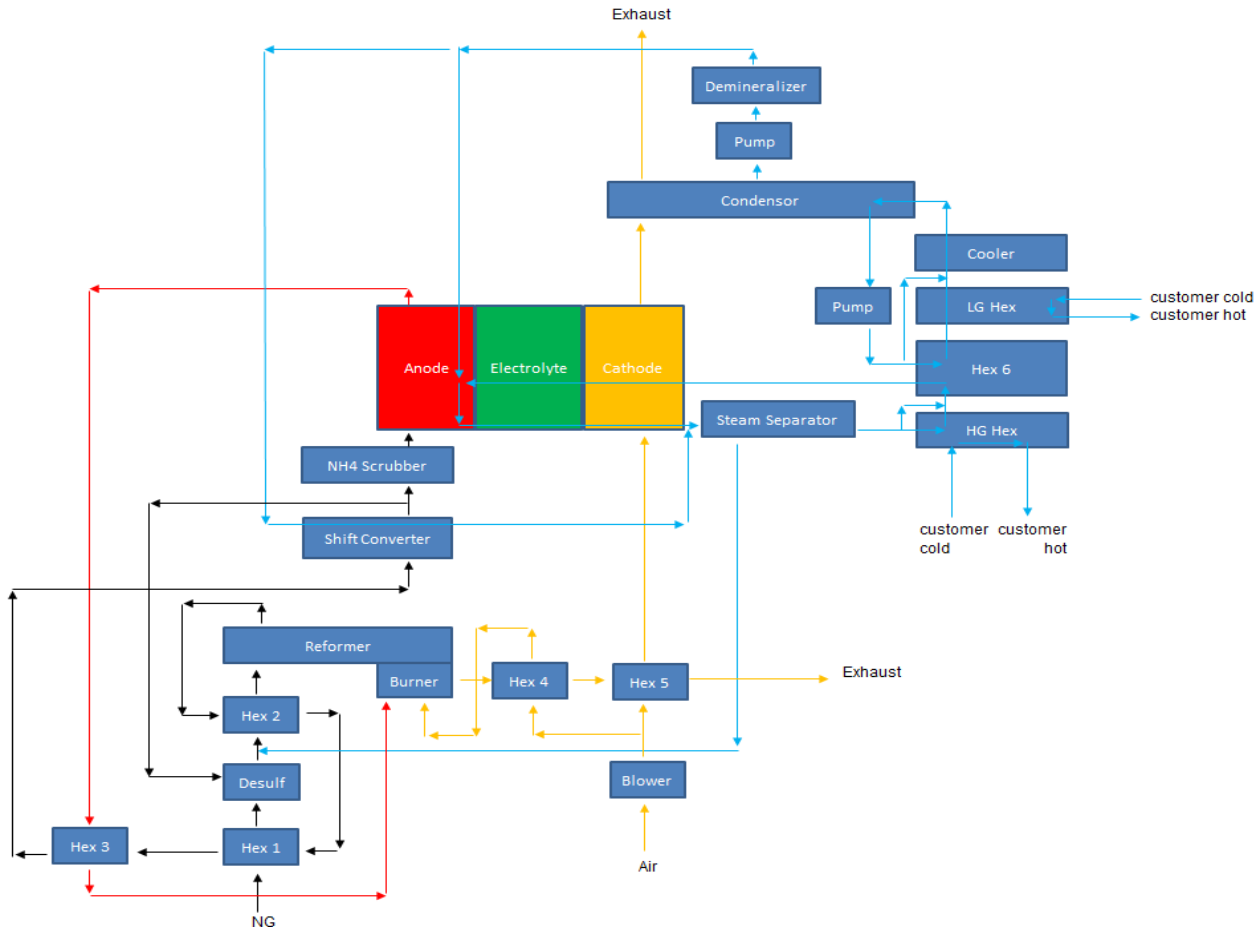

Figure 2-5. PAFC Mechanical BOP

The reformer technology assumed in this study is similar to that described in US Patent 6,296,814 B1 where natural gas is reformed in an array of closely spaced catalyst tubes filled with nickel catalyst.[12] Depleted fuel in the anode exhaust is combusted in the reformer to provide the heat required for the reforming reaction. The reformate exits the reformer and is then stepped down in temperature by providing heat for the aforementioned heat exchanger duties in Hex 1 and Hex 2. Next, the reformer effluent is cooled once more in Hex 3 by warming anode exhaust before it (anode exhaust) is combusted in the reformer burner. The reformer effluent then enters the integrated low temperature shift converter modeled after US Patent 6,306,354 B1.[13] Here, the CO concentration in the fuel stream is reduced by the water gas shift reaction in the presence of a copper, zinc oxide, and alumina catalyst to a level tolerable by the anode catalyst. The water gas shift reaction entails reacting carbon monoxide with water to form carbon dioxide and hydrogen. The integrated low temperature shift converter consists of two zones: an adiabatic zone followed by an actively cooled zone. In the adiabatic zone, the fuel's temperature rises as the exothermic shift reaction proceeds and no heat is transported out of the system. Allowing the temperature to rise improves reaction kinetics so that the shift reaction proceeds quickly. In the actively cooled zone, pressurized cooling water from the fuel cell cooling loop removes heat from the fuel causing its temperature to drop to a level suitable for introduction into the fuel cell anode without causing damage. The patent owners' contend that an integrated low temperature shift converter such as the one described is optimal with respect to

minimizing the quantity of catalyst required for achieving an acceptably low level of carbon monoxide in the fuel stream. After leaving the shift converter, the fuel stream enters an ammonia scrubber, such as the one described in US Patent 2010/0024648 A1, whose function is to reduce the concentration of this contaminant.[14] The undesirable production of ammonia occurs in the reformer if nitrogen is present in the natural gas stream. The fuel stream passes through the ammonia scrubber in a counter flow arrangement with respect to a stream of phosphoric acid flowing over a support material. Ammonia present in the fuel stream reacts with phosphoric acid to form ammonium dihydrogen phosphate which remains in the phosphoric acid solution as a solute. Next, the fuel stream is introduced into the anode where the fuel cell electrochemical reaction takes place. Exhaust exiting the anode is then directed to the reformer burner and combusted, becoming the source of heat for the endothermic reforming reaction.

Oxidant for the reformer burner and the fuel cell cathode is provided by a blower also depicted in Figure 2-6. Exhaust from the reformer burner first heats the reformer burner oxidant in Hex 4 and then the cathode oxidant in Hex 5 before being exhausted to the environment. Air then enters the cathode where the fuel cell electrochemical reaction takes place. The cathode exhaust passes through a condenser where entrained water vapor is condensed to liquid water by transferring heat to the low grade heat exchange loop. The remaining cathode exhaust is vented to the environment. A pump forces the condensed water through a demineralizer before being split into two streams. One stream passes through the actively cooled zone of the integrated low temperature shift converter where it cools the fuel stream and exits as a two phase water/steam mixture which is then introduced into the stack cooling loop, i.e. the second stream exiting the demineralizer. Cooling water in the stack cooling loop extracts heat from the stack and exits the stack as a two phase water/steam mixture. Steam is separated from the two phase mixture and is mixed with desulfurized natural gas before being introduced to Hex 2. Cooling water exiting the steam separator passes to the high grade heat exchanger where heat is transferred to a water stream supplied by the customer. If the quantity of heat recovered by the customer at the high grade heat exchanger is insufficient for stack cooling requirements, then surplus heat is transferred to the low grade heat loop at Hex 6. Low grade heat is recovered by an additional water stream supplied by the customer at the low grade heat exchanger. Surplus heat not recovered at the low grade heat exchanger is rejected to the atmosphere with a fan-driven cooling unit such that cooling water is returned to the condenser at a temperature low enough for condensing sufficient quantities of water for stack cooling and reforming requirements. Bypass loops are provided to bypass one or both of the high grade and low grade heat exchangers for rejecting heat directly to the fan-driven cooler if no customer heat sink is supplied to these heat exchangers.

2.3 HIGH LEVEL MANUFACTURING SYSTEM DESIGN

The manufacturing system design adopted for this study is depicted in a high level process flow diagram below in Figure 2-6.

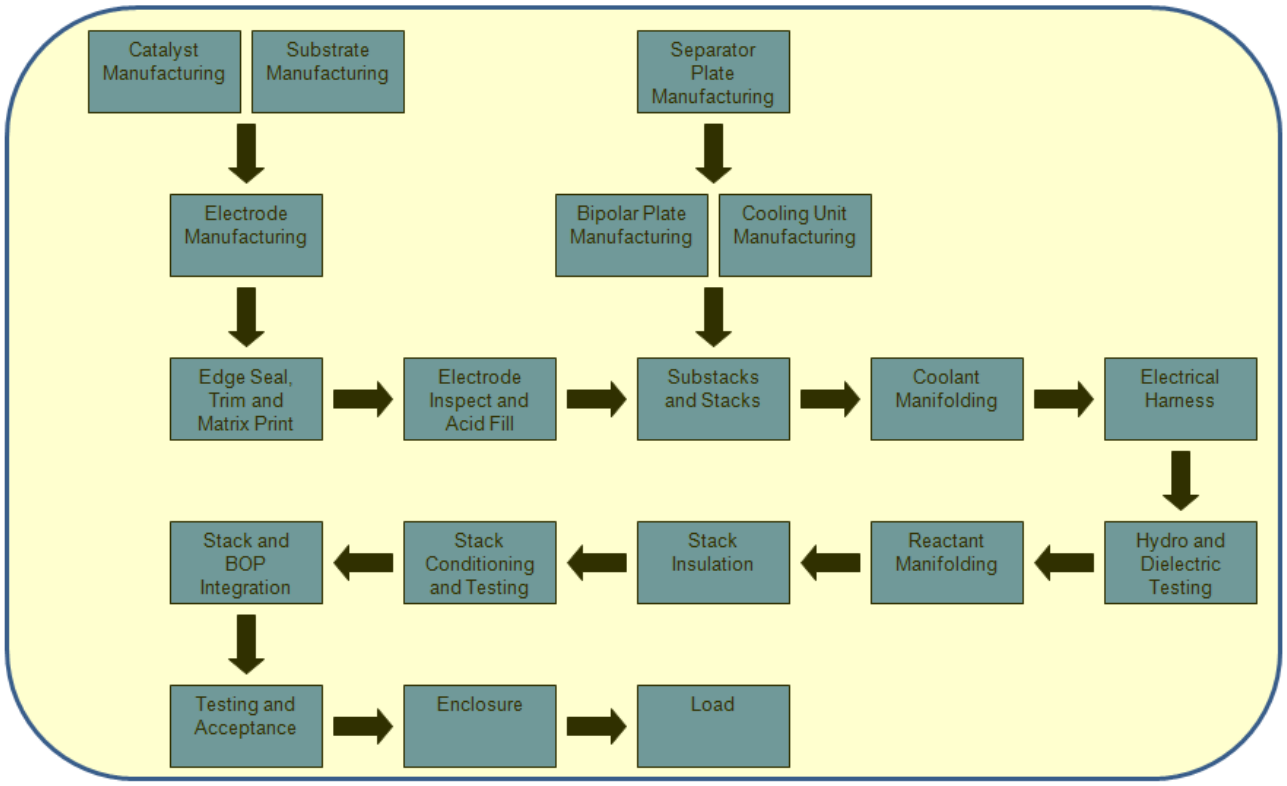

Figure 2-6. High Level PAFC Manufacturing Process Steps

Catalyst manufacturing and substrate manufacturing are independent processes outputting carbon supported platinum catalyst and carbon paper, respectively. Electrodes are manufactured by depositing catalyst on the carbon paper substrates to make electrodes. Electrodes passing quality control inspection are given an edge seal and then have excess material trimmed from their edges. A matrix layer is then printed on both anodes and cathodes. Next, electrodes are inspected, repaired if necessary, and then dipped in a bath to fill with phosphoric acid. Separator plate manufacturing precedes both bipolar plate and cooling unit manufacturing. Electrodes, bipolar plates, and cooling units are integrated into substacks which in turn are integrated with stack end plates and tie rods to create stacks. Stacks then receive coolant manifolding and electrical harnessing which is followed by a quality control step to ensure no water leaks or electrical short circuits. Stacks then receive reactant manifolds and an insulation jacket. A conditioning and testing step follows to ensure stacks are operational. Next, stacks are integrated with balance of plant components and system level testing is performed. After the verification of system performance, an enclosure is placed over the system and the system is loaded onto a trailer for shipping. In the following sections, the above manufacturing steps are expanded and described in detail. In total, 48 manufacturing steps and 224 cost components were examined.

2.4 CATALYST MANUFACTURING

Because carbon supported catalysts such as those used in PAFC have wide commercial availability from multiple suppliers, catalyst has been modeled as a direct material in this cost

analysis. However, it is nonetheless instructive to consider the evolution of catalyst manufacturing and the particular challenges to overall fuel cell system cost imposed by catalyst cost and performance. Electrode reaction kinetics are proportional to catalyst surface area. As such, increasing catalyst surface area (more or less equivalent to decreasing catalyst particle size) in electrodes has been a central theme in catalyst development over the years. First generation catalysts (1960s era) for phosphoric acid fuel cells were platinum blacks having a particle size of 10 nm and requiring a cost prohibitive areal loading of 5 mg Pt/cm^2. The next generation of catalysts, which evolved in the 1970s and is still widely used today, employed carbon black particles as supports for platinum crystals, represented diagrammatically in Figure 2-7.

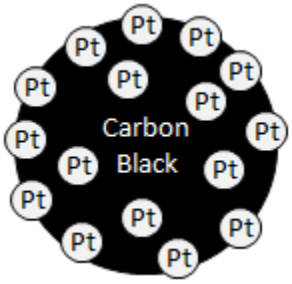

Figure 2-7. Platinum Supported on Carbon Black

In these catalysts, platinum crystals are caused to attach to carbon black particle by procedures well documented in patent literature.[15,16] This advancement led to a roughly 5 fold decrease in mean platinum crystal particle size from 10nm for platinum blacks to 2 nm for platinum supported on carbon black. In addition, this and other advancements have produced a roughly 10 fold decrease in Pt areal loadings which are currently on the order of 0.25-0.50 mg Pt/cm^2 per electrode. This sharp reduction in platinum loading has been pivotal in easing cost challenges associated with PAFC. However, platinum costs have recovered some of their lost influence in recent history due to a sharp increase in the market price of platinum over the last decade as indicated in Figure 2-8. Recovery and recycling of Pt from decommissioned stacks is important for reducing catalyst cost.

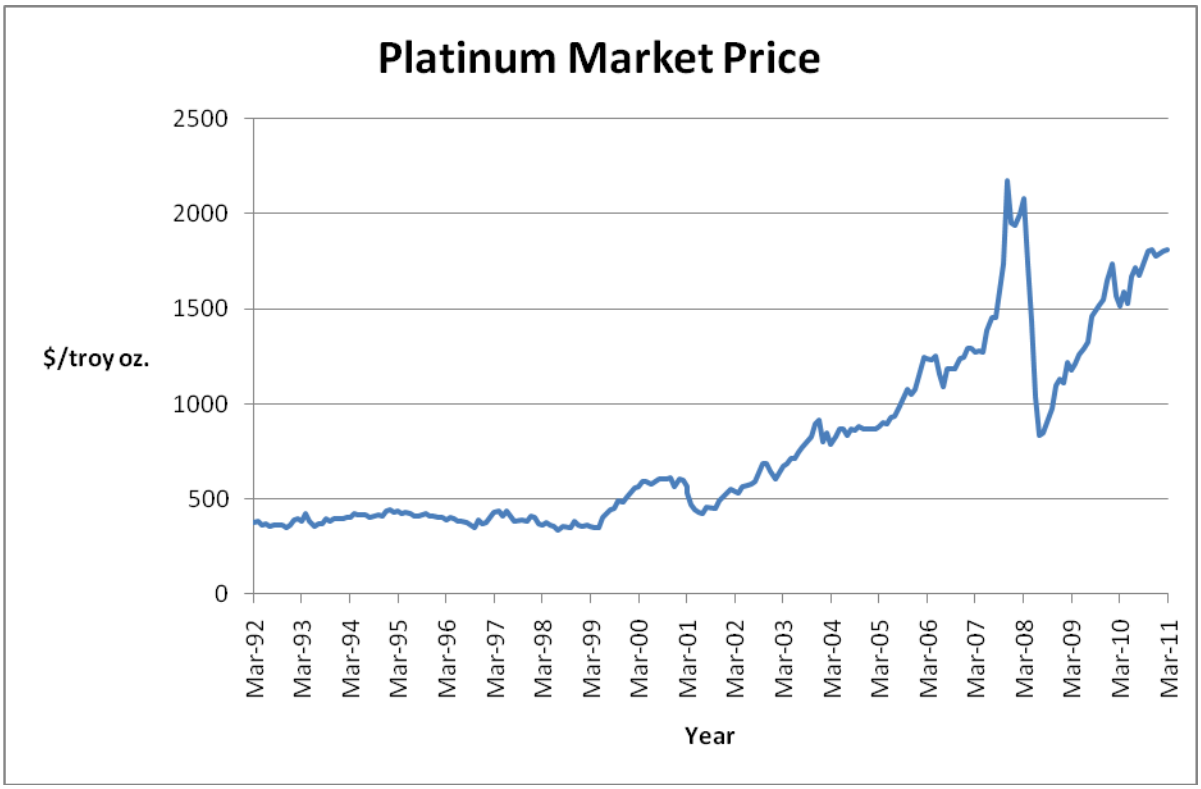

Figure 2-8. Platinum Market Price History

A famous study by Bregoli showed that reducing the particle size of platinum crystals below 2 nm would not lead to an increase in catalyst activity.[17] The results of the Bregoli study led researchers to direct attention to the careful control of spacing between adjacent platinum atoms as a means of increasing catalyst activity, particularly in the cathode. These efforts produced the third generation of catalysts which entail alloying platinum with one or two other metals on a carbon black support. For instance, Luczak and Landsman describe a process for alloying platinum with chromium and cobalt, producing a particularly active and stable catalyst.[18] In addition to controlling the space between adjacent platinum atoms, alloying attempts have been motivated by the need to control platinum surface area loss. Over the course of a fuel cell's life, mean platinum crystal particle size increases and catalyst surface area is lost as platinum from different crystals unite to form larger crystals. Also complicating catalyst utilization is the phenomenon of anion absorption whereby phosphate anions slow the reaction kinetics of oxygen reduction in the cathode. Relatively large catalyst loadings are required in state of the art PAFC to mitigate the effects of platinum surface area loss and anion absorption. For instance, in the present study, catalyst loadings are assumed to be 0.25 mg Pt/cm^2 for the anode and 0.50 mg Pt/cm^2 for the cathode (0.75 mg Pt/cm^2 total per cell) as indicated in Figure 2-3. By comparison, platinum loadings for PEM fuel cells are on the order of 0.15 mg/cm^2. Clearly, reducing platinum surface area loss and anion absorption are important R&D needs which have the potential to significantly lower costs by allowing electrodes to be manufactured with reduced platinum loadings.

For modeling purposes, the anode catalyst is assumed to be 10 wt% Pt on Vulcan XC72 and the

cathode catalyst is assumed to be 10 wt% Pt alloyed with cobalt and chromium on graphitized XC72. Graphitization of the cathode catalyst support improves its corrosion resistance but at a cost of reduced surface area for platinum attachment. Consequently, the platinum areal loading for the cathode must be higher as compensation for reduced catalyst surface area. In this model, the cost of platinum catalyst is disaggregated into two components: the platinum direct material cost and a "processing cost" which encompasses all other costs such as manufacturing, carbon black, alloying metals, profit, and overhead. The market price of platinum is a particularly stochastic input to the cost model as already demonstrated in Figure 2-8. As such, the model randomly samples from a theoretical distribution fitted to the most recent 5 year history of the market price of platinum. This randomly selected market price is added to the processing cost to generate a total cost for carbon supported catalyst. The processing cost itself is a function of the assumed fuel cell manufacturer's yearly production volume and was developed through consultation with an industry partner.[19] Discounts from suppliers are expected to be realized with the larger orders that would be placed as production volume increases from 5 to 500 MWe/yr.

2.5 SUBSTRATE MANUFACTURING

As is the case for carbon supported catalysts, carbon paper substrates have been modeled as direct materials purchased from a supplier by the fuel cell manufacturer due to wide commercial availability from multiple suppliers. Substrates have evolved from woven mesh tantalum screens in the 1960s to today's carbon paper substrates. Miwa's procedure [20] for making the carbon paper substrates used in the PC-25^{TM} is summarized below:

1. Chop polyacrylonitrile (PAN) fiber bundles into fibers having lengths on the range of 3 to 20 mm and diameters on the range of 4 to 9 μm
2. Disperse the chopped fibers in water or methanol
3. Add a temporary binder such as polyvinyl alcohol, hydroxyethyl cellulose, etc.
4. Remove the dispersant by drying to create a carbon fiber mat mechanically bound by the temporary binder
5. Dissolve both a self-curable resin and a non-self-curable resin in water, methanol, or other solvent
6. Impregnate the carbon fiber mat obtained in step 4 with the solvated resin obtained in step 5 by dipping the mat into the resin solution or spraying the resin solution onto the mat to create a prepreg
7. Hot press one or more prepreg layers to obtain a cured substrate of the desired thickness
8. Carbonize substrates in an inert environment at 750-1000^{0}C to convert resin to carbon and to dissipate the temporary binder

9. Graphitize substrates in an inert environment at 2000-3000^{0}C to convert carbon to graphite

A 2010 patent owned by Breault shows that improving the substrate manufacturing process remains an active research and development interest.[21] Here, Breault indicates that a substrate may be obtained by eliminating the impregnation step (step 6 above). By substituting uncured, chopped, cross-linkable resin fibers for the solvated resin described in the Miwa example, the impregnation step, which represents 16% of the total cost of a substrate, can be eliminated. For modeling purposes, low volume and high volume quotes from multiple vendors were obtained for graphitized carbon paper having thicknesses and porosities suitable for PAFC substrates. These substrates are assumed to be manufactured in a process similar to Miwa.[20]

2.6 ELECTRODE MANUFACTURING

Methods developed in the late 1970s and early 1980s [22,23,24] for depositing carbon supported catalyst onto carbon paper substrates are still in use today by UTC and its suppliers.[25] These processing techniques have been modeled in the present study and appear diagrammatically in Figure 2-9.

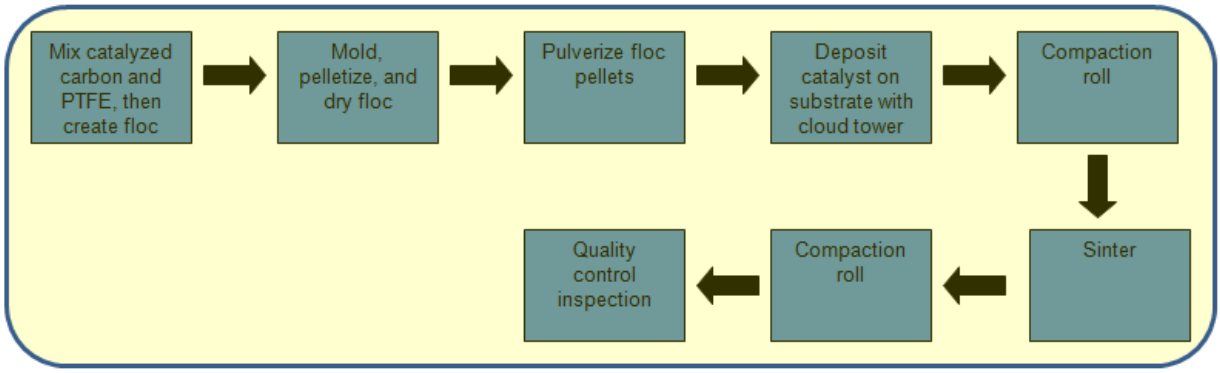

Figure 2-9. PAFC Electrode Manufacturing Process Steps

An aqueous co-suspension of carbon supported catalyst and PTFE particles is prepared in a vat with mixing capabilties and caused to floc by heating to 135^{0}F. The heat source is removed and the vat contents are cooled to room temperature. A small amount of phosphoric acid is added to prevent an undesirable reaction in a subsequent step. However, the phosphoric acid treatment has its own undesirable side effect in that it causes dried floc to absorb water from the atmosphere, complicating handling and accurate weighing. To respond to this challenge, floc is molded into pellets during the drying process. Pelletizing the floc greatly improves its resistance to water absoprtion from the atmoshpere. Pelletizing is performed by pouring the vat contents into a honeycomb shaped mold where water is extracted by vacuum filtration while floc particles are retained in the mold. A substrate beneath the mold allows the transmittance of water out of the mold while floc is retained. The honeycomb mold and substrate are transferred to an oven where the floc is dried into pellets having the shape of the honeycomb mold. After drying, the pellets are separated from the mold and either stored or used immediately in the following steps.

For electrode manufacturing, catalyst pellets are introduced into a hopper having a scale which automatically weighs the proper amount of catalyst necessary for deposition onto a single electrode. The catalyst pellets are conveyed from the scale to a micropulverizer which grinds the pellets into a high surface area, low particle size cloud of catalyst. A carbon paper substrate is positioned beneath a bottomless, pyramid-shaped chamber with the substrate essentially forming the base of the pyramid. The substrate and chamber are pressed against each other so as to form a seal. The catalyst cloud is introduced into the chamber and a turbine beneath the substrate creates a low pressure environment that pulls the catalyst cloud toward the substrate. Air passes through the substrate while catalyst particles are retained on the surface forming a uniform layer on top of the substrate. The cloud tower principle is depicted in Figure 2-10.

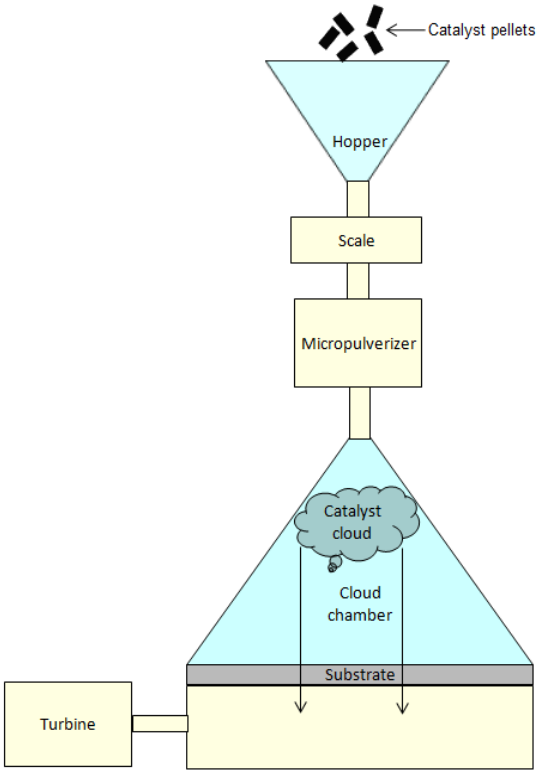

Figure 2-10. Cloud Tower

After the catalyst layer has been deposited by the cloud tower, a substrate is conveyed to a low temperature drying oven to remove moisture absorbed from the atmoshpere by the phosphoric acid added to the catalyst in the floccing stage. Immediately after drying, substrates are conveyed to a compaction roller to lightly press the catalyst layer onto the substrate. The preceeding drying step prevents moist catalyst from adhering to the rollers. Substrates then enter a two stage continuous sintering oven with an assumed 8 minute residence time. The first stage, assumed to occur at 290^0C, removes a wetting agent present in the PTFE suspension used in the floccing stage. The second stage, assumed to occur at 337^0C, forces the PTFE present in the catalyst to slighly exceed its glass transition temperature. Upon cooling, the PTFE resolidifies, binding the catalyst layer to the substrate. Electrodes exiting the sintering oven pass through a second compaction roll before before undergoing a quality control inspection that examines electrodes for substrate and catalyst layer thicknesses as well as the areal loading of platinum.

2.7 EDGE SEAL AND MATRIX PRINT

Edge seals must be incorporated into electrodes to prevent oxidant from entering the anode and fuel from entering the cathode as demonstrated previously in Figure 2-2. In PAFC, the liquid electrolyte provides a convenient mechanism for edge sealing called a wet seal. When the mean pore size in an electrode's edge is controlled to be sufficiently small, the edges become wettable to phosphoric acid. Capillary forces draw phosphoric acid into the small pores of the edge seal region where the acid is retained, creating a liquid barrier which blocks the flow of the unwanted reactant stream. In designs using relatively thick substrates or thick, ribbed, electrolyte reservoir plates, low porosity edge seals have been made using densified edge seals and integral edge seals. Densified edge seals entail adding extra carbon fiber to the edges of substrates in the initial carbon paper manufacturing process.[26] When a substrate such as this is pressed and cured, its two sealing edges are more dense and thus of a lower porosity than the remaining portions of the substrate. The lower porosity draws phosphoric acid into the edge seal by capillary forces. Integral edge seals are formed by inserting extra layers of material into the edges of electrolyte reservoir plates that are formed not as a single piece but by a lamination process.[27] As with the densified edge seal concept, this results in more material being present in edges which in turn results in a lower porosity and higher propensity to retain acid. When substrates are sufficiently thin (less than about 0.35 mm) such as the ones modeled in present study, edge seals may be created by a screen printing process. Carbon paper substrates are manufactured with identically distributed porosity over the entire substrate. Porosity in the edge seals, however, is reduced by screen printing an ink containing matrix material into the two substrate edges where an edge seal is desired.

In the 1970s, Breault showed that silicon carbide (SiC) is particularly stable in a hot phosphoric acid environment and very suitable as an electrolyte retaining matrix material when mixed with a small amount of PTFE as a binder.[28] Matrix layers have been applied to electrodes in a variety of ways including spraying, screen printing, and Gravure printing. Gravure printing has proven to be the most satisfactory and is described by Spearin.[29] The Gravure printing process begins with preparing an ink consisting of SiC, ammonium hydroxide, deionized water as a solvent, polyethylene oxide as a thickener, and PTFE as a binder. Depressions of a controlled size, shape, depth, and pattern are created in a roller by etching or engraving. These depressions receive and hold a precisely controlled volume of ink from an ink bath. The roller contacts an electrode that is passed under the roller and ink is transferred from the roller depressions to the electrode surface. Electrodes are heated to evaporate the solvent and to soften the PTFE binder such that upon cooling and resolidification of the binder, the matrix layer is secured to the electrode. Applying a matrix layer to both anodes and cathodes is a method for controlling printing errors as any potential flaws in the matrix print on one electrode are unlikely to align with another flaw in the opposing electrode with which it is mated.

The preceding inputs were used to develop the edge seal and matrix manufacturing model whose process steps are depicted below in Figure 2-11.

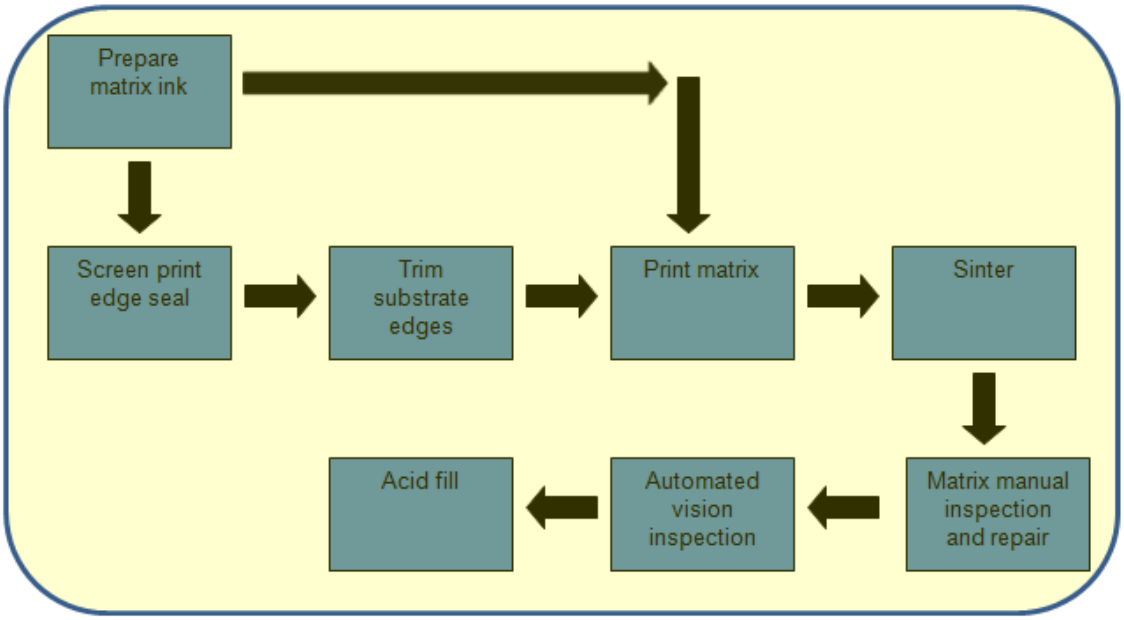

Figure 2-11. PAFC Edge Seal and Matrix Manufacturing Steps

Electrodes passing the quality control inspection step in electrode manufacturing are inputted to the edge seal screen printing step. Matrix ink preparation precedes edge seal screen printing and matrix printing. It is assumed for modeling purposes that the ink for matrix printing as described by Spearin is similar to the ink used in edge seal screen printing which can be prepared by ball milling. Because graphitized carbon paper substrates are inherently brittle and fragile, UTC minimizes human touches throughout the electrode manufacturing process by using high levels of automation.[5] Substrates are especially susceptible to damage along their edges. As such, it assumed that electrode edges are trimmed after edge sealing as shown below for an anode in Figure 2-12

.

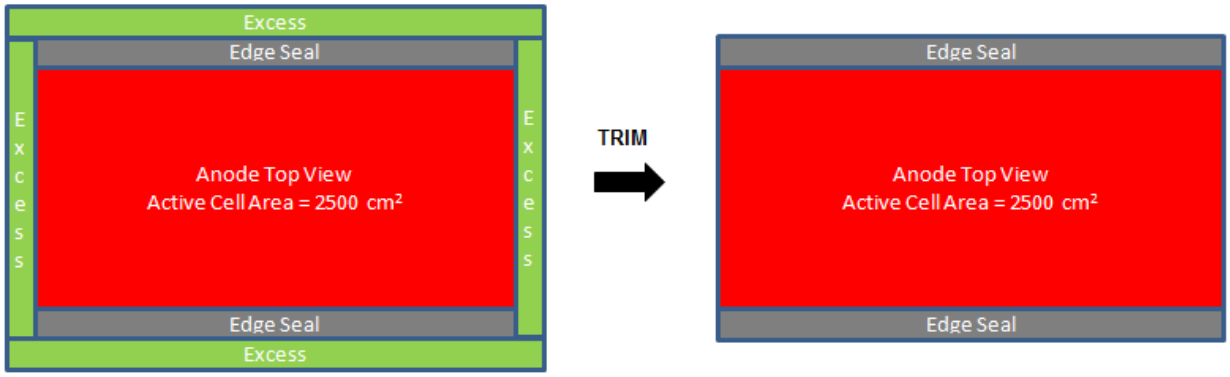

Figure 2-12. PAFC Electrode Edge Sealing and Trimming

After trimming, both anodes and cathodes have a matrix layer printed onto their catalyst layers by Gravure roll printers such that when the matrix layers are dry and anode and cathode are mated, the total thickness of the matrix layer is 0.05 mm. Electrodes with freshly printed matrix

layers enter a continuous sintering furnace and are subjected to an assumed 8 minute heat treatment at 325-350^{0}C to dry the matrix ink and secure the PTFE binder in the matrix to the electrode. Electrodes exiting the furnace are allowed to naturally cool before a manual inspection and repair step. In this step, a worker visually examines electrodes for defects in the matrix print and repairs them by applying matrix ink over the flaw with a brush. Manually inspected and repaired electrodes are next passed to an automated vision machine where matrix layers are once again examined for defects. Electrodes failing the automated vision inspection are rejected. Electrodes passing the automated vision inspection are dipped in a dilute (85%) acid bath to load the matrix, edge seals, and substrates with the appropriate quantity of phosphoric acid. In the fuel cell, the phosphoric acid is reconcentrated to 100% by driving off water with the heat of the fuel cell reaction. The concentrated phosphoric acid (which would be solid at room temperature) remains liquefied at the fuel cell's operating temperature.

2.8 SEPARATOR PLATE MANUFACTURING

A collection of stringent and varied functional requirements have complicated the development of reliable, low cost separator plates. Separator plates must simultaneously be:

- impermeable to reactant and product gas transfer between cells
- impermeable to acid transfer between cells
- nonporous so as not to absorb acid from the cell
- excellent heat conductors
- excellent electrical conductors
- resistant to corrosion in reducing environments
- resistant to corrosion in oxidizing environments
- mechanically strong to provide structural support to cells
- coefficient of thermal expansion (CTE) matched with other cell components
- relatively inexpensive

Graphite has been found to be the material that best meets the above requirements. Separator plates have traditionally been created by molding graphite particles with resin binder. Emanuelson et al. describe a procedure for making a molded separator plate using 50 wt% 0.5µm spheroidal graphite particles mixed with 50 wt% thermosetting carbonizable resin binder.[9] The Emanuelson procedure is represented diagrammatically in Figure 2-13 below.

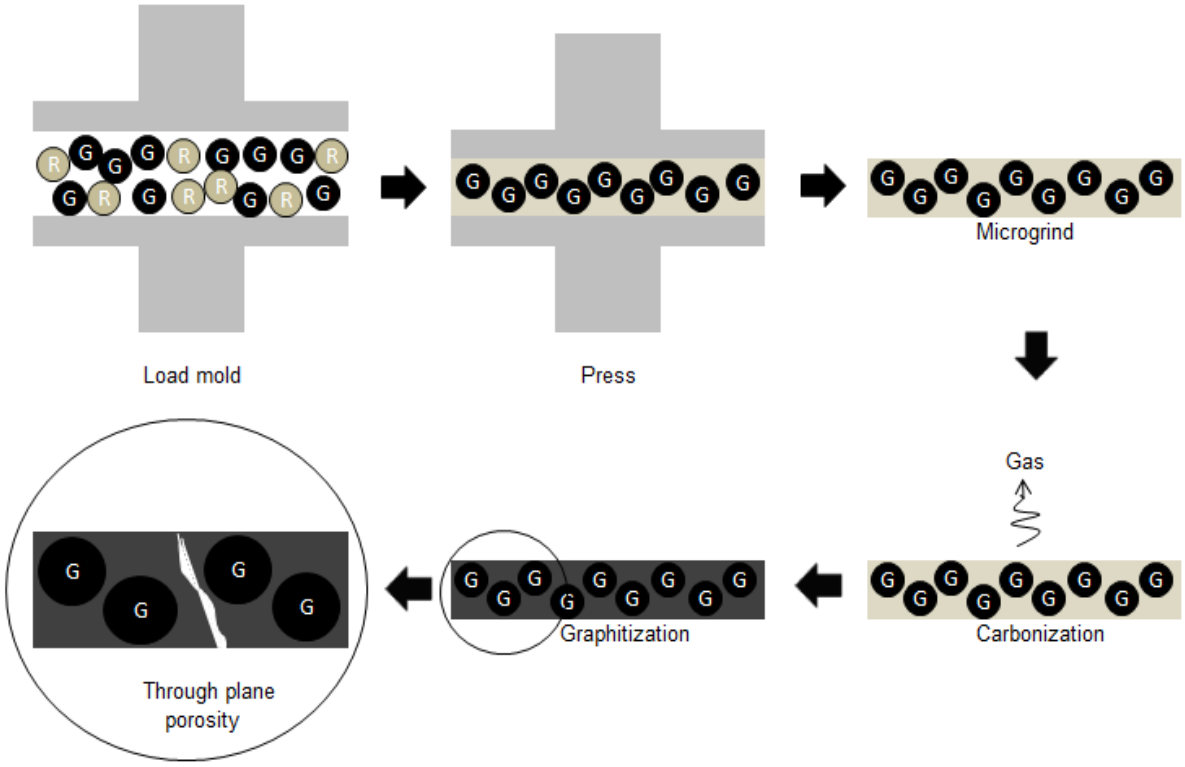

Figure 2-13. Manufacturing Steps for PAFC Separator Plate Comprised of Graphite Particles and a Resin Binder

The graphite/resin mixture is placed in a mold and hot pressed to partially cure the resin. Next, plates are microground to a predetermined thickness with variation less than +/- 0.001 inch. Plates are then subjected to a carbonization heat treatment during which the resin is converted to carbon. About half of the resin mass is converted to carbon while the other half is volatilized and outgassed from the separator plate. A slow carbonization process is required so that disruptive outgassing does not occur, which would result in open pores, blisters, and cracks in the separator plates. Emanuelson indicates a programmed temperature rise in an inert environment such as nitrogen or vacuum from ambient to 1000^0C over the course of 80 to 160 hours. A graphitization treatment in an inert environment lasting 48 hours and reaching 2800^0C follows carbonization to convert the carbon remaining from the resin binder into graphite. A completely graphitized separator plate has strong corrosion resistance in a hot phosphoric acid environment. However, despite careful control of the carbonization process, some through-plane porosity (shown as the last step in Figure 2-14) still develops in separator plates manufactured according to this procedure, creating avenues for acid and/or gas communication between cells which inevitably leads to stack failure.

Dettling and Terry showed that separator plate permeability could be reduced by hot pressing together two separator plates into one composite separator plate assembly having a layer of thermoplastic film such as fluorinated ethylene-propylene (FEP) or polyethersulphone (PES) sandwiched between the plates.[10] The pressing action causes the film material to flow into and thereby seal the pores of the two adjacent separator plates, bonding them into one composite

separator plate assembly.

More recently, Grasso et al. describe separator plates created by laminating together several layers of carbon fiber felt that have been impregnated with a matrix consisting of graphite particles and phenolic resin binder.[11] The Grasso procedure has been incorporated into this model and the manufacturing steps are presented below in Figure 2-14.

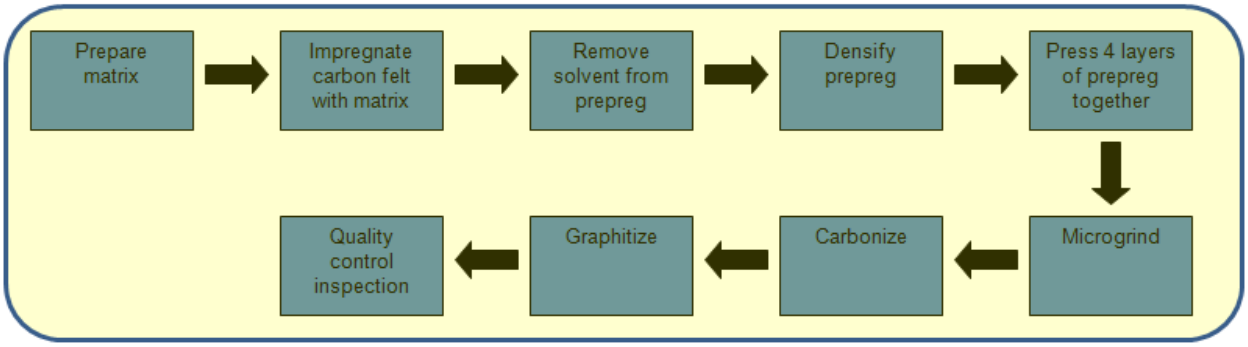

Figure 2-14. Manufacturing Steps for PAFC Separator Plate Comprised of Carbon Fiber Felt, Graphite Particles and a Resin Binder

A matrix for impregnating carbon felt is prepared by mixing graphite particles, phenolic resin binder, and methanol as a solvent in a high energy mixer. Carbon fiber felt is then impregnated with matrix by dipping the felt in a bath of matrix. Next, the prepreg is oven dried to remove the methanol solvent. A dried prepreg layer is then densified by hot pressing (but not curing) to expel trapped gases and close voids. A composite separator plate is formed by hot pressing together four prepreg layers to cure the resin binder such the prepreg layers bond with one another. The lamination of multiple prepreg layers into one composite separator plate is useful for minimizing through plane porosity as defects in one layer are not likely to align with defects in the other layers. After curing, the composite separator plates are assumed to be microground, carbonized, and graphitized in a manner similar to that as described for Emanuelson. A quality control inspection follows graphitization to examine plates for permeability.

2.9 BIPOLAR PLATE MANUFACTURING

The term bipolar plate in this report strictly refers to a separator plate and its associated anode and cathode flow fields. Flow fields may be incorporated into separator plates in several ways and have varying characteristics. Flow fields may be porous or nonporous, hydrophilic or hydrophobic, etc. Some designs use flow fields that are machined directly into the separator plate itself. Other designs use preformed separator plates to which additional material is added that becomes the flow fields. For example, Breault et al. describe a bipolar plate manufacturing procedure in US Patent 5,558,955 that begins with a preformed, graphitized separator plate to which a preformed ERP is added by hot pressing to serve as both the anode flow field and an electrolyte reservoir.[8] In this same hot pressing step, additional material is bonded to the other side of the preformed separator plate which subsequently has flow field channels machined into it to become the cathode flow field. A layer of FEP film is placed between the separator plate

and ERP which binds them together upon pressing. Another layer of FEP film is placed between the separator plate and the cathode flow field material which likewise binds the separator plate and cathode flow field material together upon pressing. Pressing both the ERP and the cathode flow field material to the separator plate in one step helps reduce costs. In their 2010 patent, Breault and Fredley indicate that the procedures indicated in US Patent 5,558,955 with regards to cathode flow field manufacturing are also preferred for anode flow field manufacturing for a fuel cell system having long life characteristics.[2] As such, the bipolar plate manufacturing model assumed in this study is one where separator plates are first manufactured according to the model described in the preceding section. Additional material is bonded to the separator plates for both cathode and anode flow fields as is described in US Patent 5,558,955 for cathode flow fields alone. Flow field channels are machined into the added material. The bipolar plate manufacturing process model assumed in this study is depicted in Figure 2-15.

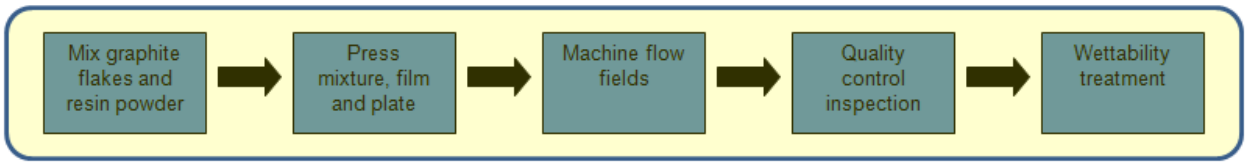

Figure 2-15. PAFC Bipolar Plate Manufacturing Steps

Graphite particles specifically having a flat, flake-like shape are mixed with resin powder. A layer of this graphite/resin mixture is placed in the bottom of a mold. Next, a sheet of FEP film is placed on top of the layer of mixture, followed by a separator plate on top of the FEP film. Another layer of FEP film is placed on top of the separator plate followed once more by a layer of graphite/resin mixture. The molding process is depicted in Figure 2-16.

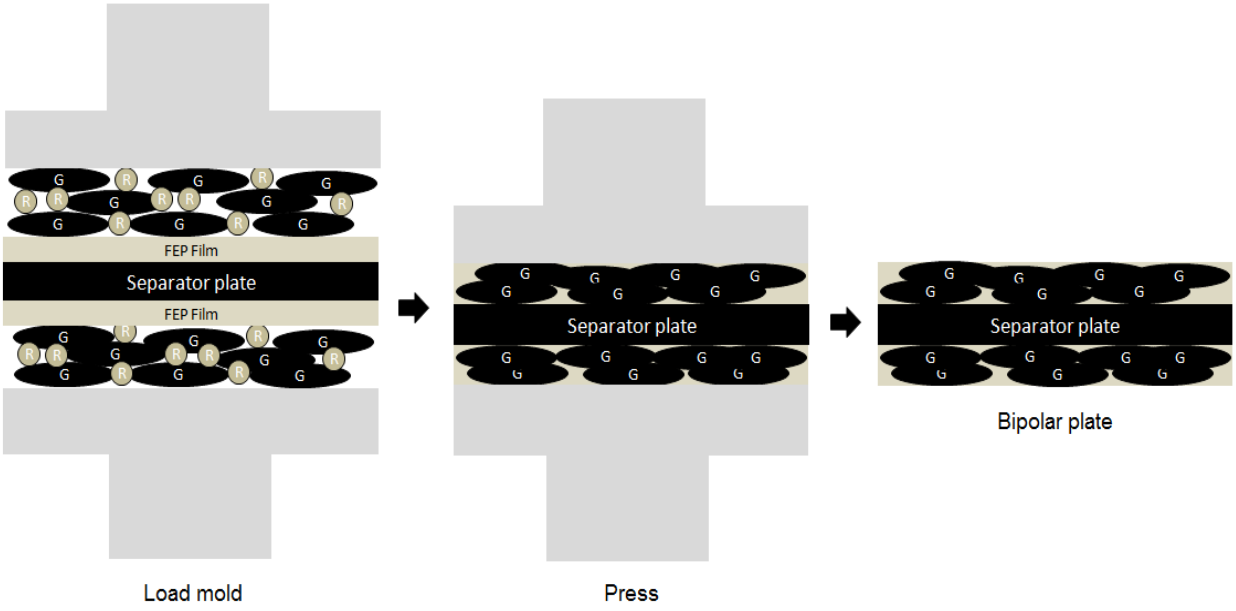

Figure 2-16. PAFC Bipolar Plate Molding Process

Hot pressing produces a cured bipolar plate which subsequently has channels machined into the flow field layers. A quality control inspection after machining is assumed to check that the dimensions of the flow field channels are within tolerance. Flow field channels are assumed to be sprayed with a suspension of XC-72 in methanol to make channels wettable and hence able to wick condensed phosphoric acid back to the cell as described in US Patent 5,558,955.[8]

2.10 COOLANT PLATE ASSEMBLY MANUFACTURING

A water/steam conducting coolant plate is assumed to be included in the stack for every eight cells as demonstrated previously in Figure 2-5. Breault et al. describe the characteristics of a coolant plate assembly in US Patent 6,050,331.[30] A highly engineered component, a coolant plate has in its center a serpentine stainless steel tube which is encapsulated in a graphite housing. The graphite housing is itself sandwiched between two separator plates with each separator plate having an attached flow field. The CTE of the graphite housing is relatively high in its center in order to accommodate the thermal stresses imposed by the expansion and contraction of the serpentine stainless steel cooling tube which it contains. The CTE transitions to a relatively lower value near the surfaces adjacent to the separator plate/flow field assemblies. The cooling plate manufacturing process model assumed in this study is shown below in Figure 2-17.

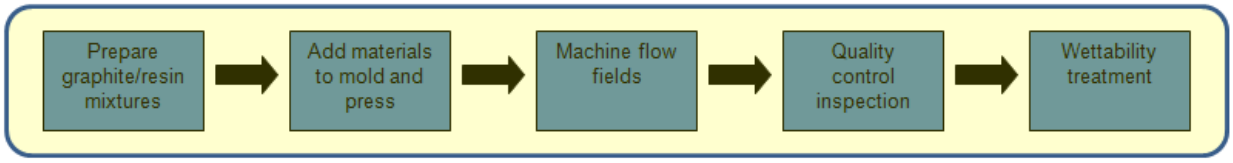

Figure 2-17. PAFC Coolant Plate Assembly Manufacturing Steps

Three different types of graphite/resin mixtures are prepared: one for the two flow fields, one for the two low CTE zones of the graphite housing, and one for the high CTE zone of the graphite housing. These mixtures, along with resin films, preformed graphitized separator plates, and stainless steel coolant tubing are placed into a mold in the order indicated in Figure 2-18 and hot pressed to form a cured coolant plate assembly.

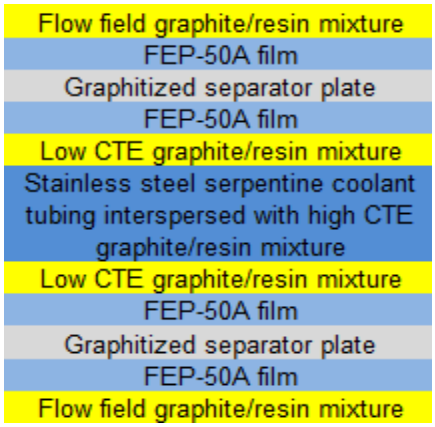

Figure 2-18. PAFC Coolant Plate Assembly Molding Process

Flow field channels are machined into the flow field layers after which cooling units undergo quality control inspection. A wettability treatment is assumed to be applied to the flow field channels as was described for bipolar plates.

2.11 SUBSTACK, STACK, AND SYSTEM ASSEMBLY

The remainder of the manufacturing process is according to Figure 2-6 beginning with the "substacks and stacks" block. A substack consisting of a cooling unit and eight cells interspersed with seven bipolar plates (described previously in Figure 2-4) is assembled by robotic pick and place equipment. Automated assembly ensures accurate alignment of parts and minimizes human touches of fragile components. Completely assembled substacks have sufficient mechanical strength for human touches and therefore can be manually integrated with end plates and tie rods into stacks. Coolant manifolding and electrical harnessing are followed by hydro and dielectric tests which in turn precedes reactant manifolding. After reactant manifolding, stacks are first insulated and then operated in a conditioning and testing step. Next, stacks are integrated with BOP components and the completed system is tested to ensure functionality. Finally, an enclosure is placed over the system and the system is loaded onto a truck for shipping.

2.12 MODEL RESULTS

Annual production volumes of 5, 20, 50, and 500 MWe/yr are shown in Figure 2-19 to have total manufacturing costs of $3821, $3049, $2838, and $2724/kWe, respectively.

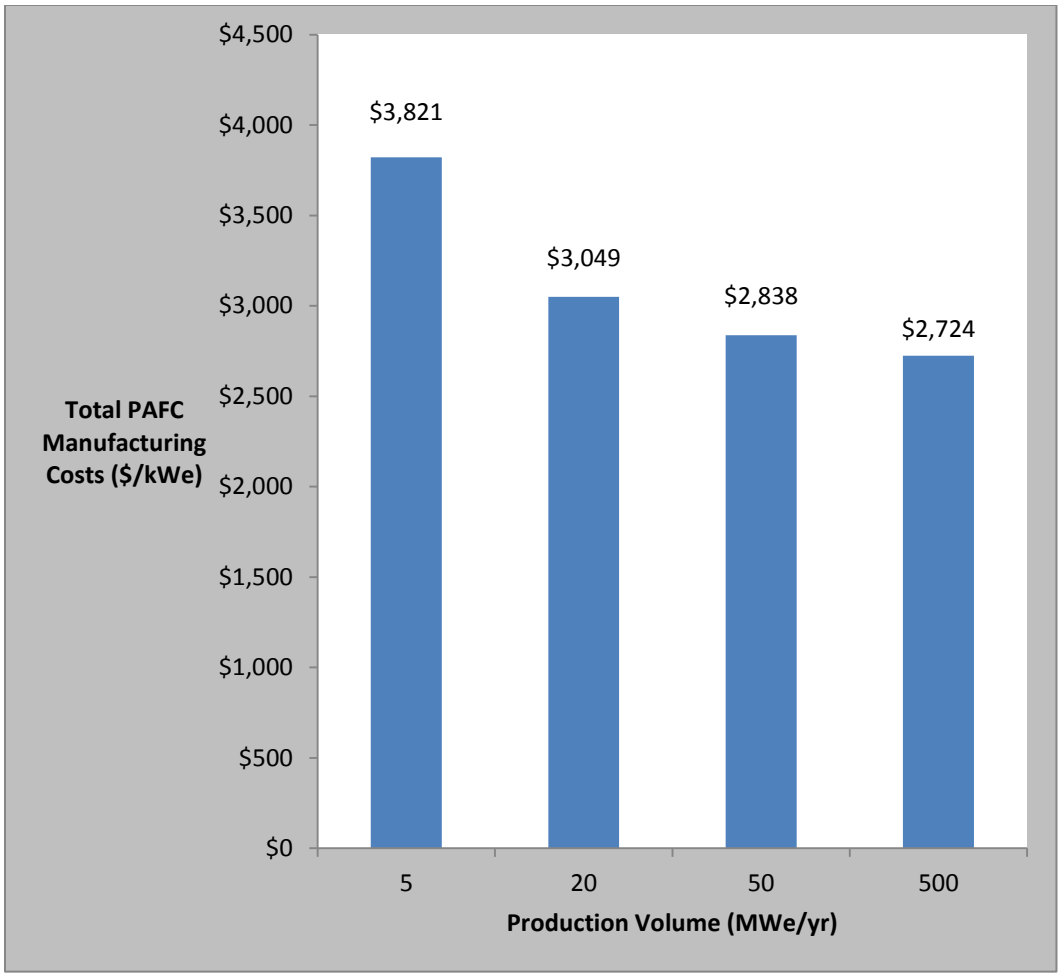

Figure 2-19. Total PAFC Manufacturing Costs for Varying Production Volumes

As can be inferred from the behavior of Figure 2-20, the manufacturing cost curve exhibits a hyperbolic pattern, becoming essentially horizontal for production volumes exceeding several hundred MWe/yr after which a limiting cost of approximately $2725/kWe is attained. The baseline production volume of 20 MWe/yr (roughly equivalent to UTC's current demand) is estimated to have a manufacturing cost of $3049/kWe as stated previously. This represents a 20% reduction from the low volume scenario of 5 MWe/yr, where manufacturing costs are estimated to be $3821/kWe. An 11% reduction in cost appears achievable just by increasing production volume from 20 to 500 MWe/yr, even if manufacturing technology is assumed unchanged (i.e. production lines are replicated in parallel) and no learning curve is experienced. As production volume increases from 5 to 500 MWe/yr, cost reductions accrue from:

- reduced contribution of fixed costs (capital and floor space) to total system cost on a per unit basis.
- reduced indirect labor requirement (modeled as a decreasing percentage of direct labor as production volume increases).
- volume discounts on materials and components purchased from suppliers (developed in consultation with suppliers and with economy of scale factors).

In order to highlight how costs are distributed and where they are concentrated, total manufacturing costs were disaggregated into seven cost components - labor, energy, floor space, capital, cell materials, stack materials and components, and BOP components and subsystems. Definitions and assumptions pertaining to labor, energy, floor space, and capital costs are detailed in section 1.2. The remaining three cost components – cell materials, stack components and materials, and BOP components and subsystems - represent those items which are purchased from suppliers by the PAFC manufacturer. Utilizing capital, floor space, energy, and labor resources, the PAFC developer manufactures and assembles these purchased items into a fuel cell system. Figure 2-20, below, is an elaboration of Figure 2-19 in that total cost has now been disaggregated into the seven cost components mentioned above.

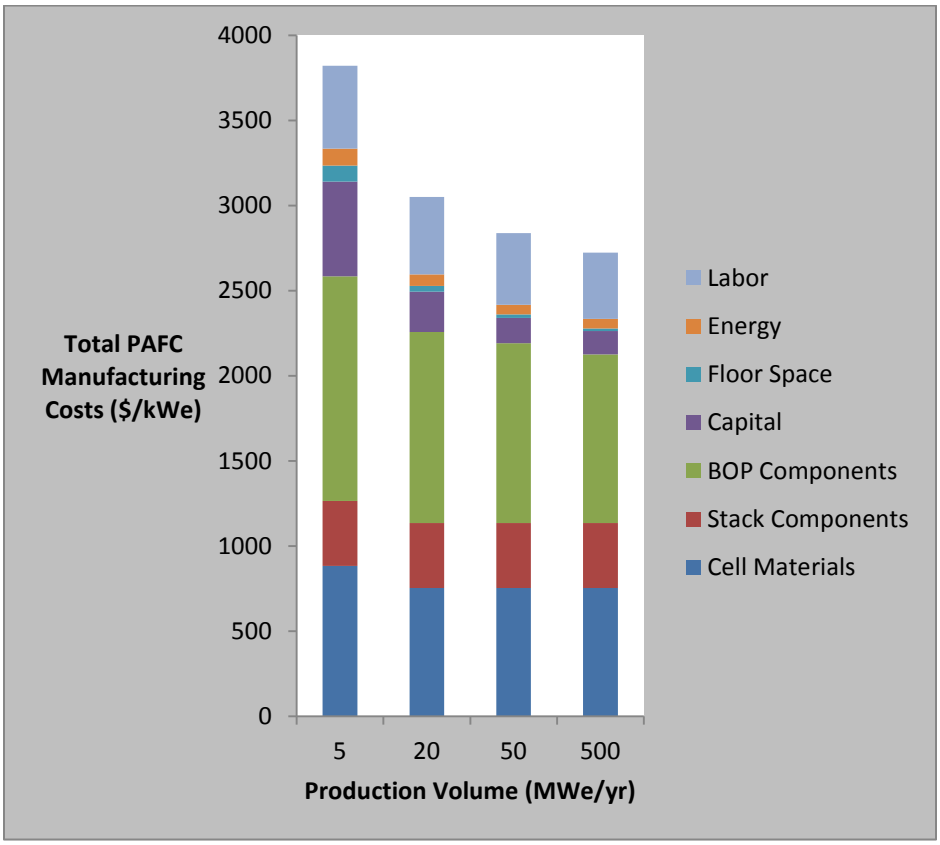

Figure 2-20. Total PAFC Manufacturing Costs and Cost Components for Varying Production Volumes

It may be readily observed in Figure 2-20 that items purchased from suppliers (cell materials, stack materials and components, and BOP components and subsystems) collectively comprise the largest manufacturing costs incurred by the PAFC manufacturer. Figure 2-21, below, shows that purchased materials and components, when taken in aggregate, are estimated to constitute 67% to 78% of total manufacturing cost. The fixed costs of capital and floor space are noted to decrease from 17% to 6% with increasing production volume, while labor and energy costs remain more or less constant at approximately 2% and 14%, respectively.

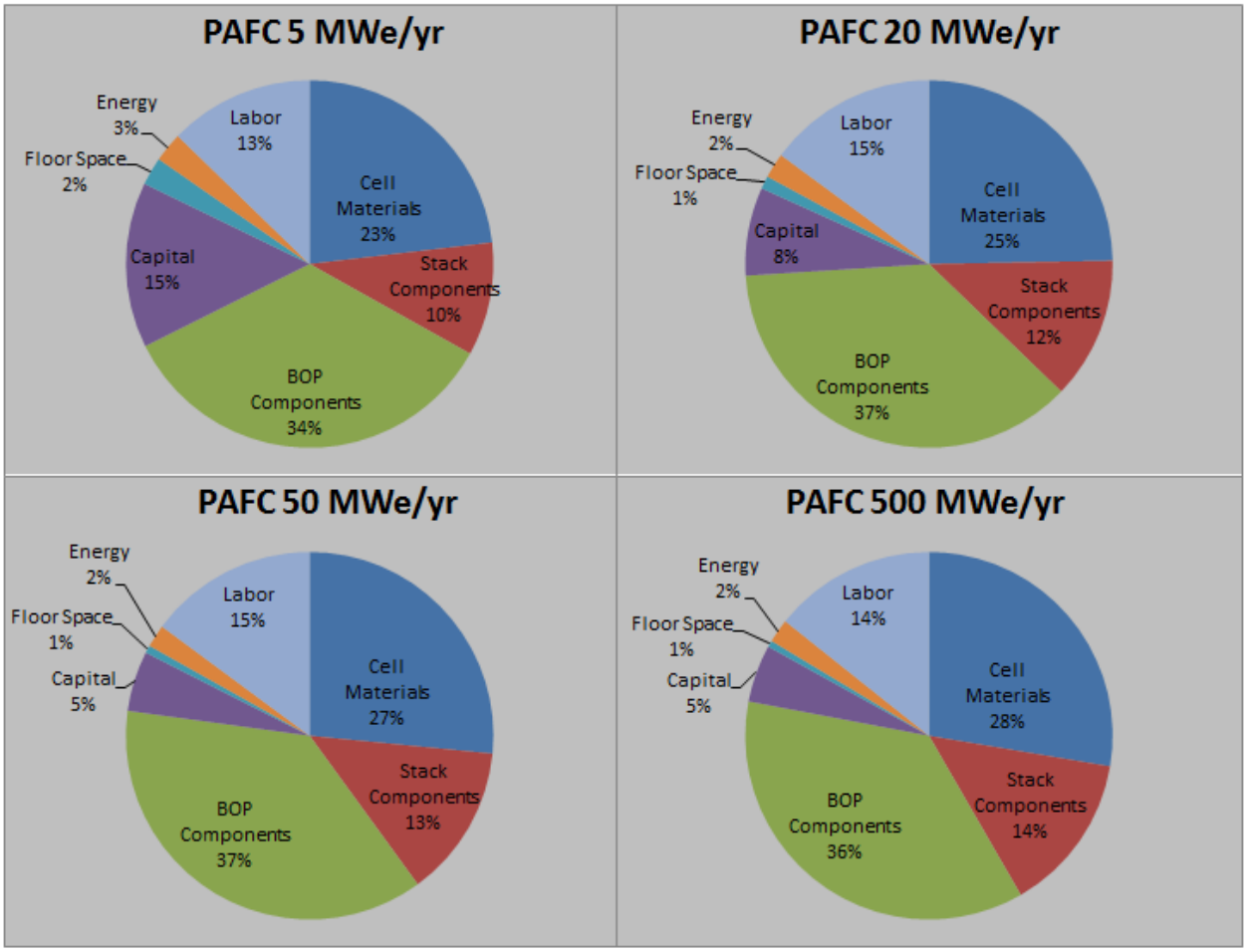

Figure 2-21. Total PAFC Manufacturing Cost Distribution for Varying Production Volumes

Because materials and components purchased from suppliers are estimated to constitute approximately three-fourths of total manufacturing costs, these cost components are examined in further detail in the following paragraphs. Major purchased items are listed in Table 2-2, and categorized as either cell, stack, or BOP.

Table 2-2. Major PAFC Cell Materials, Stack Materials and Components, and BOP Components and Subsystems Purchased from Suppliers

PURCHASED MATERIALS, COMPONENTS, AND SUBSYSTEMS		
CELL	**STACK**	**BOP**
Pt-catalyzed carbon	Graphite	Desulfurizer
Fluoropolymer	Phenolic resin	Reformer
Carbon paper substrates	Carbon fiber felt	Integrated low temp shift converter
Silicon carbide	Methanol	Ammonia scrubber
Polyethylene oxide	Carbon black	Heat exchangers
Ammonium hydroxide	Fluoropolymer	Inverter and power conditioning
Phosphoric acid	SS serpentine cooling tube	Oxidant supply
	Coolant manifolds	Instruments and controls
	End plates	Structure and enclosure
	Tie rods	Piping, fittings, joints, valves, pumps
	Electrical harness/dielectric mounts	Wiring and busbars
	Reactant manifolds	Demineralizer
	Insulation	

Major cell materials identified in Table 2-2 include Pt-catalyzed carbon, which is bound to carbon paper substrates with a fluoropolymer. After the catalyst layer has been deposited, an ink consisting of silicon carbide, fluoropolymer, polyethylene oxide, and ammonium hydroxide is applied atop the catalyst layer and to the substrate perimeters to become matrix layers and edge seals, respectively. Carbon paper substrates which have received catalyst layers, edge seals, and matrix layers are then imbibed with phosphoric acid.

Major stack materials and components are also identified in Table 2-2. Materials used in separator plate, bipolar plate, and cooling unit manufacturing include graphite flakes and powders, phenolic resin, and fluoropolymer powders and films. Carbon fiber felt is a material specific to the type of separator plate modeled in the present study. Methanol is employed as both a solvent for the phenolic-based separator plate resin and as a dispersant for the carbon black wettability treatment applied to flow fields. Stainless steel serpentine cooling tubes and coolant manifolds are also major purchased items required for regulating stack temperatures. Top and bottom stack end plates, tie rods, electrical harnesses, dielectric mounts, reactant manifolds, and insulation are the remaining major purchased stack components listed in Table 2-2.

Lastly, major balance of plant components and subsystems purchased from suppliers are also identified in Table 2-2. The desulfurizer, reformer, integrated low temperature shift converter, and ammonia scrubber are the major fuel processing components. Heat exchangers are employed throughout the fuel cell system for fuel and air heating, stack temperature regulation, combined heat and power applications, and for condensing water vapor entrained in the cathode exhaust stream. Major electrical balance of plant subsystems include the inverter and power conditioning components, instruments and controls, and wiring and busbars. The remaining BOP components and subsystems identified in Figure 2-23 include oxidant supply; structure and enclosure; piping, fittings, joints, valves, and pumps; and the water demineralizer system.

Figure 2-22 is a Pareto chart showing the estimated costs of all purchased items listed in Table 2-2 for the baseline manufacturing volume of 20 MWe/yr. An item's bar color – blue, red, or green – indicates whether it is a cell material, stack component, or BOP component, respectively.

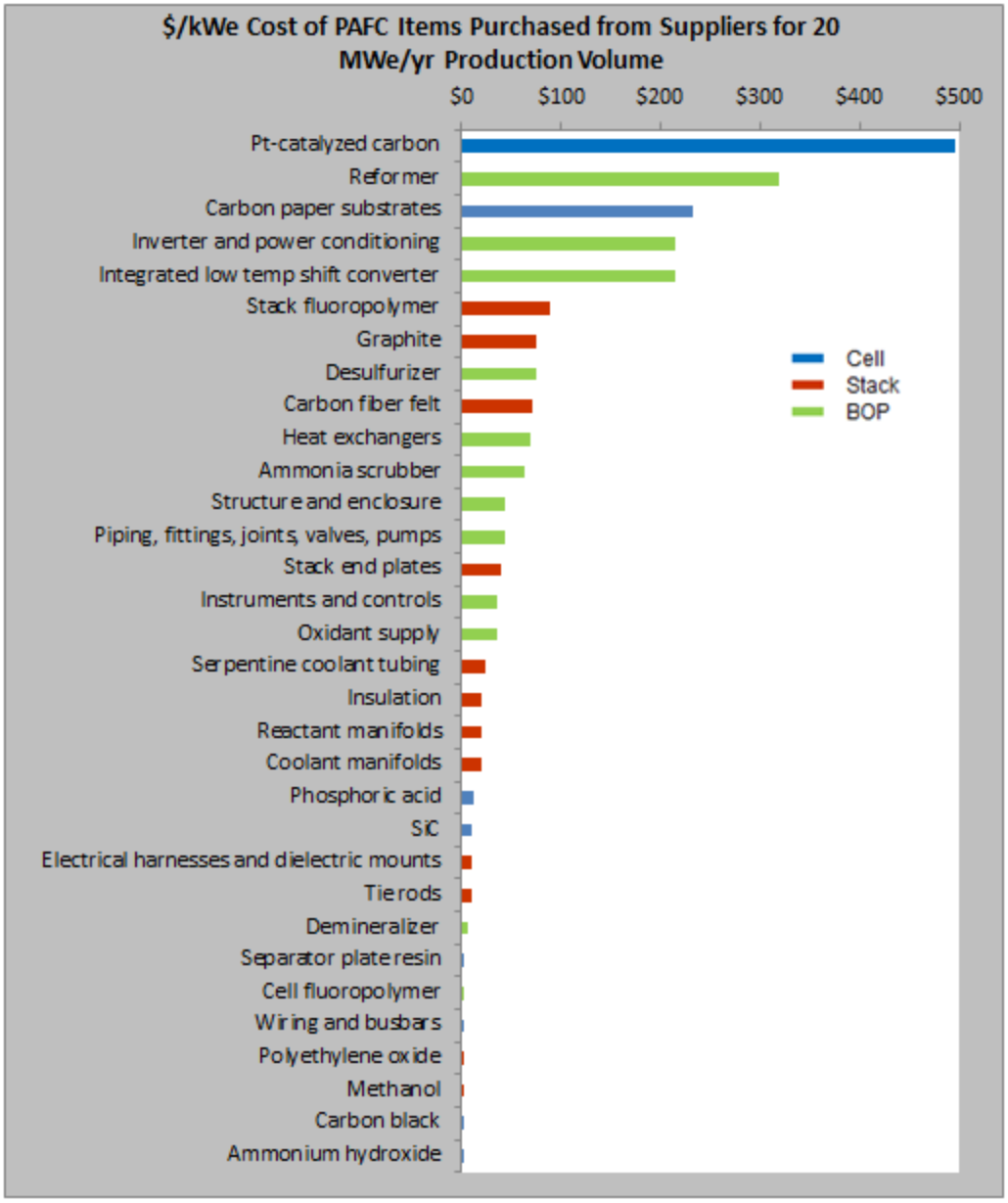

Figure 2-22. PAFC Pareto Chart of Cost of Items Purchased from Suppliers for 20 MWe/yr Production Volume

As indicated in Figure 2-22, Pt-catalyzed carbon and carbon paper substrates are two direct materials belonging to the cell category which have clearly significant cost impact. Three members of the BOP category - reformer, inverter and power conditioning, and integrated low temperature shift converter – complete the top five of highest cost purchased items. Fluoropolymer, graphite, and carbon fiber felt are significant stack costs. For the baseline production volume of 20 MWe/yr, total purchased item costs (i.e. exclusive of labor, capital, floor space, and energy) are estimated to be distributed as 33% cell, 17% stack, 50% BOP.

Figure 2-23 lists all manufacturing steps examined in this study, and the costs incurred at each step. Steps are grouped and classified according to component or task. For example, the electrode manufacturing process was described with sixteen steps beginning with catalyst flocculating and ending with the filling of electrodes with acid. These sixteen steps are grouped under the heading "Electrodes" in Figure 2-23. Steps are listed in a sequence which reflects the chronology of the actual manufacturing process, with first steps occurring at the top of the graph and final steps at the bottom. The relatively large contribution of items purchased from suppliers (cell materials, stack materials and components, and BOP components and subsystems) to total manufacturing cost is clearly reemphasized in this graph.

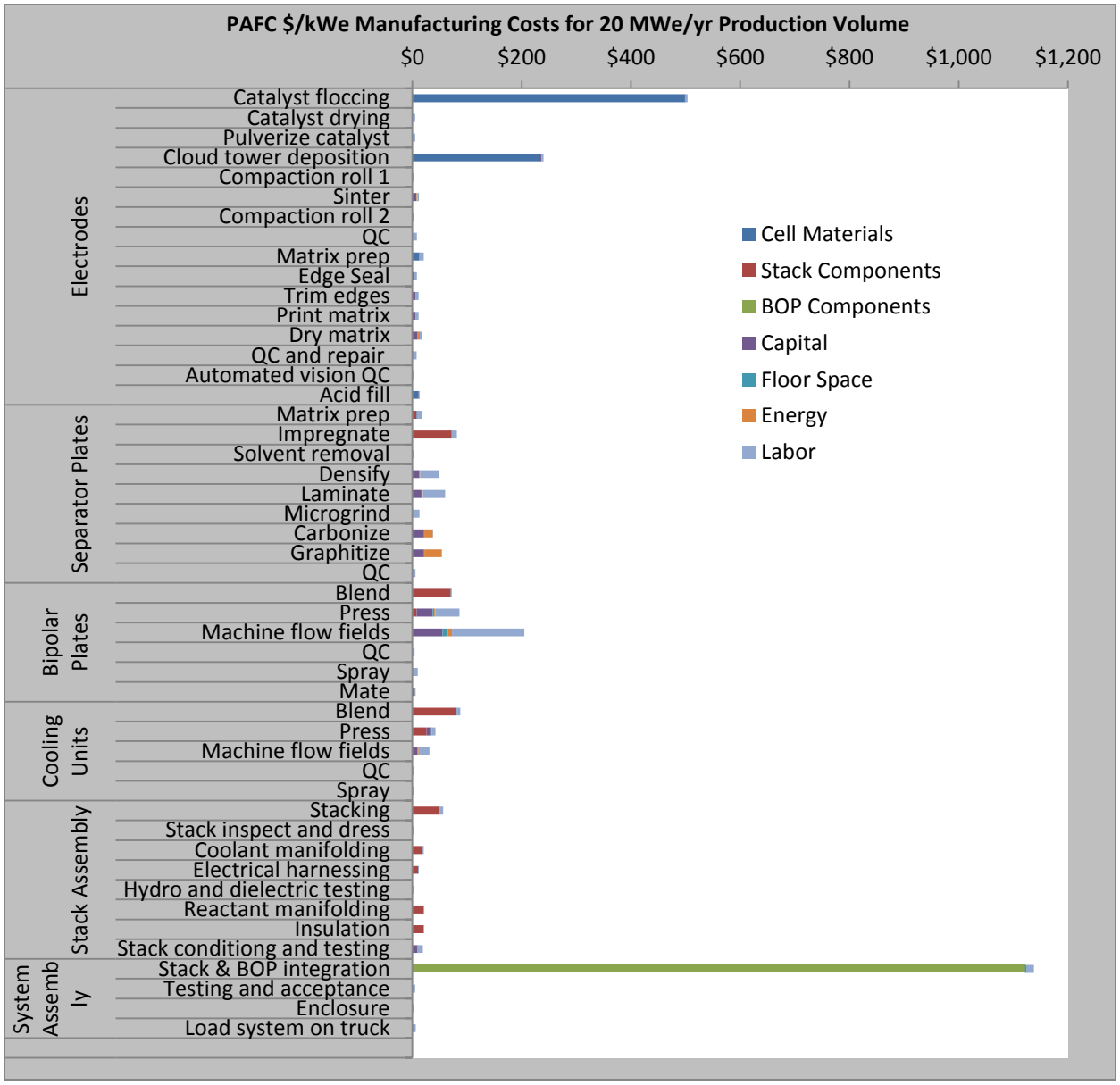

Figure 2-23. Total PAFC Manufacturing Cost Disaggregated by Process Steps and Cost Components for 20 MWe/yr Production Volume

As discussed previously, materials and components purchased from suppliers are estimated to constitute roughly 75% of total system cost, implying the remaining cost components (i.e. capital, floor space, energy, and labor) are estimated to collectively represent approximately 25% of total costs. To better describe these cost components, Figure 2-24 lists all costs other than purchased item costs for each step in the manufacturing process. Figure 2-24 is completely analogous to Figure 2-23 above, with the exception that purchased item costs have been excluded, and the cost axis adjusted, to improve the graphical resolution of the remaining cost components.

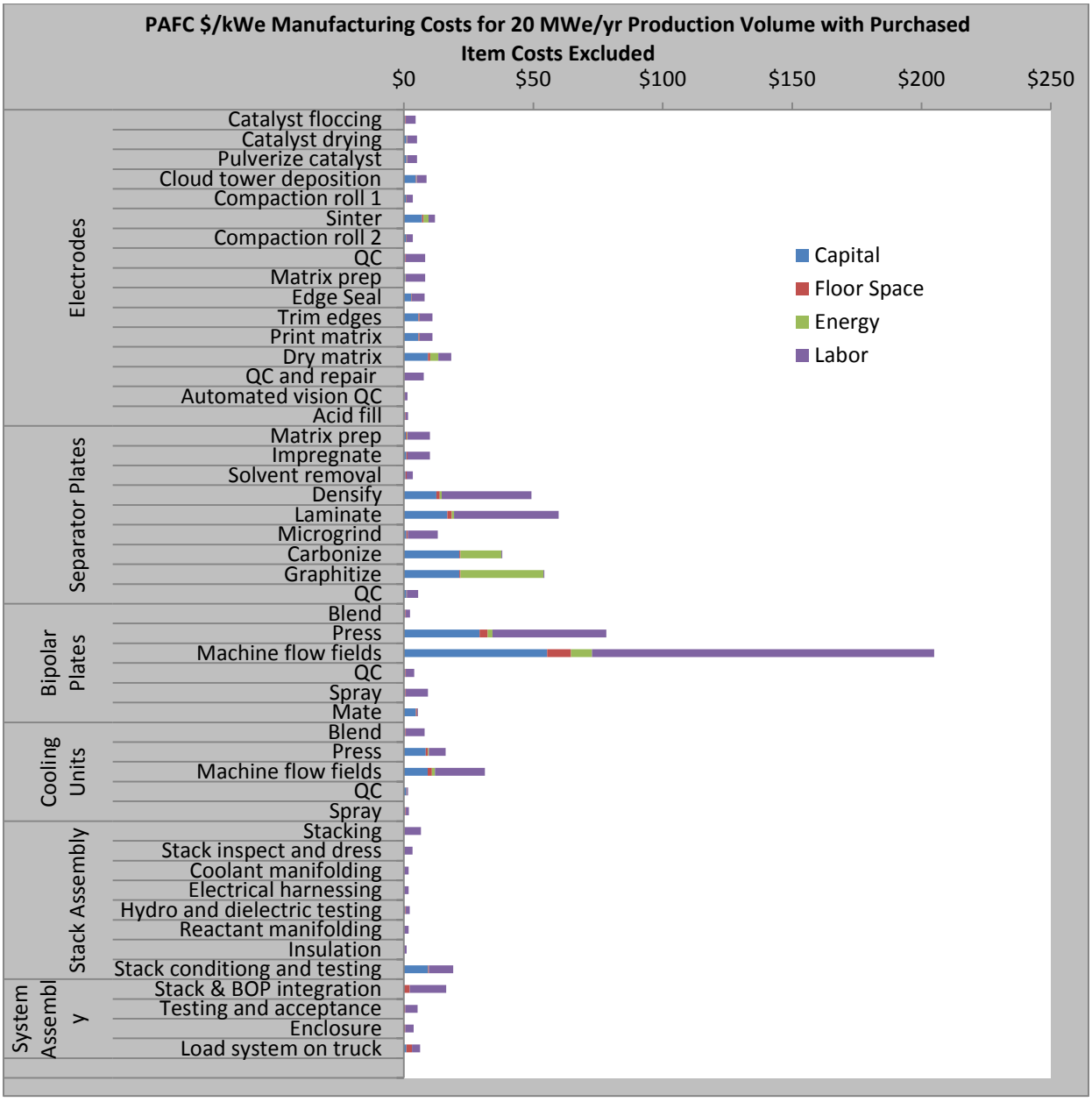

Figure 2-24. Total PAFC Manufacturing Cost Disaggregated by Process Steps and Cost Components for 20 MWe/yr Production Volume with Purchased Item Costs Excluded

The highest cost steps when purchased items are excluded from consideration are those process steps related to separator plate and bipolar plate manufacturing. The bipolar plate flow field machining step in particular is estimated to exceed $200/kWe due to large labor and capital requirements, necessary because of lengthy machining times. The hot pressing step which precedes flow field machining is likewise costly due to high capital and labor requirements. The densify and laminate steps used in separator plate manufacturing are two additional hot pressing processes with relatively high capital and labor costs. Carbonization and graphitization of separator plates show high capital costs, as well as high energy costs due to lengthy, high temperature heat treatments. The largest floor space cost is associated with bipolar plate flow field machining as a large number of CNC mills are required for the given takt time and assumed throughput of a single machine. Electrode manufacturing is broken down into sixteen steps, several of which are non-value added (e.g. catalyst pelletizing and dual matrix printing) and in need of streamlining for improved process efficiency.

Several of the larger labor, capital, floor space, and energy costs identified in Figure 2-24 are significant contributors to total manufacturing cost. Figure 2-25, similar to Figure 2-22, is a Pareto chart which compares, not only purchased item costs, but all cost component categories for the baseline production volume of 20 MWe/yr.

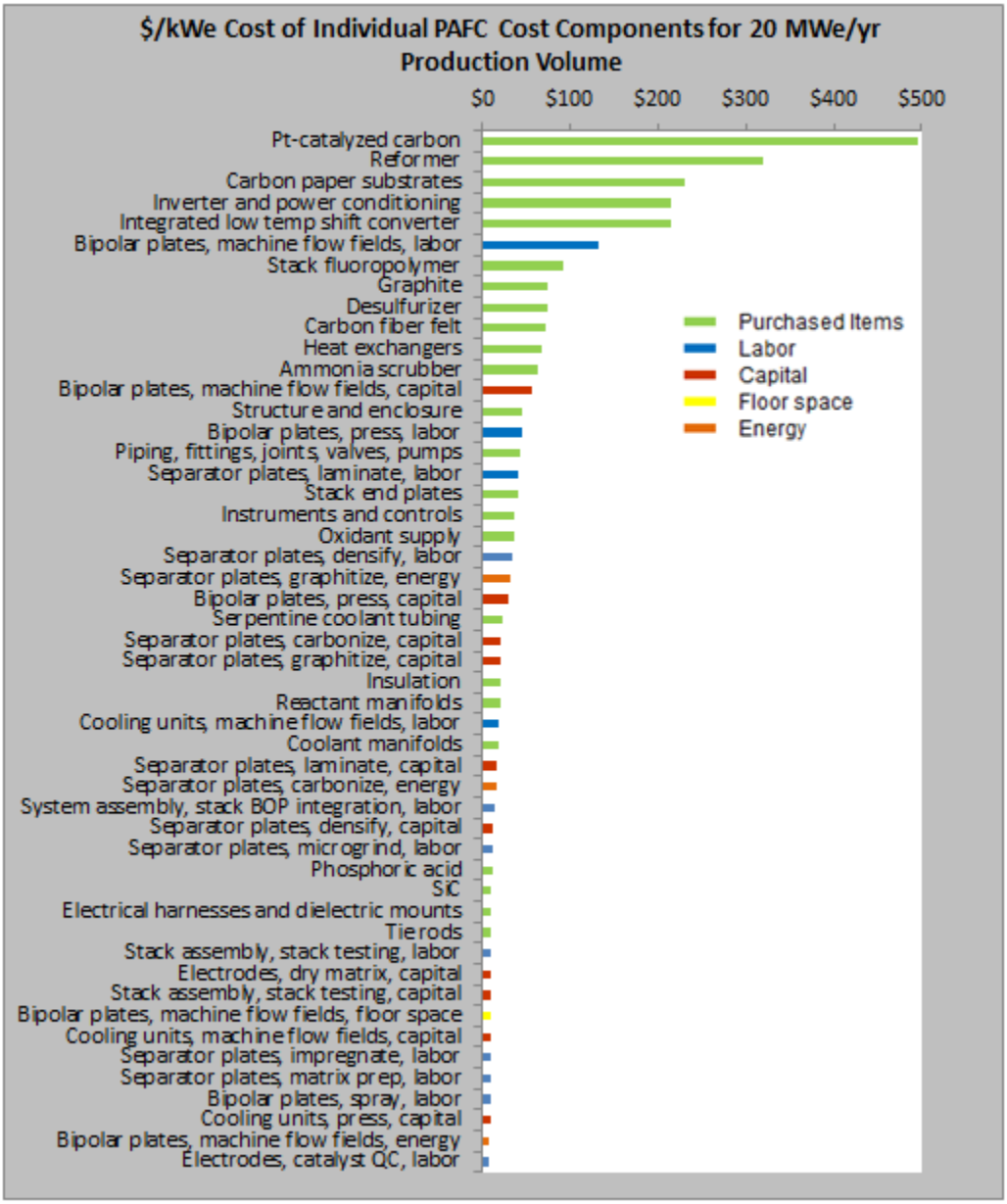

Figure 2-25. PAFC Pareto Chart for All Cost Components for 20 MWe/yr Production Volume

The top fifty highest cost components are listed using the indicated color code (note that the three purchased item cost categories – cell materials, stack components, and BOP components – have been assigned the same color, green). While 224 individual cost components were identified, it is well worth noting that the fifty most expensive constitute over 93% of total

manufacturing cost. Purchased item costs are predominant in the top half of the chart. Pt catalyzed carbon, carbon paper substrates, carbon fiber felt, graphite, and fluoropolymer are the most significant cell and stack materials. The fuel processing BOP components (desulfurizer, reformer, integrated low temperature shift converter, and ammonia scrubber) are estimated to constitute 24% of total manufacturing cost. The inverter and heat exchangers are additional high cost BOP components. Interspersed among the highest cost purchased items in the Pareto chart are several significant labor costs attributable to the machining and hot pressing steps in bipolar plate and separator plate manufacturing. The capital cost for flow field milling machines, in the thirteenth rank, is also noteworthy. The lower half of the chart is a more diverse mixture of cost component categories with purchased items, labor, and capital appearing most frequently. Three energy cost components appearing in the chart are the energy costs attributable to separator plate carbonization and graphitization, as well as the energy cost for flow field machining. The floor space cost attributable to flow field machining is the only one of this cost component category to register among the top fifty.

Figure 2-26, below, is an elaboration of Figure 2-19 in that total manufacturing cost is disaggregated into cell, stack, and BOP costs. With reference to Figure 2-23, cell costs are defined as all costs (cell material, capital, labor, energy, and floor space) associated with the steps under the Electrode category. Similarly, stack costs are defined as all costs associated with the categories of Separator Plates, Bipolar Plates, Cooling Units, and Stack Assembly. Finally, BOP costs are defined as all costs associated with the System Assembly category.

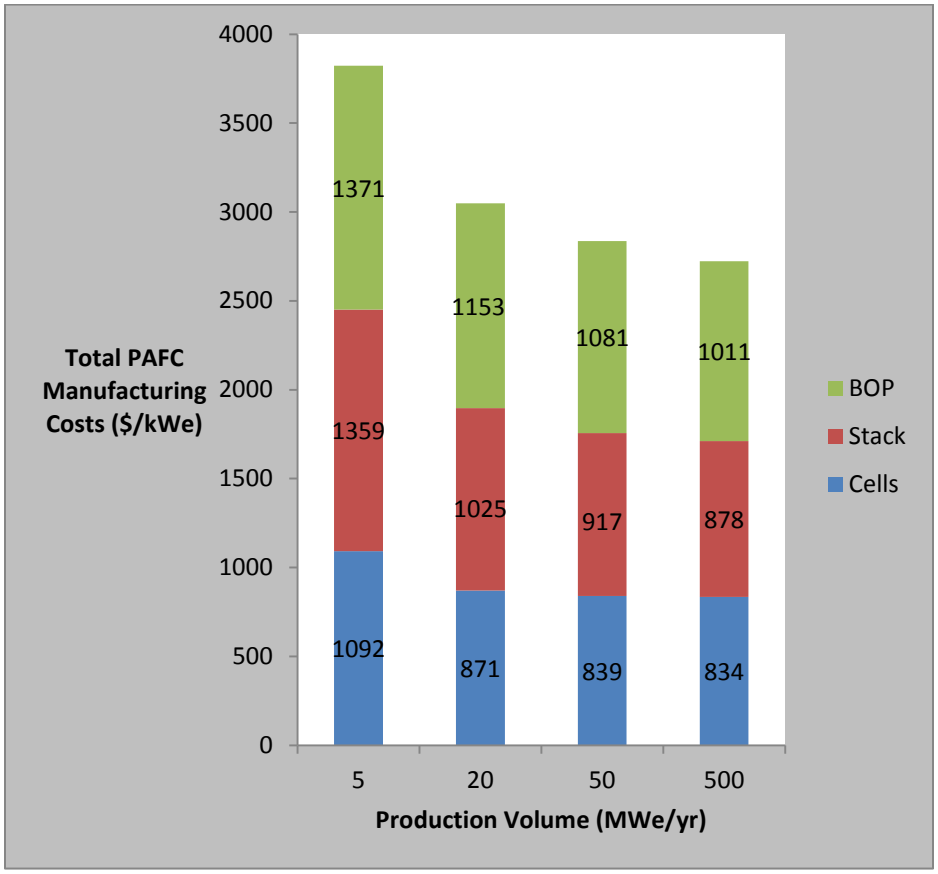

Figure 2-26. PAFC Manufacturing Costs Disaggregated by Cell, Stack, and BOP for Varying Annual Production Volumes.

All three cost categories are shown to decrease in magnitude with increasing annual production volume. The relative cost distribution, however, remains more or less constant as indicated in Figure 2-27. Cell costs range from 28 - 31%, stack costs from 32 - 35%, and BOP costs from 36 - 38% for all annual production volumes.

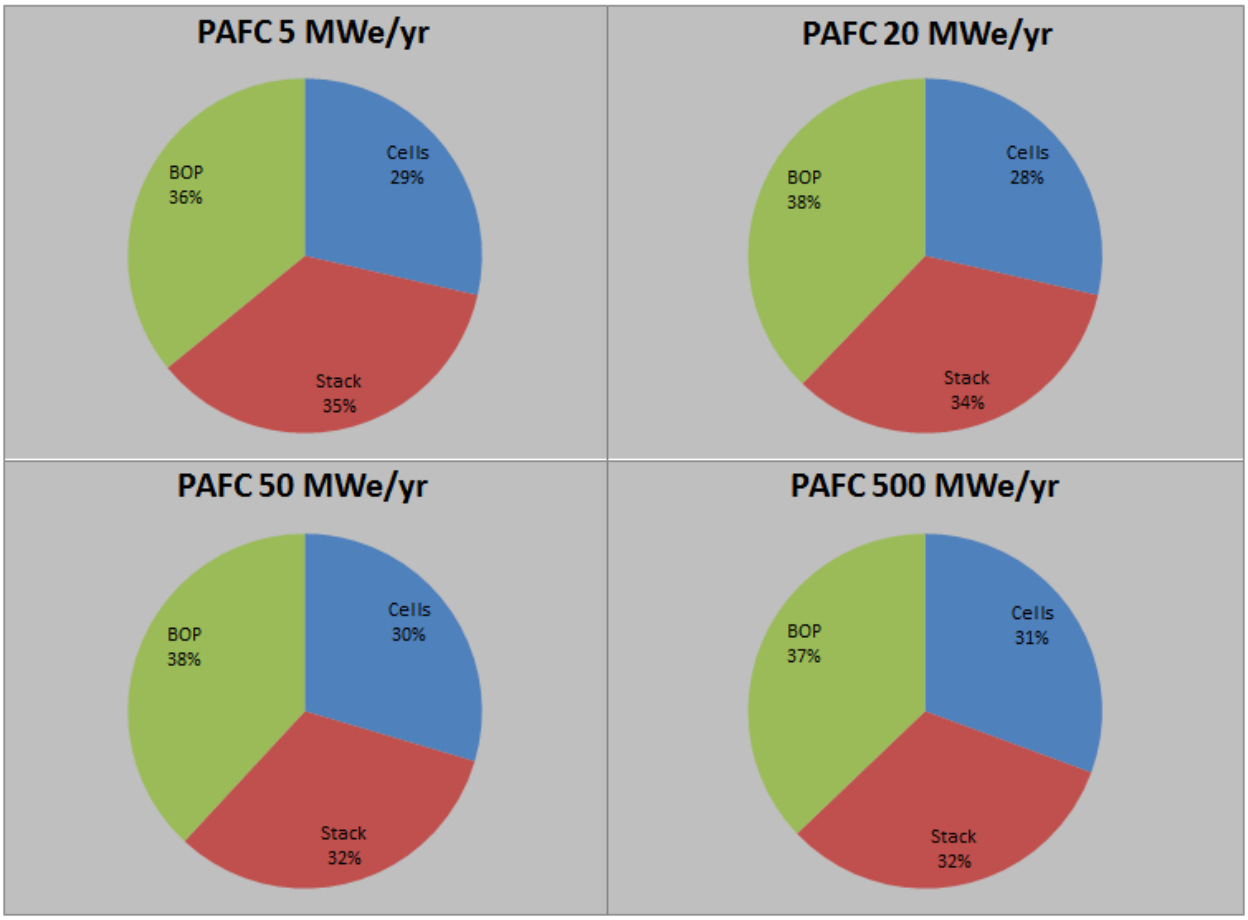

Figure 2-27. PAFC Cell, Stack, and BOP Cost Distribution for Varying Annual Production Volumes

Monte Carlo simulation was performed to assess the impact of stochastic and uncertain inputs on cost estimation. For the baseline production volume of 20 MWe/yr, total manufacturing cost is estimated to be between $2995 and $3293/kWe with 90% confidence after 10,000 trials as shown in Figure 2-28. The cost distribution is unimodal and bell-shaped, with slight skewing to the right.

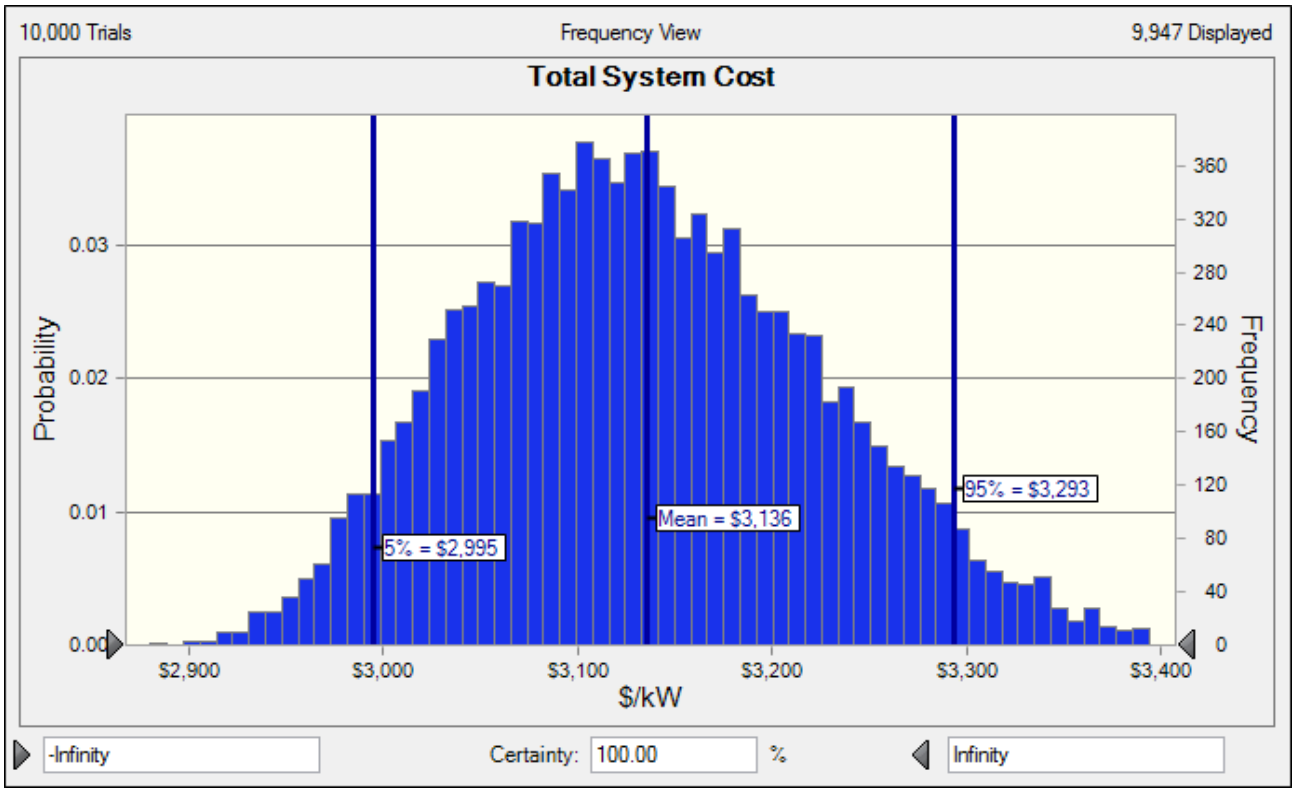

Figure 2-28. Monte Carlo Simulation of Total PAFC Manufacturing Cost for 20 MWe/yr Production Volume

Sensitivity analysis, shown in Figure 2-29, reveals that the market price of platinum represents over 70% of model variability as this commodity has had a particularly volatile recent history. The next most important contributor to variance is the cost of electricity for industrial customers, varying considerably from state to state, from $0.04/kWh in Washington to $0.23/kWh in Hawaii.[31] These top two variables, along with the assumed capital recovery rate and flow field machining time, constitute over 91% of model variance. The probabilistic assumptions used in this sensitivity analysis are listed in Table 2-3.

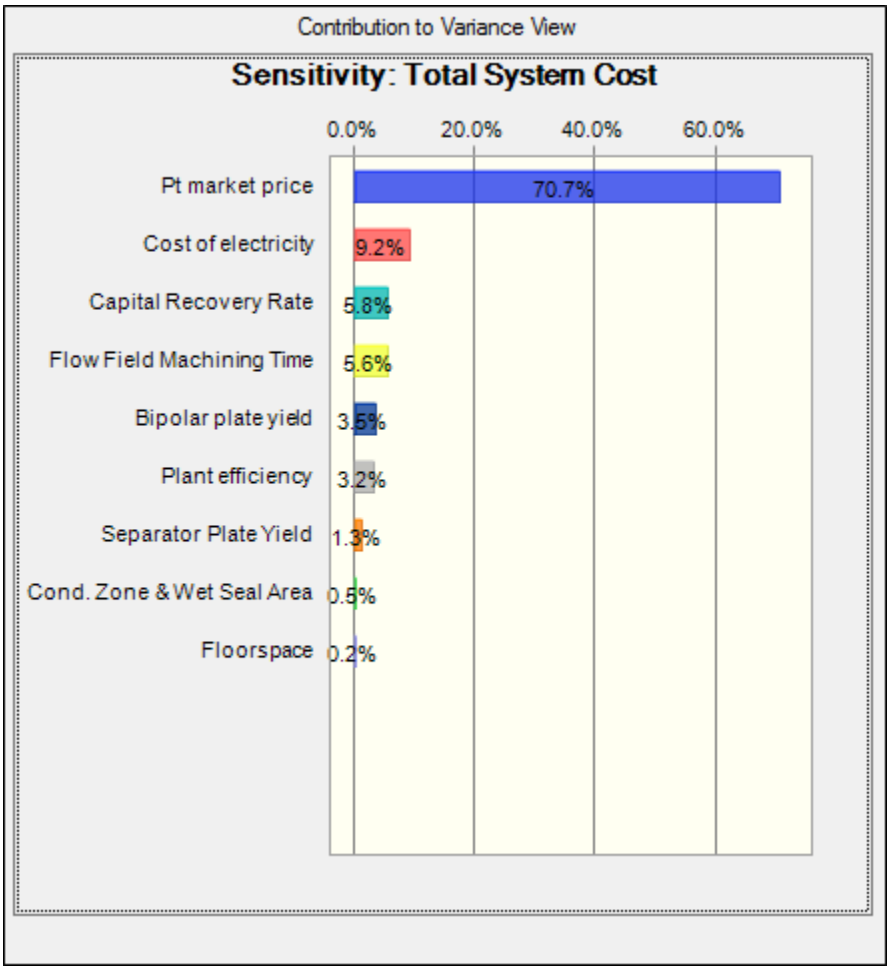

Figure 2-29. Sensitivity Analysis for Total PAFC Manufacturing Cost for 20 MWe/yr Production Volume

Table 2-3. Sensitivity Analysis Assumptions for Total PAFC Manufacturing Cost for 20 MWe/yr Production Volume

Variable	Distribution Family	Parameters	Units
Pt market price	Triangular	min = 746, most likely = 1244, max = 2302	$/troy ounce
Cost of electricity	Lognormal	mean = .08, sd = .04	$/kWh
Capital recovery rate	Triangular	min = 8, most likely = 12, max = 18	%
Flow field machining time	Triangular	min = 10, most likely = 120, max = 180	minutes
Bipolar plate yield	Triangular	min = 88, most likely = 98, max = 99	%
Plant efficiency	Triangular	min = 75, most likely = 80, max = 85	%
Separator plate yield	Triangular	min = 88, most likely = 98, max = 99	%
Cond. zone & wet seal area	Normal	mean = 15, sd = 1	%
Floorspace	Triangular	min = 12, most likely = 22, max = 24	$/ft^2

2.13 OPPORTUNITIES

While commercially acceptable stack and system lifetimes of ten and twenty years, respectively, are possible for state of the art PAFC, reductions in first costs and life cycle costs are necessary for mass commercialization of this fuel cell technology. Manufacturing related cost reduction opportunities identified in this study include:

- Volume production – For modeling purposes, a baseline production volume of 20 MWe/yr was selected because of its rough equivalence with the recent production volume experienced by actual PAFC manufacturers. An 11% reduction in cost from $3049/kWe to $2724/kWe appears achievable just by increasing production volume from the model baseline to 500 MWe/yr, even if manufacturing technology is assumed unchanged (i.e. production lines are replicated in parallel) and no learning curve is experienced. This cost is still prohibitive to mass commercialization of PAFC, indicating that widespread adoption cannot be driven production volume with massive demand from early adopters or with favorable tax code treatment. However, the demand created by early adopters and tax credits is essential for providing learning/discovery opportunities which can lead to the technological breakthroughs (such as catalyst areal loading reduction) that are necessary to reduce first costs to a competitive level of $1500/kWe or less.

- Catalyst – Reducing the areal loading of platinum from 0.75- 1.00 mg/cm^2 for PAFC to be on par with PEMFC (0.15 mg/cm^2) is a reasonable goal with the potential to reduce first costs by $300-$500/kWe. Advancements in reducing platinum surface area loss and anion absorption are needed to make this cost reduction possible.

- Fuel processing BOP – Many BOP components such as blowers and heat exchangers may be available as low cost off-the-shelf items already manufactured in large volumes for other industries. Fuel processing BOP components, however, are unique items produced in low volume, contributing significantly to their high realized cost. In this model, at the baseline production volume of 20 MWe/yr, approximately 24% of total system cost is attributable to the fuel processing BOP (desulfurization unit, reformer, integrated low temperature shift converter, ammonia scrubber, and all fuel processing related piping and heat exchangers). At this same fuel cell production volume, only fifty each of desulfurization units, reformers, integrated low temperature shift converters, and ammonia scrubbers are needed annually, an insufficient production volume to be of major concern to suppliers. In the absence of a significant increase in fuel cell demand, efforts should be directed at new, lower cost designs for fuel processing BOP components. For example, the total cost of a reformer might (perhaps counter intuitively) be reduced by using a noble as opposed to nickel-based catalyst as such a reformer could be significantly smaller in overall size. A smaller reformer would require less materials, fewer/shorter manufacturing and assembly operations such as welding, and less effort for transportation and manipulation. Furthermore, a reforming catalyst which does not

generate ammonia could lead to the elimination of an entire BOP component, the ammonia scrubber.

- Substrate – Carbon paper substrates are among the highest cost materials used in PAFC manufacturing. Paper making is a slow, discontinuous process that is followed by long, energy intensive carbonization and graphitization steps. As mentioned previously in section 2.5, PAFC developers are actively researching lower cost substrates as evidenced by Breault's 2010 patent which eliminates the prepreg step in traditional carbon manufacturing and reduces substrate cost by 16%.[21] Approaches which further reduce the number or duration of steps in substrate manufacturing, as well as approaches using new procedures or materials should be examined.

- Flow field molding – The machining of flow field channels is a long (up to 2 hours) process having substantial capital, labor, and energy requirements. A near net shape pressing procedure which results in flow field channels requiring little to no subsequent machining is estimated to provide a cost savings on the order of $65/kWe. A material which does not adhere to molds must be identified to enable near net shape pressing technology. Non-contact sensors for flow field inspection are also needed.

- Separator plate carbonization/graphitization cycle time – Separator plate carbonization and graphitization are batch processes requiring 2-3 weeks of high temperature heat treatments using capital and energy intensive furnaces. Carbonization especially must proceed very slowly to avoid disruptive outgassing of volatilized resin, which would result in open pores, blisters, and cracks in the separator plates. Approaches to shortening the cycle times of separator plate carbonization and graphitization should be examined. Reducing the cycle time of carbonization from greater than 300 hours to 48 hours (equivalent to the cycle time of a typical graphitization step) could reduce total system cost by an estimated $25/kWe. Development of new resin binders is central to reducing the manufacturing cost and increasing the reliability of separator plates.

- Hot press cycle times – Reducing cycle times for hot pressing steps in separator plate, flow field, and cooling unit manufacturing steps would result in reduced capital, labor, energy, and floor space costs. Reducing the average hot pressing step to 5 minutes for an entire sequence of mold loading, warm up, pressing, cool down, then part removal would reduce total system cost by $34/kWe for the baseline production volume of 20 MWe/yr

- Electricity – With all other factors held constant, the difference between operating a PAFC manufacturing plant in the lowest as opposed to the highest cost state for industrial electricity results in a reduction in total system cost by $191/kWe. Thus, the cost of electricity merits careful consideration when selecting a manufacturing site.

- Electrode manufacturing – State of the art electrode manufacturing uses inefficient processes. For instance, the catalyst deposition steps of floccing, drying, pelletizing, grinding, deposition by cloud tower, and sintering have been in use since the late 1970s. A streamlining of this process would eliminate inefficient steps such as pelletizing. Similarly, Gravure matrix printing currently requires both electrodes be printed to insure against defects. If the printing process is optimized, then the application of a matrix layer to only one electrode would be sufficient.

- Stack conditioning and testing cycle times – UTC indicates that stack conditioning and testing is a bottleneck in their current manufacturing process in need of acceleration. A means for bypassing rather than replacing any bad cells identified in stack testing would be desirable for reducing stack manufacturing cycle time.

Phosphoric acid fuel cell technology is continually evolving, with the first relevant patents appearing in the 1960s and many recent ones appearing in 2010. During this time, significant breakthroughs in design and manufacturing technology have occurred such as reducing platinum loadings by an order of magnitude when platinum supported on carbon black supplanted platinum black. More recently, stack life has been doubled for UTC's commercial product from 5 to 10 years. These and other advancements have led to PAFC becoming economically justifiable in certain applications where users have a combined heat and power load and reside in a state where clean energy tax credits exist and the cost of grid electricity is relatively high. More cost reduction work needs to be done to expose PAFC to a wider market.

With 500 MWe/yr production and the potential technological advancements discussed above, the manufacturing cost of PAFC can be significantly reduced from the baseline cost of $3049/kWe. Remick and Wheeler indicate that when the installed costs of PAFC systems in the 400 kWe range are under $2000/kWe, they may be economically competitive with conventional energy conversion systems (reciprocating engines and gas turbines) with respect to cost of electricity over the life cycle of the product.[32] Advances in design, materials, and manufacturing technology will be required to close the current cost gap between PAFC and other conventional energy conversion systems.

2.14 REFERENCES

1. UTC Power. http://www.utcpower.com/products/purecell400 (2010)
2. Breault, R., and R. Fredley. *Fuel cell assembly having long life characteristics*, US Patent 2010/0055541 A1, Mar. 4 (2010).
3. Breault, R. *Apparatus for reducing electrolyte loss from an electrochemical cell*, US Patent 4,345,008, Aug. 17 (1982).
4. Breaul, R. *Method for reducing electrolyte loss from an electrochemical cell*, US Patent 4,414,291, Nov. 8 (1983).
5. Kanuri, S., K. Intwala, L. Protsailo, and S. Nelson, UTC Power, Inc. *Private meeting with Joshua Warren, Wei Zhang, Surya Saripalli, and Sujit Das*, Oak Ridge National Laboratory, Oak Ridge, TN 37932, Sep. (2010).
6. Grevstad, P. *Electrolyte reservoir for a fuel cell*, US Patent 4,035,551, July 12 (1977).
7. Luoma, W., R. Martin, and R. Breault. *Electrochemical cell assembly*, US Patent 4,929,517, May 29 (1990).
8. Breault, R., R. Martin, R. Roche, and R. Kline. *Cathode reactant flow field component for a fuel cell stack*, US Patent 5,558,955, Sep. 24 (1996).
9. Emanuelson, R., W. Luoma, and W. Taylor. *Method for making improved separator plates for electrochemical cells*, US Patent 4,360,485, Nov. 23 (1982).
10. Dettling, C., and P. Terry. *Integral gas seal for fuel cell gas distribution assemblies and method of fabrication*, US Patent 4,505,992, March 19 (1985).
11. Grasso, A., R. Martin, and R. Roche. *Composite article*, US Patent 6,039,823, March 21 (2000).
12. Bonk, S., G. Scheffler, P. Foley, T. Corrigan, R. Sederquist, and F. Kocum. *Hydrocarbon fuel gas reformer assembly for a fuel cell power plant*, US Patent 6,296,814 B1, Oct. 2 (2001).
13. Szydlowski, D., T. Corrigan, D. Blake, and R. Sederquist. *Shift converter*, US Patent 6,306,354 B1, Oct. 23 (2001).
14. Breault, R. *Ammonia contact scrubber for a fuel cell*, US Patent 2010/0024648A1, Feb. 4 (2010).
15. Kemp, F., and M. George. *Sequential catalyzation of fuel cell supported platinum catalyst*, US Patent 3,857,737, Dec. 31 (1974).
16. Petrow, H., and R. Allen. *Finely particulated colloidal platinum compound and sol for producing the same, and method of preparation (of fuel cell electrodes and the like employing the same)*, US Patent 3,992,512, Nov. 16 (1976).
17. Bregoli, L.: Electrochim. Acta, 23, 489 (1978)
18. Luczak, F., and D. Landsman. *Method for making ternary fuel cell catalysts containing platinum, cobalt, and chromium*, US Patent 4,613,582, Sep. 23 (1986).
19. Hladis, A., HydroGen, Inc. *Private emails and teleconferences with Joshua Warren, Wei Zhang, and Sujit Das*, Oak Ridge National Laboratory, Oak Ridge, TN Jan. - Apr. (2011).
20. Miwa, K., K. Shimizu, and H. Fukui: *Electrode substrate for fuel cell and process for producing the same*, US Patent 4,851,304, July 25 (1989).
21. Breault, R. *Electrode substrate for electrochemical cell from carbon and cross-linkable resin fibers*, US Patent 2010/0035126 A1 Feb. 11 (2010).
22. Goller, G., and R. Breault. *Automated catalyst processing for cloud electrode fabrication for fuel cells*, US Patent 4,233,181, Nov. 11 (1980).

23. Singer, R. *Catalytic dry powder material for fuel cell electrodes comprising fluorocarbon polymer and precatalyzed carbon*, US Patent 4,177,159, Dec. 4 (1979).
24. Goller, G., V. Petraglia, and J. Salonia. *Dry mix method for making an electrochemical cell electrode*, US Patent 4,175,055, Nov. 20 (1979).
25. Kanuri, S. *PAFC Cost Challenges*, MCFC and PAFC R&D Workshop sponsored by U.S. Department of Energy, Office of Energy Efficiency and Renewable Energy, Fuel Cell Technologies Program, http://www1.eere.energy.gov/hydrogenandfuelcells/mcfc_pafc.html (2009).
26. DeCasperis, T., R. Roethlein, and R. Breault. *Method of forming edge seals for fuel cell components*, US Patent 4,269,642, May 26 (1981).
27. Breault, R., and M. Gorman. *Laminated electrolyte reservoir plate*, US Patent 5,366,825, Nov. 22 (1994).
28. Breault, R. *Silicon carbide electrolyte retaining matrix for fuel cells*, US Patent 4,017,664, Apr. 12 (1977).
29. Spearin, W. *Process for forming a fuel cell matrix*, European Patent 0 344 089, May 26 (1989).
30. Breault, R., R. Martin, R. Roche, G. Scheffler, and J. O'Brien. *Coolant plate assembly for a fuel cell stack*, US Patent 6,050,331, Apr. 18 (2000).
31. U.S. Energy Information Administration: http://www.eia.doe.gov/cneaf/electricity/epm/table5_6_a.html (2010).
32. Remick, R., and D. Wheeler. *Molten carbonate and phosphoric acid fuel cells: overview and gap analysis*, Technical Report NREL/TP-560-49072 (2010).

3. MOLTEN CARBONATE FUEL CELLS

3.1 BASIC OPERATION

As with phosphoric acid fuel cells, major development of molten carbonate fuel cells (MCFC) began in the 1960s, resulting in the second most mature technology of the three examined in this study. Development has occurred across the globe by many participants such as MTU Friedrichshafen in Europe, Ishikawajima Heavy Industries in Japan, and FuelCell Energy (FCE) in the United States. FuelCell Energy, formerly known as Energy Research Corporation, is currently the only United States producer of commercially available MCFC systems, which it has offered since 2003.

Molten carbonate fuel cells frequently use natural gas as a fuel source with the natural gas having been reformed inside the stack rather than in an external reformer as with PAFC. Reforming may be direct internal, indirect internal, or a combination of the two. Direct internal reforming means natural gas is reformed to H_2 and CO by a catalyst inside the anode. With direct internal reforming, catalyst is exposed to a degradative carbonate vapor which reduces catalyst efficacy over time. Indirect internal reforming entails reforming natural gas inside reforming units which are catalyzed, plate shaped structures present in the stack itself and placed intermittently between cells. With indirect internal reforming, catalyst is not exposed to carbonate vapor. Figure 3-1 shows the basic operation of a molten carbonate fuel cell using both direct and indirect internal reforming.

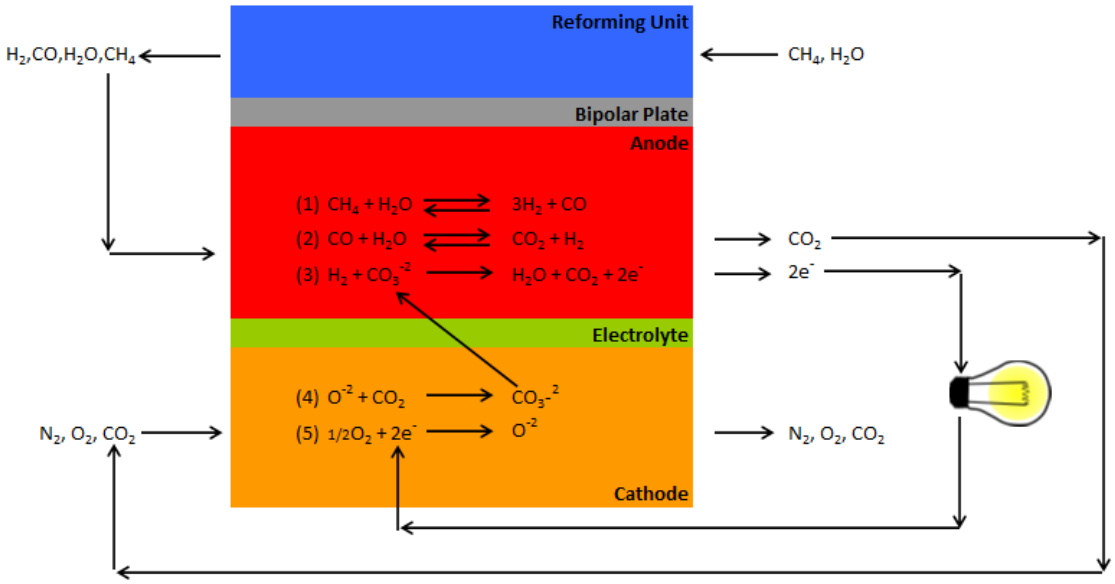

Figure 3-1. Basic Operation of a Molten Carbonate Fuel Cell Using Direct and Indirect Internal Reforming

A mixture of primarily methane and steam exits a prereformer (not shown) and enters the reforming unit from the top right. Catalyst in the reforming unit reforms most (55-70%) of the methane to hydrogen and carbon monoxide. Heat generated in the exothermic electrochemical

fuel cell reaction is communicated to the reforming unit and drives the endothermic steam reforming reaction (reforming reaction shown as reaction (1) in anode). Reformed fuel exits the reforming unit and is supplied to the anode where additional reforming occurs as shown in reaction (1). As diatomic hydrogen created in reaction (1) is consumed in the fuel cell electrochemical reaction (3), reaction (1) is driven essentially to completion by Le Chatelier's Principle such that practically 100% conversion of methane to carbon monoxide and diatomic hydrogen is achieved. Hydrogen consumption in reaction (3) similarly drives reaction (2), the water/gas shift reaction, to near completion such that most carbon monoxide is shifted to carbon dioxide and diatomic hydrogen. The fuel cell electrochemical reaction (3) shows a molecule of diatomic hydrogen and a carbonate ion (CO_3^{-2}) reacting to form water and carbon dioxide with two electrons liberated. The electrolyte layer is non-conductive to electrons. Thus, the electrons liberated in reaction (3) are forced through an external circuit where they perform work before entering the fuel cell's cathode. Air containing diatomic oxygen is supplied to the cathode by a blower (not shown). The two electrons liberated in reaction (3) are shown to reduce an oxygen atom to an oxide ion (reaction 5). Carbon dioxide created in reactions (2) and (3) is recycled to the cathode. In reaction (4), carbon dioxide and an oxide ion react to form a carbonate ion which is conducted through the electrolyte to the anode where another cycle of reaction (3) begins.

Operating temperature and pressure are classical MCFC optimization challenges with benefits and tradeoffs that must be considered carefully. For instance, higher temperatures enable higher voltages and thus higher power. However, higher temperatures also promote corrosion reactions that eventually lead to system failure. Higher pressures also enable higher voltages and power. However, higher pressures also increase the rate at which nickel (Ni) dissolves from the cathode and migrates to and precipitates in the matrix where over time an electrical short circuit develops leading to cell failure. Various fuel cell manufacturers have adopted various combinations of temperature, pressure, and other parameters into their designs, each having benefits and tradeoffs.

3.2 CELL, STACK, AND SYSTEM DESIGN ASSUMPTIONS

For MCFC specifically, limited discussion of manufacturing processes and model results is given due to the proprietary nature of information disclosed to ORNL by FCE. FCE uses an externally manifolded, atmospheric pressure design with direct and indirect internal reforming similar to the description provided in Section 3.1. Stacks are manufactured and conditioned at FCE's 70 MWe capacity manufacturing facility in Torrington, CT. After conditioning, stacks are shipped to customer sites where they are integrated with BOP components and commissioned. Because stacks and BOP are not integrated until having been shipped to the customer, the MCFC model departs from the boundaries discussed in section 1.2 to include shipping and installation costs.

FCE offers three commercially available fuel cell systems under the DFC® (direct fuel cell) trademark: DFC-300®, DFC-1500®, and DFC-3000®. All three systems use the same stack design having one, four, and eight stacks, respectively. A stack consists of 375 to 400 cells stacked in series with each cell having a planform surface area of nearly one square meter. Reforming units are incorporated into stacks at an interval of 1 reforming unit for each group of 4 to 8 cells. With no increase in total stack height, FCE has increased stack output by more than

5-fold since 1992.[3] FCE recently indicated that the DFC-300®, their single stack combined heat and power system, is currently capable of 375 kW net AC with approximately 56% electrical efficiency and 89% total efficiency (LHV natural gas).[1]

Cells are assumed to have a total planform area of 0.871 m^2 as indicated in Figure 3-2. Wet seals are assumed to require 10% of total cell area, leaving an active cell area of 0.7839 m^2.

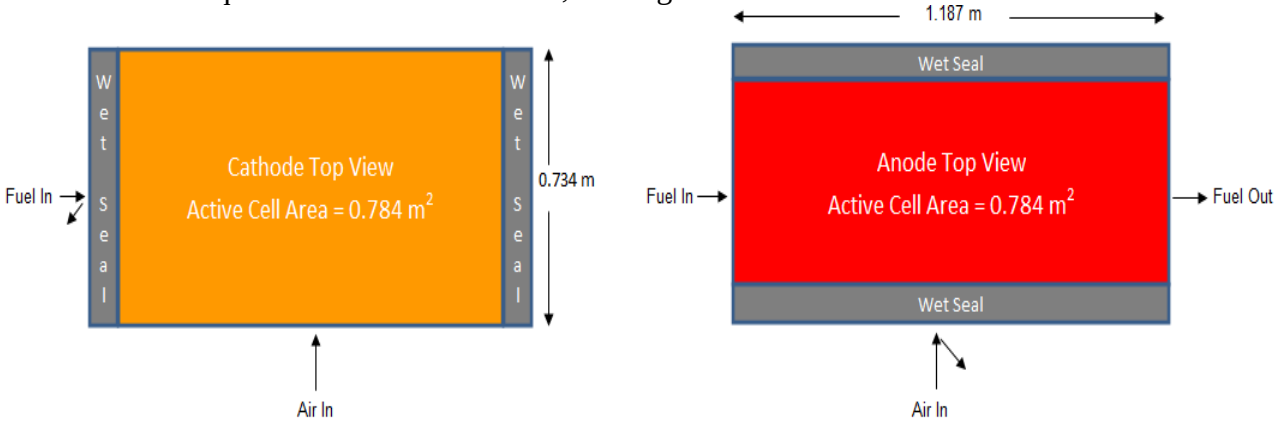

Figure 3-2. MCFC Planform Cell Geometry

At 0.798 volts per cell and a current density of 0.168 A/cm^2, a power density of 1.341 kW/m^2 is achieved. Thus, a single cell is producing direct current at a rate of 1.051 kW. If 382 cells are assumed per stack then one stack has a gross DC output of 401 kW at zero hours. A 96% efficient inverter renders the DC to 385 kW gross AC. Parasitic loads are assumed to require 2.5% of gross AC, leaving 376 kW net AC at zero hours. The above mentioned cell, stack, and power assumptions are summarized in Table 3-1.

Table 3-1. MCFC Cell, Stack, and Power Assumptions

Cell area	0.734 X 1.187 = 0.871 m^2
Percent cell area used for wet seals	10%
Active cell area	0.871 m^2 x 0.90 = 0.784 m^2
Current density	0.168 A/cm^2
Voltage	0.798 V
Power density	1.341 kW/m^2
Single cell power	1.051 kW
Gross System DC at 0hr	$\frac{1.051\ kW}{cell}$ X $\frac{382\ cells}{stack}$ = $\frac{401kW\ DC}{system}$
Losses:	
Inverter efficiency 96%	401 kW DC x 0.96 = 385 kW AC
Parasitic Losses 2.5%	385 kW x 0.975 = 376 kW net AC
Electrical efficiency (LHV natural gas)	56%
Thermal efficiency	33% → 0.76 MMBtu/hr
Total system efficiency	89%

The cell structure assumed in this study is shown in Figure 3-3.

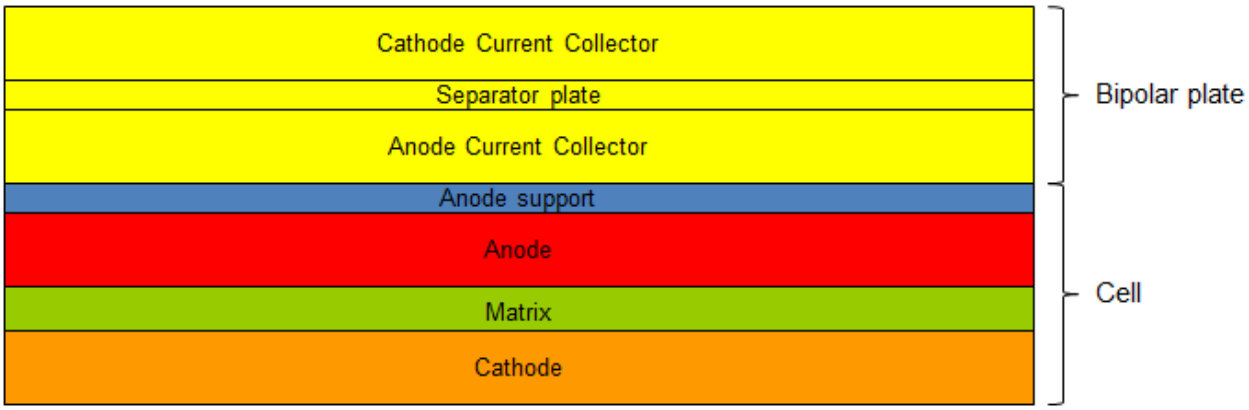

Figure 3-3. MCFC Cell Structure

A matrix layer retains an electrolyte consisting of a eutectic mixture of alkali carbonates. Adjacent to one side of the matrix layer is a nickel cathode that will be lithiated and oxidized to nickel oxide in situ during initial stack warm-up. Facing the other side of the matrix layer is a nickel alloy anode. A porous, nickel substrate is assumed to be added to anodes to provide mechanical support. The bipolar plate consists of a central, stainless steel separator plate, to

which two pocketed cathode wet seal rails are welded to one side and two pocketed anode wet seal rails are welded to the opposite side. Corrugated, stainless steel sheets are included on either side of the separator plate and fit into the pockets formed between the separator plate and wet seal rails. The corrugated sheets serve as both flow fields and current collectors. Reforming units are assumed to occur with every group of 4 to 8 cells. Manifolds direct a reforming unit's effluent to the anodes of cells near that reforming unit.

Molten carbonate fuel cells are able to operate on a wide variety of fuels including natural gas, anaerobic digester gas, coal mine methane, peak shave gas. Each fuel type places different demands on the fuel processing BOP. In this study, an MCFC system operating on pipeline quality natural gas has been assumed, using the mechanical balance of plant shown in Figure 3-4.

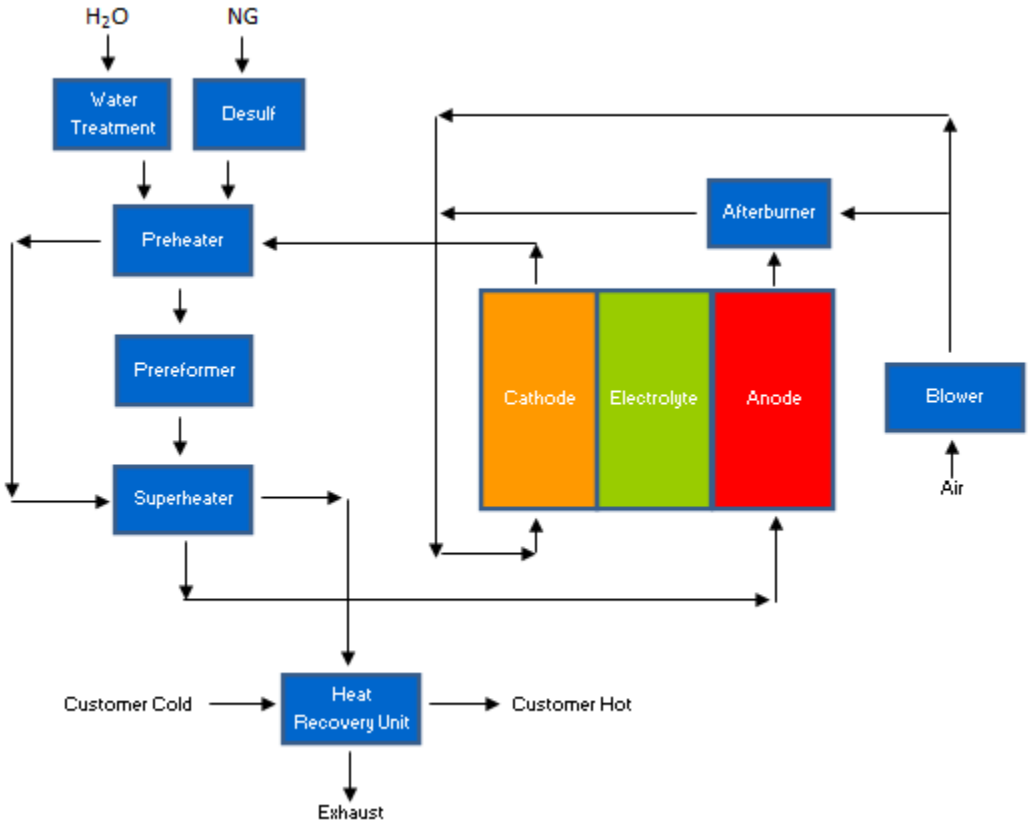

Figure 3-4. MCFC Mechanical Balance of Plant

In their 2011 patent, Katikaneni and Daly of FCE describe a fuel processing system useful for processing natural gas and/or other MCFC suitable fuels such as digester gas, coal mine methane, and peak shave gas.[7] Incoming fuel is desulfurized at ambient temperatures, preheated, and then prereformed at low temperature. The patent owners describe an integrated prereformer where fuel is first passed over a Pt-based catalyst to remove oxygen. Oxygen removal from the fuel stream is necessary as oxygen would deactivate the nickel based prereforming catalyst through which the fuel stream flows next. The prereformer converts higher hydrocarbons (higher defined as greater than 2 carbon atoms per molecule) to primarily methane, resulting in a fuel stream whose overall composition is mostly methane, hydrogen, carbon monoxide, and carbon dioxide. In some designs, a third catalyst layer that is also nickel based, is disposed between the deoxidant catalyst layer and the prereforming catalyst layer, and

serves to convert the propane and propylene present in certain fuel feedstocks to primarily methane and carbon oxides. Figure 3-5, reflecting the assumptions of the present study and the above mentioned patent, shows water and natural gas entering the fuel cell system and first being demineralized and desulfurized, respectively. The fuel and water streams are mixed and then preheated by cathode exhaust before being introduced to the prereformer. The prereformer effluent passes through a superheater where cathode exhaust again transfers heat to the fuel/steam mixture before it is introduced into the reforming units in the stack. Reformed fuel exits the reforming units and is conveyed to the anodes where fuel reforming is completed and the fuel cell electrochemical reaction takes place. Carbon dioxide rich, depleted fuel exits the anodes and is introduced into an afterburner along with air supplied by a blower. Depleted fuel is combusted with air in the afterburner and then mixed with additional fresh air supplied by the blower. This gas mixture is introduced into the cathodes, providing the carbon dioxide and oxygen required in reactions (4) and (5) in Figure 3-1. Cathode exhaust transfers heat first in a preheater, and then in a superheater to the incoming raw fuel stream as described previously. After these heat exchanger duties, the cathode exhaust transfers heat to a customer supplied CHP load before being exhausted to the atmosphere.

The fuel desulfurization process deserves special mention and elaboration as FCE indicates this to be among the most significant of challenges to reducing costs and improving reliability. In their technology development phase, FCE examined and demonstrated several desulfurization strategies including hydrodesulfurization, selective catalytic oxidation, and ambient temperature sulfur adsorption.[2] Hydrodesulfurization requires a hydrogen rich stream, which is relatively easy to obtain in externally reforming systems by harvesting hydrogen from reformer effluent. However, internally reforming systems such as FCE's MCFC product line would require complex and capital intensive BOP designs to obtain a hydrogen rich stream for hydrodesulfurization. Thus, hydrodesulfurizaton was not further pursued by FCE. Selective catalytic oxidation likewise was not further pursued due to system complexity and high capital cost. Sulfur removal by adsorption was selected as the optimal strategy.

Sulfur adsorbents can be broadly categorized as having chemisorption or physisorption mechanisms. Chemisorption involves valence forces where the electronic states of the adsorbent and adsorbed species are altered due to the exchange or sharing of electrons, resulting in the adsorbed species changing into a new chemical. Physisorption involves intermolecular forces (van der Waals forces) where the adsorbent and the adsorbed species are attracted to each other because of polarizations in their molecules. To further clarify the distinction, when a physisorbed species is desorbed from its adsorbent, it is still the same chemical compound as before it was adsorbed. A chemisorbed species that is released, however, would be a new compound.

Sulfur compounds present in pipeline natural gas are a combination of those that occur naturally and those that are inputted by the natural gas industry as odorants to facilitate human detection of leaks. The types and quantities of sulfur compounds encountered in natural gas varies widely according to geographic region of origin, distributor company, and season of the year. Whereas hydrodesulfurization systems are generally robust to all combinations and quantities of sulfur compounds likely to be encountered in pipeline quality natural gas, adsorbent systems need to be tailored to local natural gas quality. Further, the local quality must remain relatively stable to

ensure the adsorbent system is optimal, or at the very least capable as sulfur introduction into anodes will quickly lead to system failure. Different natural gas mixtures require different combinations, types, and sequential orderings of chemisorption and physisorption adsorbents into a desulfurization system. FCE has conducted extensive lab and field experiments to determine optimal adsorbent system configurations for various qualities of natural gas.

FCE cites zeolite as the most commonly used physisorption adsorbent used in their desulfurization systems.[2] Zeolite is a family of nearly 200 naturally occurring and synthetic aluminosilicates having two important properties for separating and sequestering certain compounds. The first of these properties arises from the microporous nature of zeolite. With pore diameters on the same order as small molecules such as water, zeolites can behave as "molecular sieves" (another term used for zeolites) whereby small diameter molecules may pass through the pores of the zeolite while larger diameter molecules are excluded. Secondly, zeolites exhibit non-uniform charge distribution such that polar molecules are attracted by and adsorbed to the zeolite's surface. Zeolites may be impregnated with copper, silver, or other metals to enhance their adsorption capabilities. FCE indicates physisorption adsorbents have been found useful for removing dimethyl sulfide (DMS), a major sulfur contaminant in natural gas, as well as other mono-, di-, and tri-sulfides. Tetrahydrothiophene (THT) is also removed by physisorption adsorbents. Water is actually the most challenging of natural gas contaminants. In general, water decreases the sulfur trapping capacity of zeolite adsorbents by both blocking the adsorption of incoming sulfur compounds as well as causing previously trapped sulfur compounds to desorb. Increasing temperatures also generally decrease the sulfur trapping capacity of physisorption adsorbents as increasing temperature is accompanied by increasing molecular vibration and hence increasing propensity for disruption of van der Waals forces.

Metals on activated carbons or some other support are the most frequently used class of chemisorption adsorbents by FCE.[2] These adsorbents trap carbonyl sulfide (COS), hydrogen sulfide (H_2S), THT, mercaptans, and heavier di- and tri-sulfides. Hydrodesulfurization, in fact, is a chemisorption method where all sulfur compounds in a natural gas stream are first converted to H_2S and then reacted with ZnO (a chemisorbent) to form ZnS and H_2O. However, as previously mentioned, hydrodesulfurization first requires a pure stream of hydrogen which is not easily obtained with internally reforming fuel cells. Chemisorption generally improves with increasing temperatures while increasing moisture may either improve or worsen chemisorption depending on the adsorbent and sulfur species present in the natural gas stream.

Sulfur removal by adsorption is clearly a complex interplay between natural gas quality, temperature, adsorbent types, and adsorbent arrangements. To protect fuel cell anodes from sulfur poisoning, FCE uses a lead-lag system where a lead bed of adsorbent material, performing the bulk of desulfurization, is followed by a lag bed of adsorbent material that polishes the fuel stream exiting the lead bed. An example of a lead-lag desulfurization unit using varied adsorbent types is given in US Patent 7,063,762.[8] When the lead bed adsorbent is depleted, valves are switched in the fuel supply piping such that the lag bed becomes the new lead bed. The previous lead bed has its adsorbent material regenerated or replaced, and becomes the new lag bed. Adsorbents are replenished as needed over the course of the fuel cell's life and are thus an operation and maintenance cost. FCE has realized an 80% reduction in the overall cost of sulfur removal through extending the life and reducing the quantity of adsorbents used, as well as

through the concomitant reductions in labor, transportation, and disposal costs that accrue from using less adsorbent.[2] Nevertheless, sulfur removal remains the most significant maintenance cost incurred by MCFC owners, and is an important contributor to the overall high cost of electricity from these systems. First costs for sulfur removal are also significant, ranging from $400/kWe for the cleanest fuel supplies up to $3000/kWe for anaerobic digester gas cleanup.[3] Several opportunities for potential cost reductions related to desulfurization are recognized. Currently, adsorbents are replenished at regular intervals without strict knowledge of whether or not the adsorbent is fully depleted. The development of a low cost online sulfur detection system would allow full utilization of expensive adsorbents. In addition, a system shutdown mechanism responsive to sulfur breakthrough could prevent catastrophic system failure from sulfur poisoning. The identification of an adsorbent material which does not trap benzene and other aromatics would enable adsorbents to be classified as non-hazardous waste, enabling lower cost disposal.

3.3 HIGH LEVEL MANUFACTURING SYSTEM DESIGN

The manufacturing system design assumptions adopted for this study are depicted in a high level process flow diagram in Figure 3-5. Cathodes are assumed to be manufactured from powder starting materials with a doctor blade procedure followed by sintering. Electrolyte consisting of alkali carbonates and other additives is added to cells in sufficient quantity to ensure a long stack life. Cathode current collectors are assumed to be purchased from a supplier and modified in-house before being incorporated into bipolar plates. Anodes are manufactured using a tape casting procedure and then further strengthened with an anode support. Anode current collectors purchased from a supplier are loaded with reforming catalyst. Separator plates and wet seal rails, both purchased from a supplier, are joined in a welding step. Cathodes, cathode current collectors, anodes, anode current collectors, and separator plates with associated wet seal rails are then physically mated. Matrix layers, like anodes, are assumed to be manufactured using a tape casting procedure. Reforming units are assembled in-house and delivered to the stack and compress manufacturing cell along with matrices and mated electrode/current collector/bipolar plate assemblies. Stacks are manually assembled and compressed, followed by reactant manifolding, instrumentation, and incorporation into an insulated housing/vessel. Newly formed stacks undergo a conditioning step where anode and matrix tape binders are combusted and/or volatilized out of the stack. Also during the conditioning step, electrolyte migrates into the matrix and the nickel cathodes are oxidized and lithiated. Conditioned stacks are sent to customer sites and integrated with BOP components. In the following sections, some of the challenges specific to these manufacturing steps are examined in further detail.

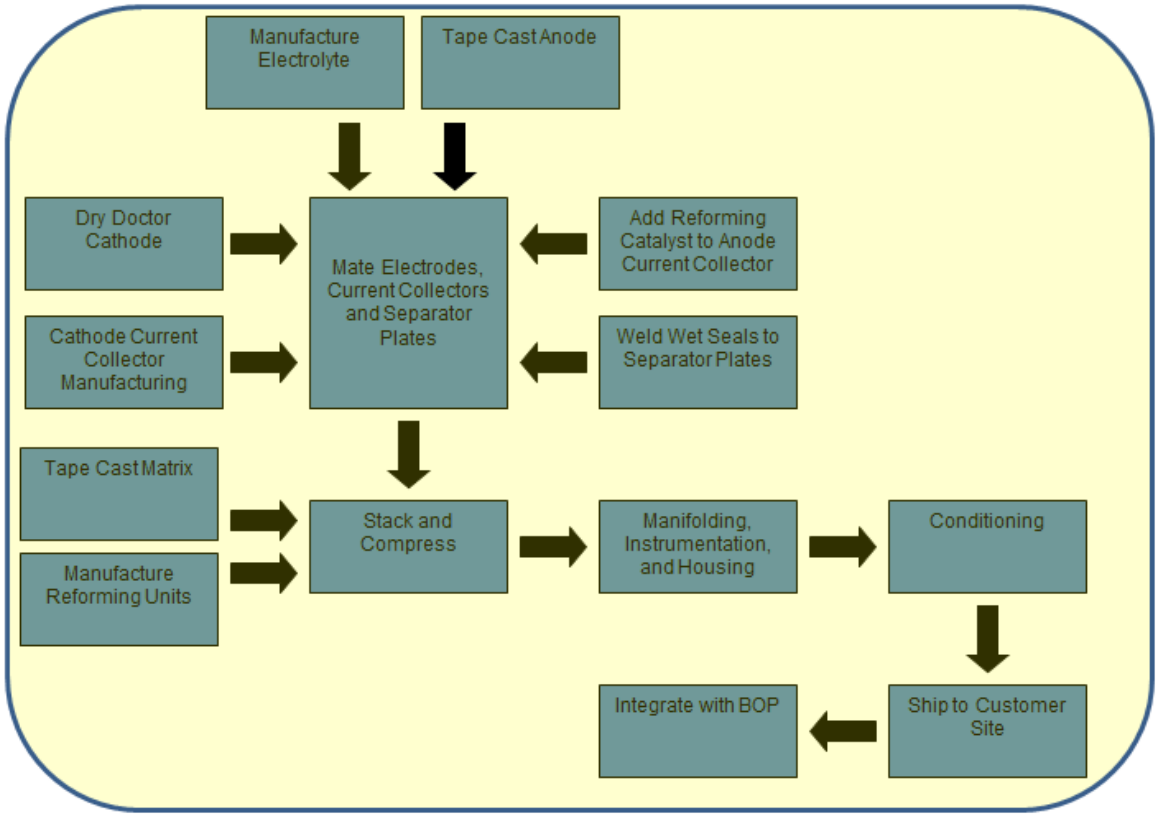

Figure 3-5. MCFC High Level Manufacturing Process Steps

3.4 CATHODE MANUFACTURING

That lithiated nickel oxide has been the cathode material of choice for decades belies the fact that cathodes present one of the greatest challenges in MCFC technology. This challenge, referred to as cathode dissolution, is a process whereby, slowly, over time, the cathode material (NiO) is dissolved into the molten electrolyte. NiO dissociates into Ni^{+2} and O^{-2}. The oxide ion is free to combine with a carbon dioxide molecule to form a carbonate ion as in reaction (4) in Figure 3-1. Indeed, the rate of cathode dissolution is well known to increase with, among other factors, an increasing partial pressure of carbon dioxide in the cathode.[9] The Ni^{+2} ion liberated in the dissociation of NiO could potentially remain solvated in the electrolyte indefinitely except that a highly reducing environment exists in the portion of electrolyte adjacent to the anode. Here, Ni^{+2} can be reduced by hydrogen to uncharged, nickel atoms which precipitate as solid nickel metal in the matrix. Over time, a bridge of nickel metal is created from successive precipitation reactions. The bridge traverses the matrix and creates an electrical short between the anode and the cathode, ultimately leading to cell failure.

Numerous factors influence nickel oxide's propensity to solvate. These include electrolyte pH and composition, operating temperature and pressure, current density, and the quantities and relative concentrations of the gases introduced into the cathode.[6] In general, cathode dissolution is minimized with increasing pH, sodium (as opposed to potassium) carbonate for the

electrolyte material, increasing temperature, decreasing pressure and current density, and relatively lean carbon dioxide and oxygen concentrations.

MCFC developers examined various strategies that led to the successful mitigation of cathode dissolution to the extent that the goal set for commercial viability (deemed to be a 40,000 hour stack life) became attainable. Perhaps the most important of these strategies is the use of additives to the electrolyte bulk materials to raise the electrolyte pH, resulting in a reduced propensity for nickel oxide to dissolve.[10] Alkaline earth metal carbonates or oxides, such as magnesium oxide (MgO), are frequently incorporated into electrolyte bulk materials to achieve this effect. Other strategies have been shown to be effective but are generally cost prohibitive from a materials or manufacturing standpoint, or they show only marginal improvement. These include the use of other electrolyte additives such as potassium tungstate and lanthanum oxide; the use of cathode additives such as iron and magnesium oxide; the use of cerium oxide as a coating on nickel oxide cathodes; and the use of cobalt based materials as either a coating on a nickel oxide cathodes, or as the bulk cathode material itself in place of nickel oxide.[6] Exact cathode and electrolyte compositions used by MCFC developers and manufactures are proprietary.

Yuh and Li describe a dry doctor blade procedure useful for manufacturing anode supports which is similar to the cathode manufacturing process assumed in the present study.[13] A dry, metallic nickel powder bed of predetermined thickness is assumed to be formed using a doctor blade procedure. Next, this powder bed is sintered with heating in a reducing atmosphere, resulting in an interconnected porous cathode. Thus, while anode and matrix tapes may be sintered in-situ as described in section 3.3, cathodes formed with a dry doctor procedure would require sintering before being incorporated into cells.

3.5 ELECTROLYTE MANUFACTURING

State of the art MCFC technology typically uses one or both of $(62K/38Li)CO_3$ and $(50Na/50Li)CO_3$ as the base electrolyte material. Electrolyte material may be purchased from a supplier or manufactured in-house. An example process for manufacturing electrolyte mixtures from raw materials can be found in the publicly available patent literature. Lucas and Doyon describe a process and apparatus useful for making either of the above mentioned electrolyte materials, including ones containing any of the common alkali earth metal carbonate or oxide additives useful for decreasing cathode dissolution.[4] Electrolyte raw materials, for example K_2CO_3 and Li_2CO_3, plus any additives, are blended at the appropriate ratios and fed into a heated vessel where the raw materials are melted to become a homogenous mixture. Molten material is allowed to drip from the bottom of the heated vessel onto a continuously rotating cylindrical roller which is internally cooled with water. A provision is made in the drip nozzle/heated vessel assembly whereby the molten carbonate enters the drip nozzle above a contaminant layer. Contaminants such as chlorine and sulfur present in commodity electrolyte raw materials can be reacted with metal containing foams, forming a complex which is heavier than the molten electrolyte. The contaminants sink to the bottom of the heated vessel at a level lower than the drip nozzle entrance. Upon contacting the cooling roller, the molten electrolyte solidifies into flakes which loosely adhere to the roller. The rotating action of the roller brings the solidified

material into contact with a blade that scraps the material off the roller. The falling material is collected and conveyed to a grinder to reduce the flakes to a small particle size powder. Figure 3-6 is a simplified diagram of the electrolyte manufacturing process described in the aforementioned patent.

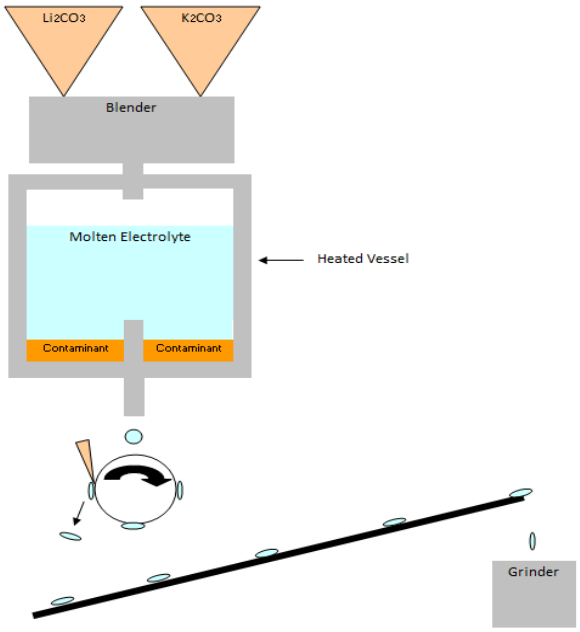

Figure 3-6. Manufacturing of MCFC Electrolyte from Raw Materials

3.6 ANODE MANUFACTURING

Early generation MCFC anodes were unalloyed porous nickel. These were abandoned as it was discovered that the compressive load of a full stack in operation caused anode creep, resulting in reaction surface area loss and hence reduced performance. Modern anodes use nickel alloyed with chromium and/or aluminum to produce anodes that are mechanically strong, electrochemically active, and cost effective.[11,12] FCE has indicated the use of nickel alloyed with aluminum in their manufacturing process to create anodes contributing only a small fraction to total system cost.[5] In general, MCFC anodes are deemed to be satisfactory with respect to performance, reliability, and cost, and as such are among the components least in need of improvement.

An example process for anode manufacturing is described by Doyon whereby nickel alloy constituents are blended into a slurry and then cast into a tape.[12] The green tape is laminated together with a preformed, porous nickel anode support. The anode support provides additional mechanical strength to the anode while retarding electrolyte creepage, which would result in poisoning of the reforming catalyst included in anode current collectors. The anode support may be a perforated nickel plate or a nickel wire mesh. Alternatively, the anode support may be a nickel plaque which is manufactured with a nickel powder dry doctoring and sintering process similar to that described in section 3.4 for cathode manufacturing.[13]

3.7 CURRENT COLLECTOR MANUFACTURING

Current collectors are corrugated sheets of stainless steel serving the dual purposes of conducting electrons and providing pathways for gas exchange. Material selection and manufacturing of current collectors are important drivers of MCFC reliability and cost challenges. Both cathode and anode current collectors have the reliability requirement of needing to withstand exposure to highly corrosive molten alkali carbonate. However, the requirements of anode and cathode current collectors differ in that the anode current collector's environment is fuel-rich and reducing, whereas the cathode current collector's environment is oxidant-rich and oxidizing. Thus, the optimal cathode current collector system may not be the optimal anode current collector system and vice versa. One source lists approximately 70 different alloys (including iron based, nickel/cobalt based, and aluminum based alloys) which have been examined by MCFC developers as current collector and/or separator plate materials.[6] Among these different materials, the 300 series (austenitic) stainless steels have emerged as one of the most acceptable. Both cathode and anode current collectors have been manufactured with austenitic stainless steels.

Cathode current collector manufacturing is closely related to what is widely recognized as one of the greatest challenges in MCFC technology, electrolyte loss. Recently published patent literature indicates that as much as 65% of all electrolyte lost in an MCFC's lifetime is due to electrolyte corrosion of the cathode current collector and the cathode side of the separator plate.[14] This corrosion produces an oxide scale which in turn leads to 25% of the internal electrical resistance realized in these fuel cell systems, significantly penalizing electrical efficiency. MCFC developers have sought to mitigate the corrosion of cathode-side hardware through various means. Baseline material choice is obviously important. Coatings are also used to slow cathode hardware corrosion. For example, in the same patent mentioned above, lithiated NiO, or alternatively, the ceramic LSC ($La_{0.8}$ $Sr_{0.2}$ CoO_3) may be applied with a spraying or dipping sol-gel process for improved corrosion resistance while maintaining high electrical conductivity. Because electrolyte loss due to corrosion has been shown to be proportional to the surface area of current collectors and separator plates, MCFC developers have also implemented strategies for reducing the surface area of these components.

Historically, the anode current collector has been clad with Ni to impart added corrosion resistance. The high cost of the Ni cladding process prompted researchers to examine other means for protecting anode current collectors. FCE indicates the use of advanced material, high temperature alloys that are not nickel clad for both cathode and anode current collectors.[5] Molten carbonate fuel cells which employ both direct and indirect internal reforming such as the DFC® product line typically have reforming catalyst loaded into their anode current collectors. Optimal catalyst/current collector systems are being actively pursued as evidenced in the patent literature.[17,18] Specifically, the catalyst should have a physical shape and be oriented in the current collector in such a way that minimizes fuel pressure drop and distributes fuel as evenly as possible within individual cells and throughout the stack as a whole. Catalyst may adopt a tablet, pellet, rod, ring, spherical or other shape, and may be oriented in an infinite number of ways with respect to the direction of fuel flow. The catalyst also should be shielded as much as possible from the electrolyte (liquid and vapor) as electrolyte poisons the catalyst. Catalyst surface area exposed to fuel should be maximized to ensure efficient utilization of the catalyst. Finally, from

a manufacturing cost standpoint, is desirable that the catalyst and current collector be designed in such a way that catalyst may be cost effectively incorporated into the current collector.

Patent literature indicates that current collectors may be augmented with perimeter baffling to minimize wet seal integrity disruption by flowing gases, as well as to force gases to remain in the active portions of the cell.[15] These baffles may be formed by adding materials, such as ceramics, to the corrugated sheet, or by a stamping process where portions of the corrugation itself are raised and turned to form a flap. Another possible function for current collectors as described in the patent literature may be to serve as substrates for holding additional electrolyte which is delivered to the matrix to replenish electrolyte lost from cells over the course of the fuel cell's life.[16,26]

3.8 BIPOLAR PLATE MANUFACTURING

In this model, a bipolar plate is defined as consisting of a central separator plate with associated anode and cathode wet seal rails and current collectors. Fuel and oxidant are precluded from entering cathodes and anodes, respectively, with a separator plate and wet seals. Typically, separator plates are thin, flat, stainless steel sheets. The separator plate occurs between the cathode and anode current collectors of adjacent cells, and thereby provides a physical barrier precluding the mixing of fuel and oxidant. Separator plates have the additional task of conducting electrons from the anode of one cell to the cathode of the adjacent cell. A wet seal is formed where the matrix layer, filled with molten carbonate during operation, contacts a metallic wet seal rail, creating at the matrix/rail interface a gas impermeable barrier of liquid which is held together by cohesive and surface tension forces. Figure 3-7 is a simplified illustration of the mechanism of wet sealing with the blue lines representing the wet seal.

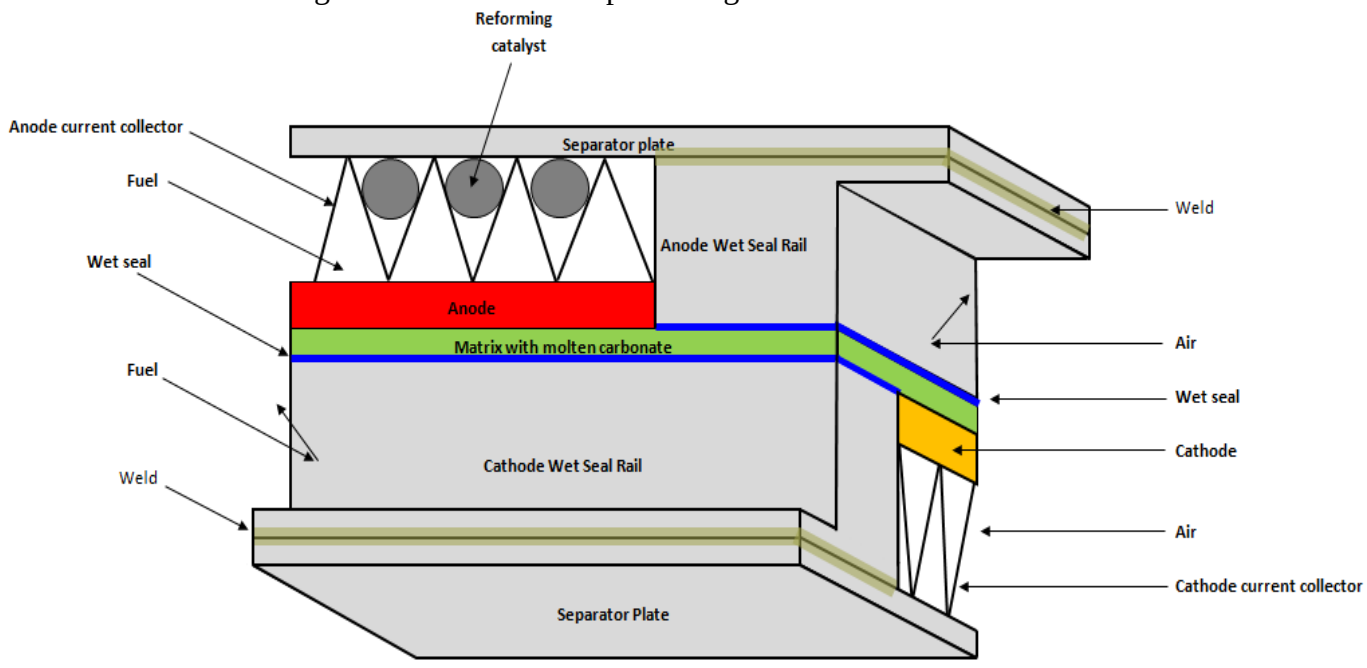

Figure 3-7. MCFC Wet Seal

Like current collectors and separator plates, wet seal rails must be comprised of materials resistant to corrosion by molten carbonate in both oxidizing and reducing environments. However, the constraints on wet seal materials are eased somewhat in that, unlike current collectors and separator plates, wet seal rails do not have the additional requirement of needing to be electrically conductive. Alumina forming alloy powders applied as a coating over low cost stainless steel wet seal rails have been shown to be sufficiently stable in molten carbonate environments. FCE indicates that a low cost aluminizing process has been identified after exploring various technologies for applying the coating including slurry painting, vacuum deposition, and thermal spraying.[5]

Li et al. describe a bipolar plate manufacturing process where aluminized wet seal rails are welded to stainless steel separator plates having a Ni-clad or other protective coating.[19] As can be appreciated from Figure 3-7, the wet seal rails form pockets into which electrode and current collector ends fit. Furthermore, the matrix-facing surface of an electrode is planar with its wet seal rails such that a continuous flat surface is created, allowing the adjacent matrix to contact both the electrode and wet seal rail simultaneously. A wet seal develops at the matrix/rail interface at operational temperatures.

3.9 ELECTRODE/CURRENT COLLECTOR/BIPOLAR PLATE MATING

As shown in Figure 3-5, cathode, cathode current collector, electrolyte, anode, anode current collector, and bipolar plate manufacturing all converge at a mating step where these components are integrated into a single, easily manipulated unit that is delivered to the stack assembly manufacturing station.

3.10 MATRIX MANUFACTURING

Lithium aluminate ($LiAlO_2$) has been the matrix material of choice for decades with the alpha allotrope being preferred by most MCFC developers over the beta and gamma allotropes. Among the three, the alpha allotrope has the smallest rate of particle growth. Particle growth is undesirable as this leads to an increase in mean pore size and hence reduced ability of the matrix to retain electrolyte.

Matrix material may be purchased from a supplier or manufactured in-house. It is recognized that substantial cost reductions could be realized by optimizing the manufacture of this material as its cost can be greater than 10 times the cost of the raw materials from which it is produced, traditionally Li_2CO_3 and Al_2O_3.[5] Recent patent literature attests to the need to reduce the cost of producing α-$LiAlO_2$, and describes a novel manufacturing technique whereby high purity α-$LiAlO_2$ is produced by first mixing Li_2CO_3 and $Al(OH)_3$ and then heat treating at 500-800^oC for 18-48 hours.[20] This procedure represents an improvement over prior processes in that it eliminates a washing step, saving time, reducing the probability of introducing impurities, and reducing particle agglomeration.

Improving matrix strength is a research focus area. Typically, a matrix is supplied to the stack in

a "green" state meaning that is held together by organic binders. During initial stack warm-up, these binders are burned off at a temperature lower than the melting point of electrolyte. In the interim temperatures between binder burn off and electrolyte melting, i.e. when the matrix is largely devoid of both binders and electrolyte, the matrix is particularly susceptible to cracking from mechanical and thermal stresses. Additional stresses would also occur over the fuel cell's lifetime due to cycling, uneven temperature distributions, and shut downs. Steps taken to increase matrix strength have included the incorporation of ceramic fibers, metal wire mesh screens, or metal particles having a platelet or spherical shape. Huang and Yuh describe a low cost method for manufacturing a mechanically strong matrix by tape casting an organic slurry of $LiAlO_2$ containing reinforcement additives for strength and alkali earth additives for decreased NiO dissolution from the cathode.[21] The slurry was prepared with high energy milling and mixing such as with attrition milling, fluid energy milling, and/or ball milling. Multiple tapes may be laminated together to achieve the desired matrix thickness.

3.11 REFORMING UNIT MANUFACTRUING

Indirect internal reforming is accomplished with reforming units, plate shaped structures loaded with reforming catalyst and placed directly in the stack. They are interspersed between cells at a regular interval of one reforming unit for each group of 4 to 8 cells. Fuel outputted from a prereformer is introduced into the reforming units where the majority of the methane will be converted to hydrogen. Fuel outputted from reforming units is introduced into the anodes of cells where the remaining methane is reformed to hydrogen. The hydrogen is electrochemically reacted with carbonate anions to form water and carbon dioxide with two electrons liberated (see reactions 1 through 3 in Figure 3-1).

Several benefits accrue from internal reforming. First, reforming units are less complex and less costly than external reformers, and thus help to lower the overall cost of fuel cell systems. In addition, a nearly 100% conversion of methane to hydrogen can be realized when indirect and direct internal reforming are coupled as the reforming reactions (1 and 2) in Figure 3-1 are driven to the right by Le Chatelier's Principle when hydrogen is consumed in the fuel cell electrochemical reaction (3). Also, stacks are cooled by the endothermic reforming reaction, which translates into smaller cooling demands placed on the cathode blower, which further translates into smaller parasitic loads and a gain in net electrical efficiency.

A closer look at the cooling effect of internal reforming shows that stack cooling with reforming units can be targeted to specific areas of the stack where temperatures are naturally higher by carefully controlling the distribution of catalyst within reforming units. Figure 3-8 is a simplified representation of a reforming unit developed by FCE and described by Ma et al.[22]

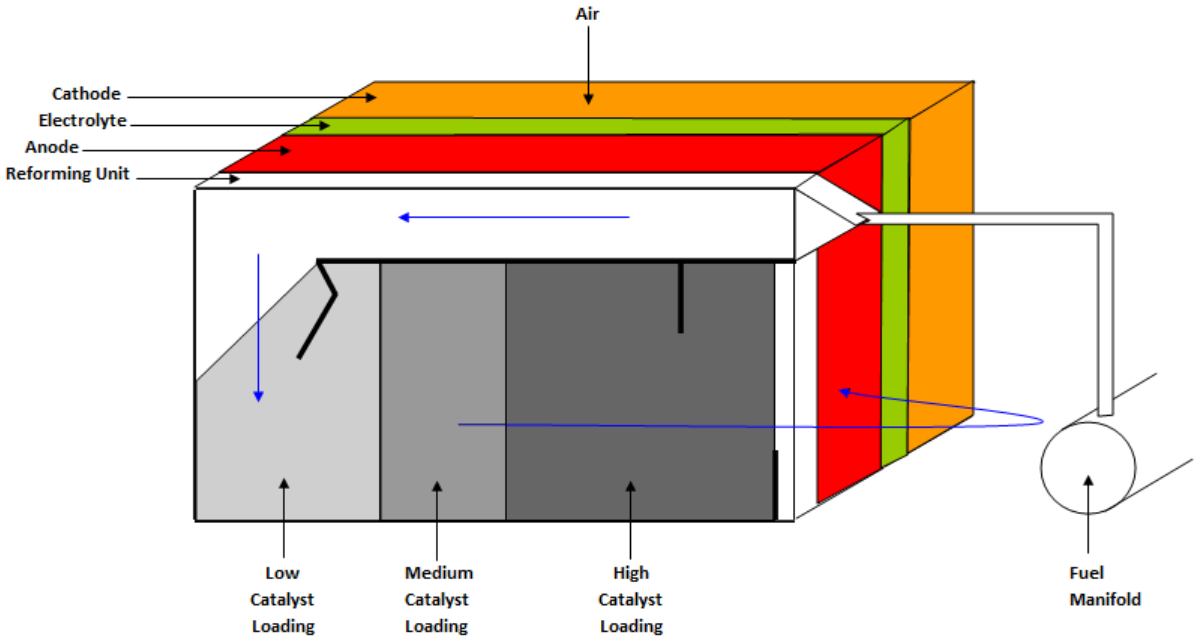

Figure 3-8. MCFC Reforming Unit

In this design, fuel exits a header and passes through tubing to a plenum connected to the reforming unit entrance. The reforming unit itself consists of a housing made of sheet metal foils. Inside the housing are plates of corrugated sheet metal. The housing walls and internal baffles direct fuel flow in a substantially U-shaped pattern through the reforming unit as shown by the blue arrows. The first leg of the fuel path through the reforming unit is uncatalyzed and thus no reforming takes place in this section. The fuel stream, however, is warmed in this section in preparation for the reforming reaction with heat transferred from air flowing into the cathodes of cells adjacent to the reforming unit. The second leg of the fuel path has a relatively low catalyst loading and is where the fuel reforming reaction is initiated. Catalyst loading increases from medium to high along the third and last leg of the fuel path through the reforming unit, with the highest degree of cooling occurring in the high catalyst loading section. Moreover, baffles perpendicular to the direction of fuel flow in this section are incorporated to augment fuel flow such that the area of maximum indirect internal reforming (and hence cooling) is shifted somewhat more to the center of the stack than would be otherwise. Reformed fuel exits the reforming unit and an external manifold (not shown) directs fuel into the anodes adjacent to the reforming unit. The hydrogen rich fuel stream (shown entering the anodes from the right) is quickly reacted in the fuel cell electrochemical reaction such that the highest current density and heat generation is observed in the right half of the cells. It is also in this section where the remaining methane undergoes direct internal reforming, providing additional stack cooling. Strategic placement of catalyst thus results in a desirable overlapping of the areas of high reforming (cooling) with the areas of high electrochemical reaction (heat generation). By doing so, heat is more effectively removed from the area of high current density. Thus, local temperatures in the high current density area are reduced, enabling improved system efficiency.

3.12 STACK AND SYSTEM ASSEMBLY

The remaining portions of the MCFC manufacturing model are assembly processes where outsourced stack and BOP components are integrated with the components the MCFC manufacturer has produced. As can be appreciated in Figure 3-6, electrode/current collector/bipolar plate assemblies, matrices, and reforming units are all delivered to the stack and compress manufacturing station. Here, these components are layered one on top the other in a pattern similar to that shown in Figure 3-9 with a reforming unit included for each group of 4 to 8 cells.

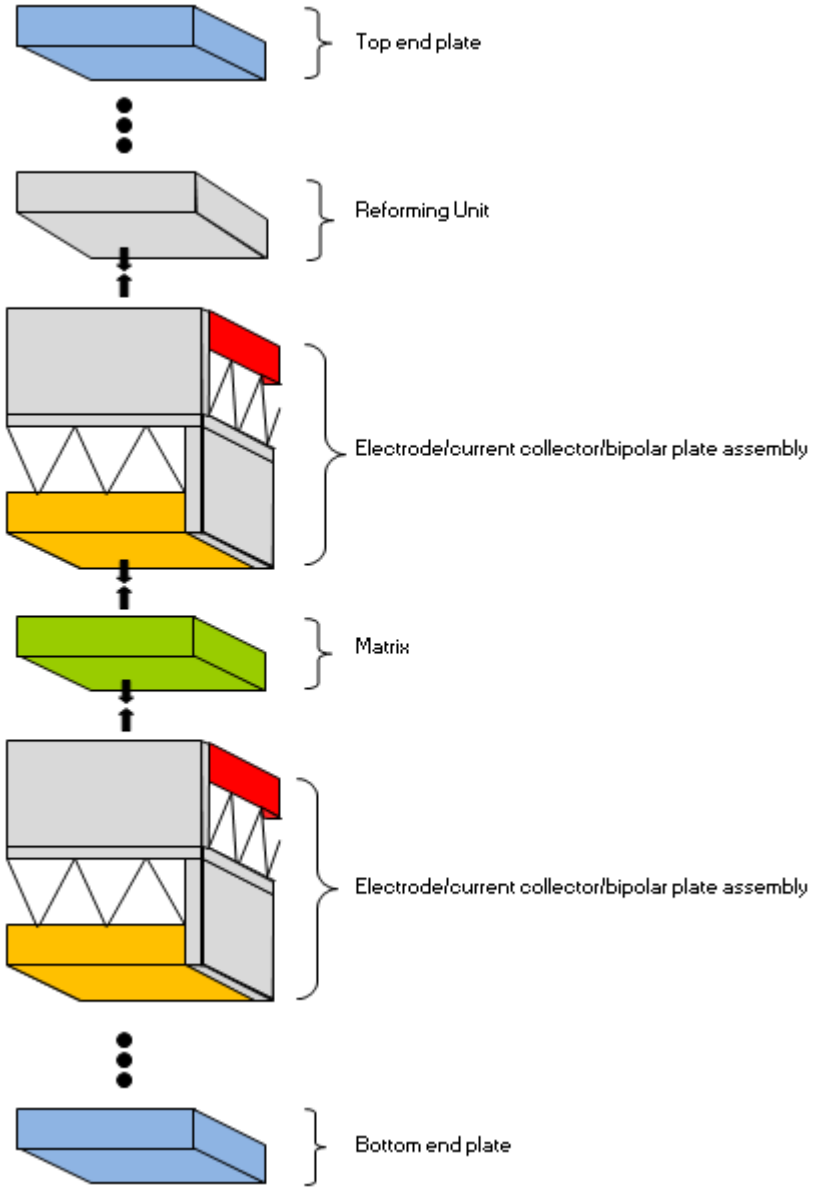

Figure 3-9. MCFC Stacking Process

End plates are incorporated at the top and bottom of the stack. Compressive force must be applied to the stack to insure good electrical contact between the conductive surfaces. Moreover,

this compressive force must be adjustable over the course of the stack's life as the stack shrinks with time due to creepage. An exemplary stack compression design is given by Blanchet.[23] In this design, compressive force is generated by springs. Springs beneath the stack communicate the compressive force through rods connected to a compression plate on top of the stack. The compressive force is in turn communicated downwardly through the stack and against a bottom compression plate.

After the compressing step, a header for supplying fuel to the reforming units is assumed to be coupled with the fuel feeder tubes and plenums as shown in Figure 3-9. External manifolds for fuel and oxidant supply are joined to the stack along with gaskets to seal the manifold/stack interfaces. Instrumentation for assessing stack performance and conditions is added, and the stack is incorporated into an insulated housing. Next, the stack is integrated with a complete balance of plant present at the manufacturing facility where the stack undergoes initial warm-up and a conditioning phase. In this conditioning phase, a variety of processes transpire including anode and matrix binder burn out, matrix impregnation with electrolyte, and corrosion reactions of electrolyte with stainless steel stack hardware. Following the conditioning phase, stacks and BOP components are shipped to the customer's site where all piping, wiring, and other connections are made and the system is commissioned. Arneson et al. may be referenced for a detailed description of a loading tool useful for inserting a BOP module into a container that serves as both its shipping container and its permanent housing at the customer site.[24]

3.13 MODEL RESULTS

For MCFC specifically, limited discussion of manufacturing processes and model results is given due to the proprietary nature of information disclosed to ORNL by FCE. Cost results are presented in relative terms.

The baseline production volume of 20 MWe/yr was assigned a relative value of 1.00 for total manufacturing cost. For annual production volumes of 5, 50, and 500 MWe/yr, total manufacturing costs are estimated to be 1.40, 0.87, and 0.81, respectively, as shown in Figure 3-10.

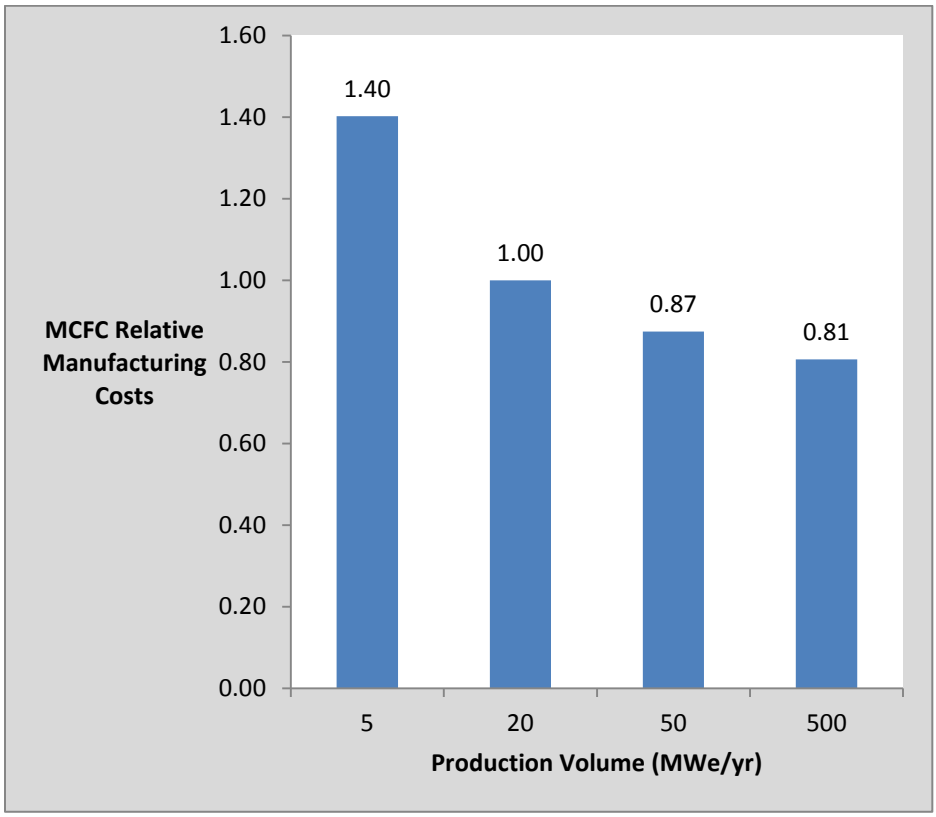

Figure 3-10. Relative Total MCFC Manufacturing Costs for Varying Production Volumes

As with PAFC, the total manufacturing cost curve follows a hyperbolic pattern, reaching a limiting value of approximately 0.81 for annual production volumes in excess of several hundred MWe/yr. Manufacturing costs for the low volume scenario of 5 MWe/yr are estimated to be 40% higher than the baseline production volume of 20 MWe/yr. Furthermore, manufacturing costs may be expected to decrease by approximately 19% just by increasing production volume from 20 MWe/yr (i.e. roughly equivalent to FCE's recent annual production volume) to 500 MWe/yr even if manufacturing technology is assumed unchanged (i.e. production lines are replicated in parallel) and no learning curve is experienced. As production volume increases from 5 to 500 MWe/yr, cost reductions accrue from:

- reduced contribution of fixed costs (capital and floor space) to total system cost on a per unit basis.
- reduced indirect labor requirement (modeled as a decreasing percentage of direct labor as production volume increases).
- volume discounts on materials and components purchased from suppliers (developed in consultation with suppliers and with economy of scale factors).

In order to highlight how costs are distributed and where they are concentrated, total manufacturing costs were disaggregated into seven cost components - labor, energy, floor space, capital, cell materials, stack materials and components, and BOP components and subsystems. Definitions and assumptions pertaining to labor, energy, floor space, and capital costs are detailed in section 1.2. The remaining three cost components – cell materials, stack components and materials, and BOP components and subsystems - represent those items which are purchased from suppliers by the MCFC manufacturer. Utilizing capital, floor space, energy, and labor resources, the MCFC developer manufactures and assembles these purchased items into a fuel cell system. Figure 3-11, below, is an elaboration of Figure 3-10 in that total cost has now been disaggregated into the seven cost components mentioned above.

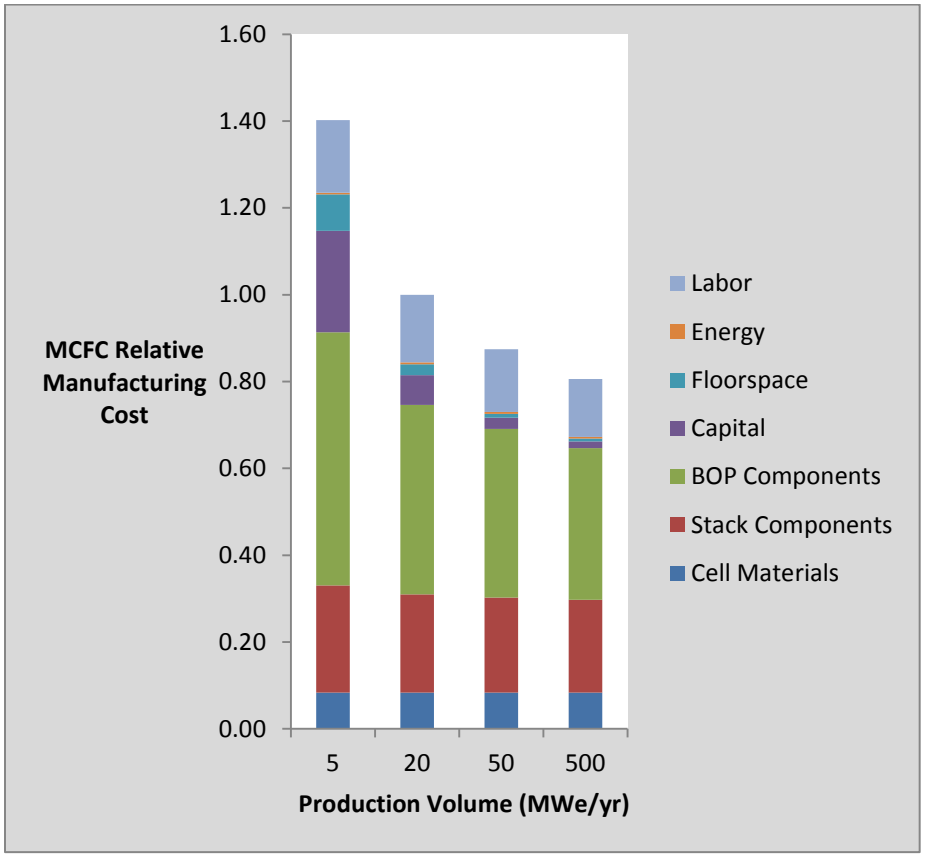

Figure 3-11. Relative Total MCFC Manufacturing Costs and Cost Components for Varying Production Volumes

It may be readily observed in Figure 3-11 that items purchased from suppliers (cell materials, stack materials and components, and BOP components and subsystems) collectively comprise the largest manufacturing costs incurred by the MCFC manufacturer. Figure 3-12, below, shows that purchased materials and components, when taken in aggregate, are estimated to constitute 65% to 80% of total manufacturing cost. The fixed costs of capital and floor space are noted to decrease in cost proportion with increasing production volume, while labor and energy costs remain more or less constant.

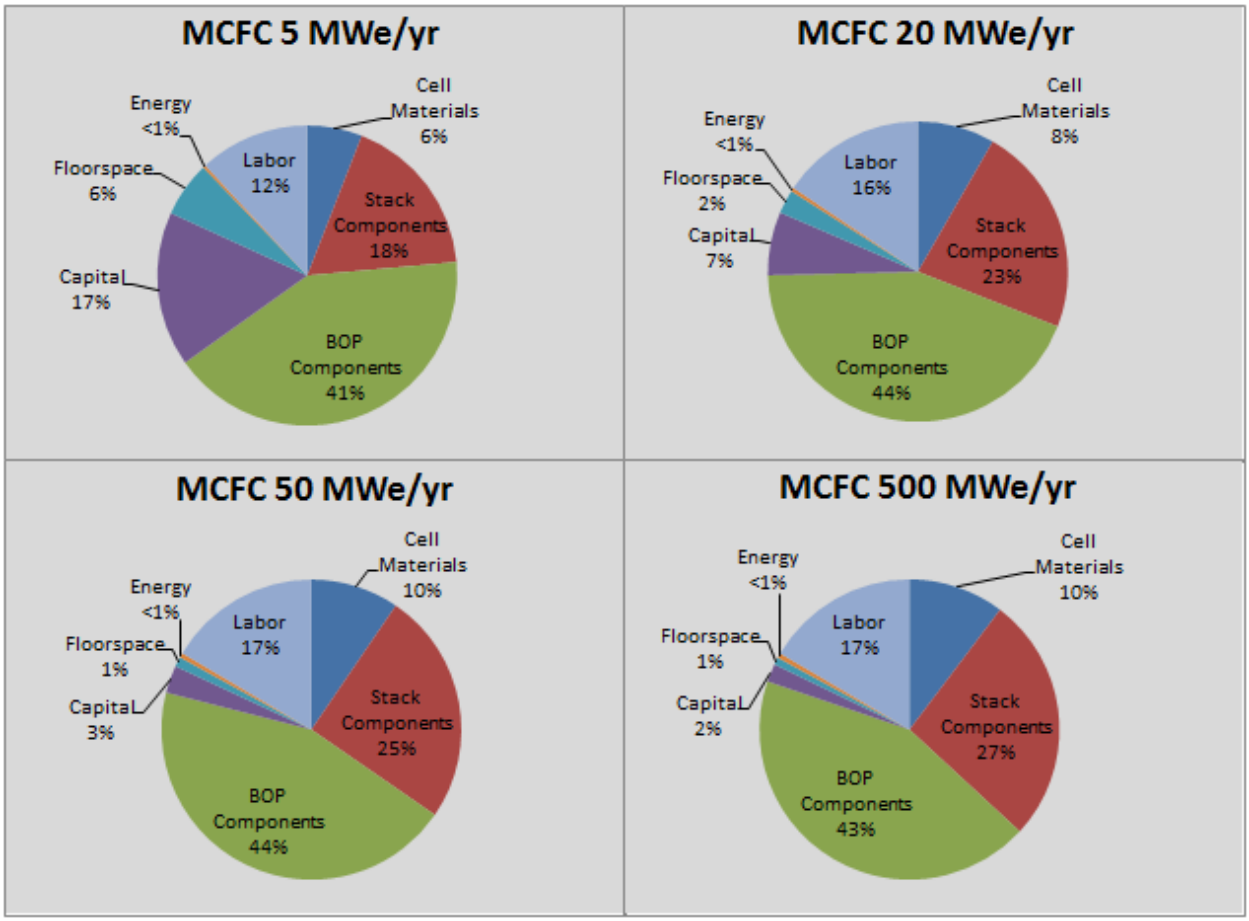

Figure 3-12. Total MCFC Manufacturing Cost Distribution for Varying Production Volumes

Figure 3-13 lists all manufacturing steps identified in this report, and the relative costs incurred at each step. Steps are grouped and classified according to component or task. For example, the cathode manufacturing steps are listed as A through F and appear under the heading "Cathodes." Steps are listed in a sequence which reflects the chronology of the actual manufacturing process, with first steps occurring at the top of the graph and final steps at the bottom. The relatively large contribution of items purchased from suppliers (cell materials, stack materials and components, and BOP components and subsystems) to total manufacturing cost is clearly reemphasized in this graph.

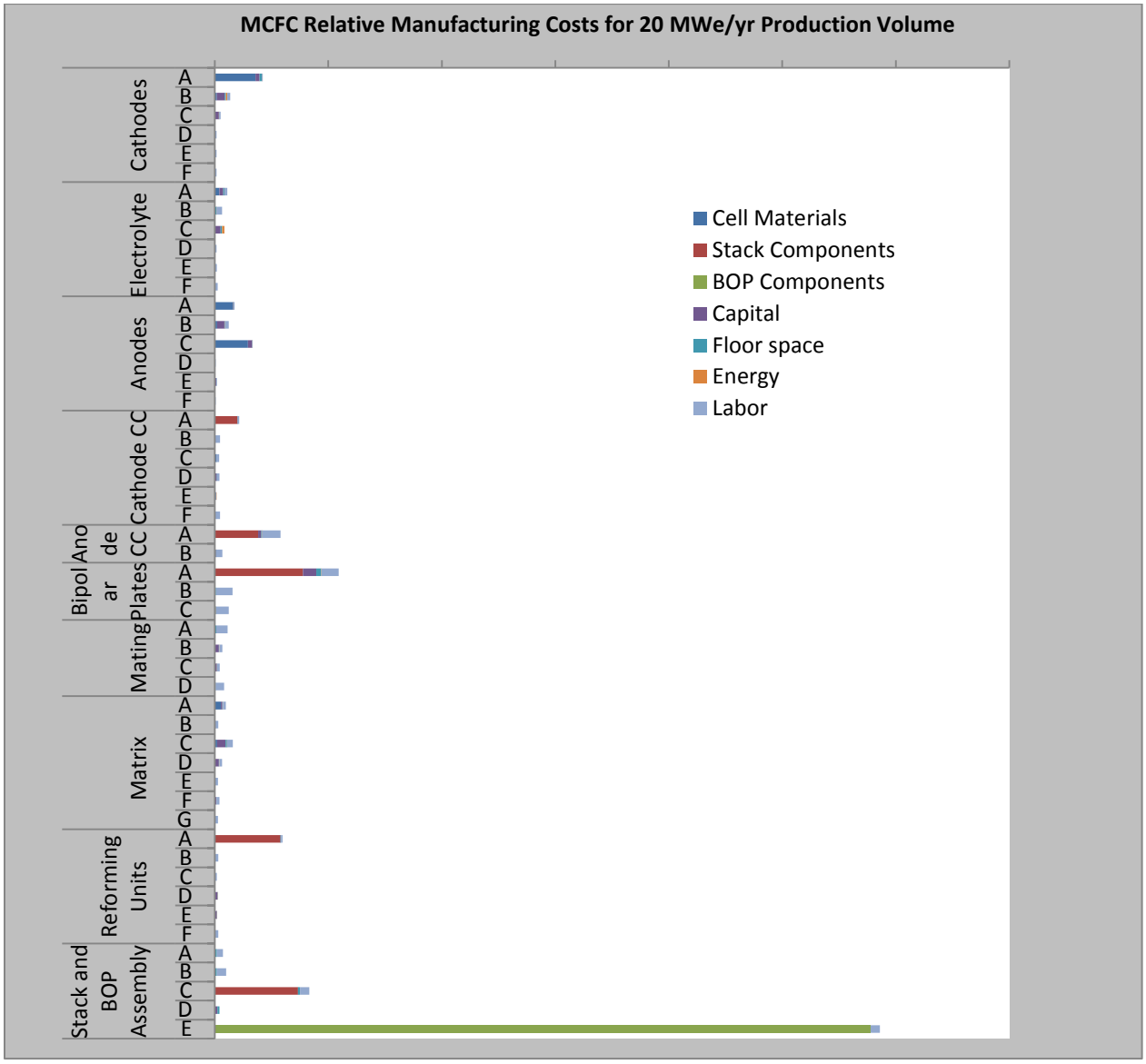

Figure 3-13. Total MCFC Manufacturing Cost Disaggregated by Process Steps and Cost Components for 20 MWe/yr Production Volume

As discussed previously, items purchased from suppliers are estimated to constitute roughly 75% of total system cost, implying the remaining cost components (i.e. capital, floor space, energy, and labor) are estimated to collectively represent approximately 25% of total costs. To better describe these cost components, Figure 3-14 lists all costs other than purchased item costs for each step in the manufacturing process. Figure 3-14 is completely analogous to Figure 3-13 above, with the exception that purchased item costs have been excluded, and the x-axis adjusted, to improve the graphical resolution of the remaining cost components.

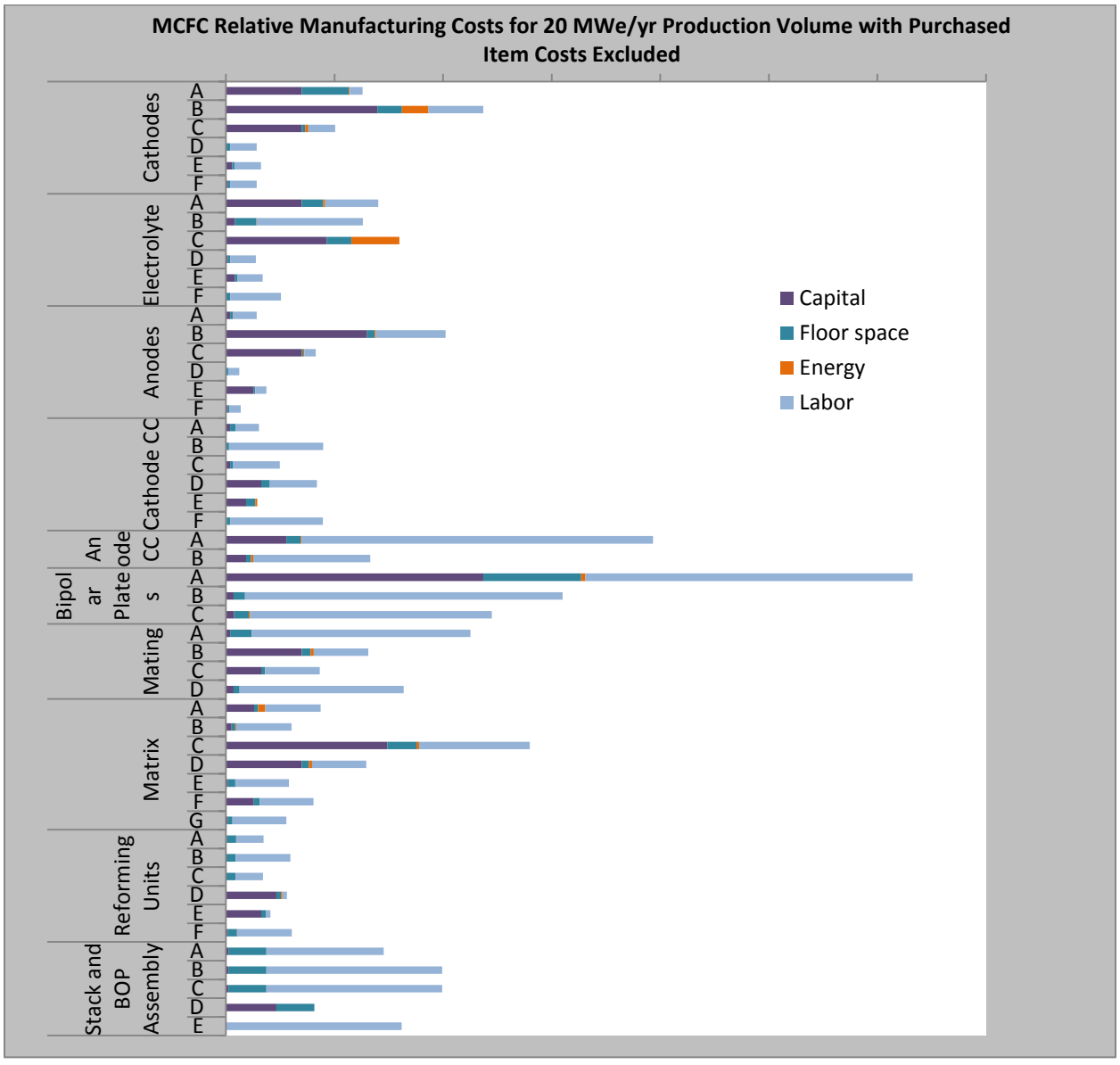

Figure 3-14. Total MCFC Manufacturing Cost Disaggregated by Process Steps and Cost Components for 20 MWe/yr Production Volume with Purchased Item Costs Excluded

The highest cost steps when purchased item costs are excluded from consideration are those steps associated with anode current collectors, bipolar plates, mating, and stack and system assembly. In these steps, high costs are largely driven by labor, suggesting opportunities for cost reductions through automation exist. Cell manufacturing (cathode, electrolyte, anode, and matrix) employs capital intensive doctor blade and other equipment, yet has generally lower costs due to labor saving automation. The highest energy costs can be observed in cathode and electrolyte manufacturing where high temperature heat treatment steps are used. The largest floor space costs are associated with bipolar plate, cathode, and electrolyte manufacturing, as well as stack and system assembly.

Figure 3-15, below, is an elaboration of Figure 3-10 in that total manufacturing cost is now disaggregated into cell, stack, and BOP costs. With reference to Figure 3-13, cell costs are defined as all costs associated with cathode, anode, matrix, and electrolyte manufacturing. Similarly, stack costs are defined as all costs associated with cathode current collector, anode current collector, bipolar plate, and reforming unit manufacturing, as well as all costs incurred for stack assembly, conditioning, and shipping to the customer's site. Finally, BOP costs are defined as all remaining manufacturing costs which include the purchase cost of BOP components and the costs for integrating stacks and BOP. As in Figure 3-10, the baseline production volume of 20 MWe/yr has been assigned a relative cost of 1.0, giving values of 1.40 and 0.81 for the low and high volume scenarios, respectively.

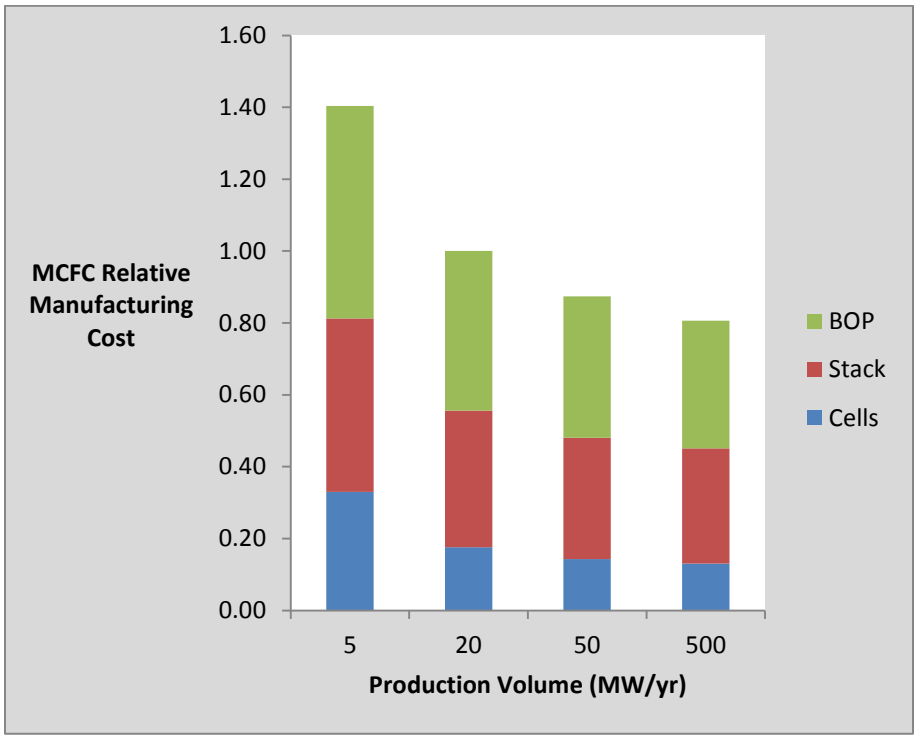

Figure 3-15. Relative MCFC Manufacturing Costs Disaggregated by Cell, Stack, and BOP for Varying Production Volumes

All three cost categories decrease in magnitude with increasing production volume. The distribution of cell, stack, and BOP costs, however, remains more or less constant as indicated in Figure 3-16. For production volumes equal to or greater than 20 MWe/yr, cell, stack, and BOP costs are approximately 16%, 40%, and 44% of total cost, respectively.

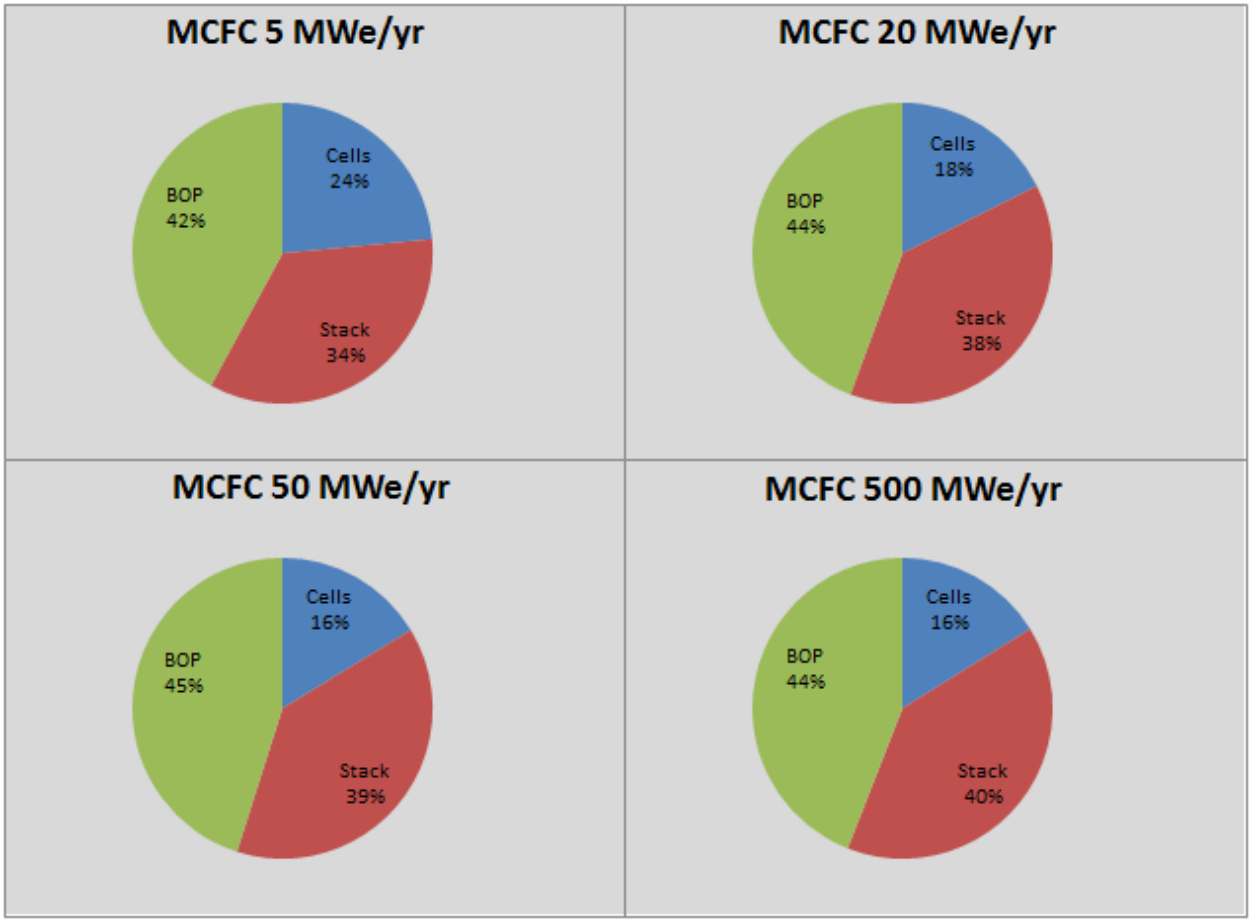

Figure 3-16. MCFC Cell, Stack, and BOP Cost Distribution for Varying Production Volumes

Monte Carlo simulation was performed to assess the impact of stochastic and uncertain inputs on cost estimation. For the baseline production volume of 20 MWe/yr, the pre-simulation point estimate for total manufacturing cost was assigned a value of $1.00. Figure 3-17 shows the outcome of a 10,000 trial simulation, resulting in an interval estimate of ($0.98, $1.04) with 90% confidence. Thus, the stochastic and uncertain inputs employed in this model produce an estimate whose margin of error equals approximately 3% of the estimated total manufacturing cost with 90% confidence after 10,000 trials. The cost distribution is unimodal, symmetrical, and bell-shaped.

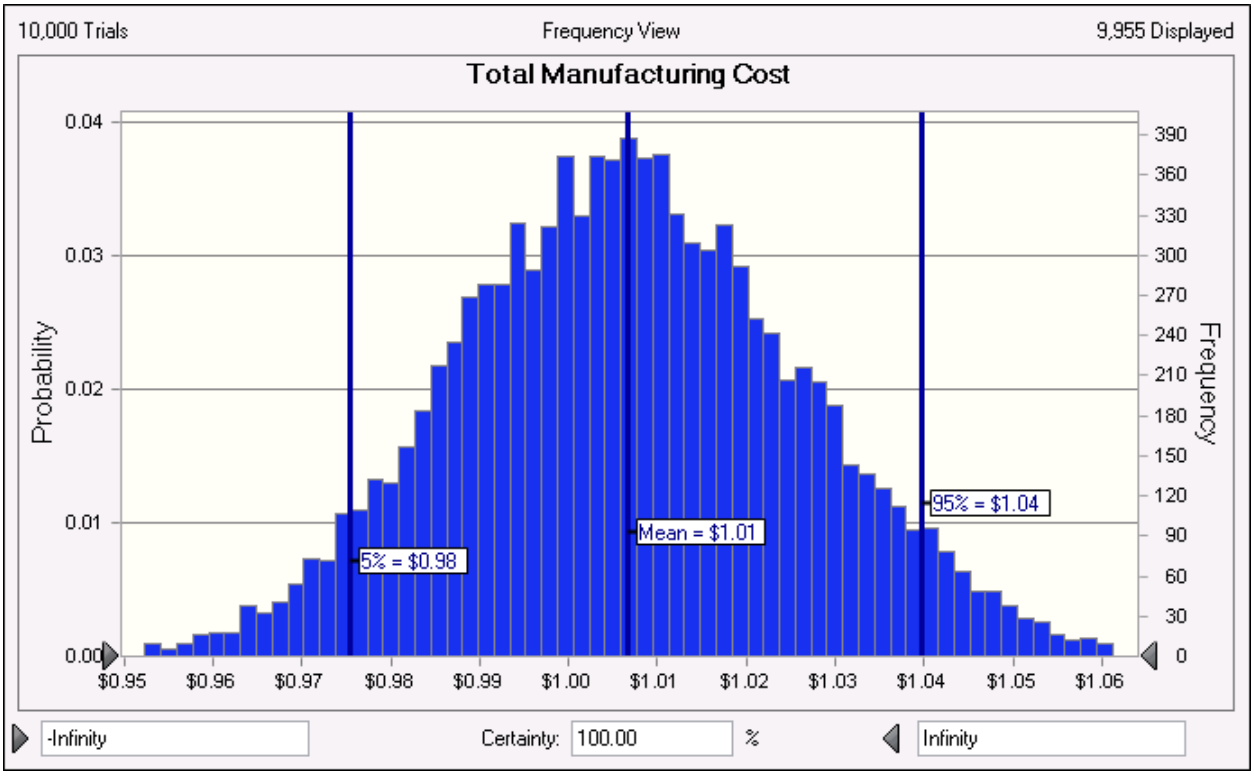

Figure 3-17. Monte Carlo Simulation of Total Relative MCFC Manufacturing Cost for 20 MWe/yr Production Volume

Sensitivity analysis, shown in Figure 3-18, shows that the market price of nickel and the desulfurizer cost constitute the majority share (about two-thirds) of model variance. MCFC costs are expected to be sensitive to the market price of nickel as this is the base material for cathodes, anodes, and anode supports. Following the market price of nickel is the inherent uncertainty in the purchase cost of the desulfurizer as this component must be tailored in each individual fuel cell system to the particular fuel feedstock that system will be utilizing. Manufacturing capital, the capital recovery rate, and stack and BOP assembly time complete the top five contributors to model variance. The final category listed in Figure 3-18 (i.e. "Other") is the collective contribution to variance of multiple other stochastic and uncertain inputs. These are not addressed in detail as their contribution to cost estimate variance is relatively small even when considered in aggregate. Although not modeled as a stochastic input in this analysis, the market price of stainless steel is also likely a substantial contributor to actual manufacturing cost variance. The probabilistic assumptions used for Monte Carlo simulation are listed in Table 3-2 with any proprietary details excluded.

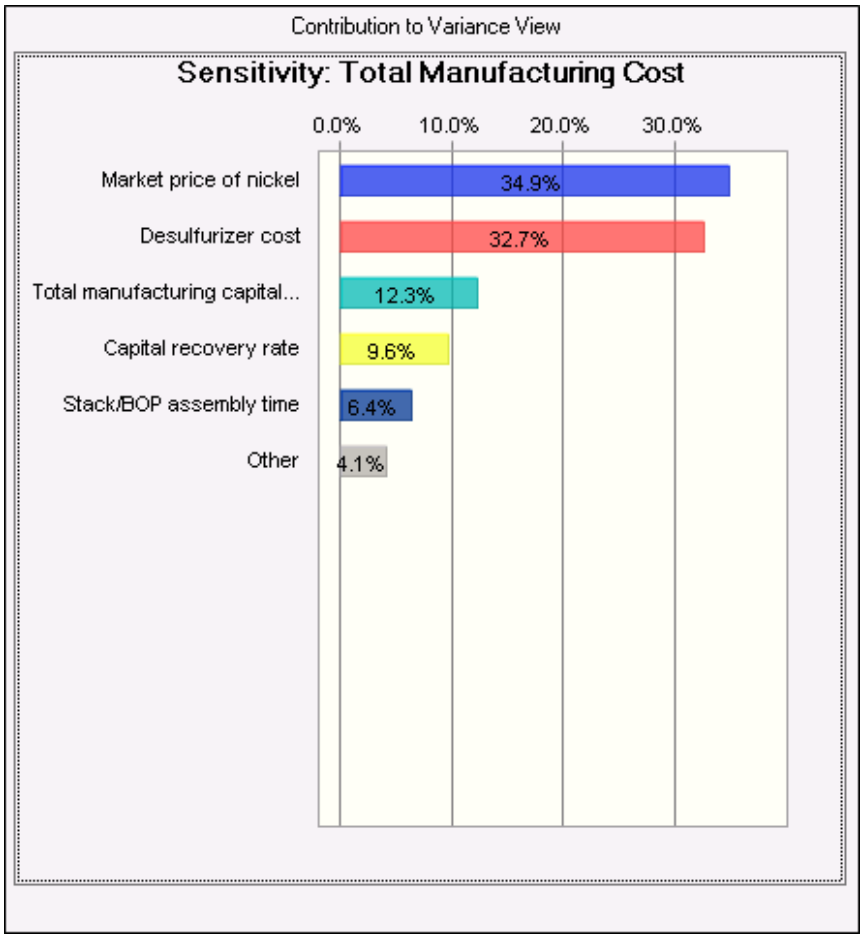

Figure 3-18. Sensitivity Analysis for Total MCFC Manufacturing Cost for 20 MWe/yr Production Volume

Table 3-2. Sensitivity Analysis Assumptions for Total MCFC Manufacturing Cost for 20 MWe/yr Production Volume

Variable	Distribution Family	Parameters	Units
Market price of nickel	Triangular	min = 4, most likely = 12, max = 24	$/lb
Desulfurizer cost	Normal	standard deviation = 10% of mean estimate	$
Total manufacturing capital cost	Normal	standard deviation = 10% of mean estimate	$
Capital recovery rate	Triangular	min = 8, most likely = 12, max = 18	%
Stack/BOP assembly time	Normal	standard deviation = 20% of mean estimate	hours

3.14 OPPORTUNITIES

While stack and system lifetimes of five and ten years, respectively, are possible for state of the art MCFC, reductions in first costs and life cycle costs are necessary for mass commercialization of this fuel cell technology. Manufacturing related cost reduction opportunities identified in this study include:

- Volume production - For modeling purposes, a baseline production volume of 20 MWe/yr was selected because of its rough equivalence with the recent production volume experienced by actual MCFC manufacturers. A 19% reduction in costs appears achievable just by increasing production volume from the model baseline to 500 MWe/yr, even if manufacturing technology is assumed unchanged (i.e. production lines are replicated in parallel) and no learning curve is experienced. However, the cost reductions to be expected from high volume production alone are of insufficient magnitude to reduce first costs to a competitive level of $1500/kWe or less needed for mass commercialization. Early adopters and favorable tax treatment are essential for sustaining demand and providing opportunities for technological breakthroughs needed for significant cost reduction.

- Purchased materials and components – With any product or process, the single largest cost component is a natural starting point when searching for potential cost reductions. Model results indicate that materials and components sourced from suppliers constitute approximately 75% of total manufacturing cost

    - Cell materials – The most important MCFC cell materials in terms of quantity used and total cost are nickel (cathodes, anodes, and anode supports), lithium aluminate (matrix), and alkali carbonates (electrolyte). Among the three, nickel is unique in that it is an exchange traded commodity with relatively wide commercial availability from numerous suppliers. The market for matrix and electrolyte materials, however, is comparatively much smaller with fewer suppliers. Opportunities for cost savings through vertical integration of matrix and/or electrolyte production are evident in the publicly available literature.[5] For instance, the matrix material, lithium aluminate, may be as much as ten times the cost of its raw material inputs. Recent patent literature shows that researchers are investigating lower cost production methods for this important MCFC material.[20] Likewise, patents have been filed for electrolyte production methods.[4] Vertical integration of the production of these materials affords MCFC manufacturers the potential for lower costs, more control over product quality, and better response to supply constraints.

    - Stack materials and components – Many stack components such as current collectors, separator plates, wet seal rails, and reforming units are manufactured from stainless steel parts which undergo typical metal-working operations such as

stamping, bending, welding, etc. Low fuel cell production volume necessitates that many of these operations be outsourced, contributing significantly to the total cost of these components. With high fuel cell production volumes, bringing these operations in-house might be justifiable. In the absence of high production volume, lower cost metal-working procedures which produce higher quality stack component parts should be investigated. Also contributing to the high cost of these components are the required protective coatings needed to minimize corrosion by electrolyte. Efforts directed at developing lower cost coating procedures, coating materials, or corrosion-proof substrate materials which do not require protective coatings in the first place are warranted.

- BOP components and subsystems – Many balance of plant components and subsystems are well known to be significant contributors to fuel cell cost. For MCFC, the adsorbent based desulfurizer is on the order of 15-40% of total system cost based on fuel feedstock quality. Online sulfur detection systems would enable optimal utilization of this high cost BOP component. Inverters, heat exchangers, and blowers also register among the highest cost BOP components.

- Automation –High labor cost steps identified in this study include certain process steps associated with anode current collector manufacturing, bipolar plate manufacturing, electrode/current collector/bipolar plate mating, and stack and system assembly. Many of these procedures may be difficult to duplicate with automated machinery because of complex motions. High production volume may be required before custom, automated assembly equipment is economically justifiable. DFMA redesign studies of components which currently show high labor inputs may lead to designs with a reduced labor requirement or ones conducive to low cost automated assembly.

- System size as way of reducing cost – The present study was commissioned to examine stationary fuel cells in the 100 – 400 kWe range. As such, emphasis was placed on creating a model representative of the DFC-300®, FCE's 375 kWe unit. However, FCE sees the greatest economic opportunity (translation, lowest cost of electricity for the customer) in its larger units.[25] It is well-known that the capital cost of chemical plant hardware, such as BOP components, scales nonlinearly. Specifically, FCE has observed that balance of plant equipment is cheaper on a per kilowatt basis for larger as opposed to smaller fuel cell systems. An indication of the impact of the BOP scaling effect is given by Remick and Wheeler where it is noted that the installed cost of the DFC-300® in recent times was on the order of $5500/kWe, while the DFC-3000® installed cost was $3500/kWe, implying a cost difference of 36%[3]

- Matrix tape casting – State of the art matrix layer manufacturing uses tape casting which is a well-established manufacturing technique. While the anode tape casting process is adequate, matrix tape casting is slow due to long drying times with the possible need to

laminate multiple layers of tape to achieve the appropriate thickness. Any lamination steps would further decrease the productivity of the matrix casting manufacturing station as the lamination process is both time consuming and an opportunity for introducing yield diminishing quality control errors. Methods for speeding up and improving the yield of matrix manufacturing should be examined.

- Extending stack life – One cost reduction opportunity which encompasses not only manufacturing but also materials, design, etc. is through stack life extension. With all other factors held constant, stack life extension results in lower life cycle cost by effectively reducing the cost of electricity. MCFC developers have attained the initial goal of a 5-year stack life. Efforts now are focused on extending stack life to 10 years. Electrolyte loss and cathode dissolution, the two major life limiting factors in state of the art MCFC operation, must be addressed if stack life is to be doubled.

    - Two strategies for mitigating the life limiting effects of electrolyte loss are 1) reduce the rate of electrolyte loss in the first place, and 2) increase the amount of electrolyte present in the cell. Electrolyte is lost through evaporation, creep, and corrosion, with corrosion being the most significant. As mentioned previously in section 3.7, 65% of electrolyte loss is due to its participation in corrosion reactions with the cathode side stainless steel hardware to produce oxide scales having poor electrical conductivity. These oxide scales, in turn, are responsible for 25% of the internal resistance in a MCFC. Coatings which mitigate this pathway for electrolyte loss (and internal resistance) have been identified, but more work is warranted. Electrolyte loss is also addressed by increasing the amount of electrolyte present in cells. Recent patent literature indicates that 10% of all electrolyte lost over the course of a fuel cell's life occurs during the first 2000 hours, reducing the life of the fuel cell by 20,000 hours.[26] The same patent goes on to describe a procedure for replacing this lost electrolyte by loading current collectors with a paste containing electrolyte of a different composition (and more importantly a higher melting temperature) than the baseline electrolyte which first enters the matrix upon initial stack warm-up. This electrolyte is released slowly, over time, based on surrounding temperatures, and replaces the large quantity of electrolyte lost in the first 2000 hours. Replenishment of electrolyte at this stage with this method results in an extension of stack life by nearly two years. Other means for mitigating electrolyte loss are also being explored. However, more research and development is needed to mitigate electrolyte loss before a ten-year stack life is attainable.

    - Cathode dissolution leads to the well-known phenomenon of nickel shorting. Numerous factors influence the rate of nickel precipitation as discussed previously in section 3.4. Further technology development is needed to reduce the propensity of nickel to become solvated in the electrolyte and/or reduce its

propensity to precipitate if solvated. Alternatively, efforts could be focused on the development of a new, low cost, non-soluble cathode material to replace traditional nickel cathodes.

Having been in development since the 1960s, MCFC technology has within the last decade attained a level of limited commercial viability. In particular, areas with high cost grid electricity and/or extensive district heating networks such as New England, California, and South Korea represent the largest current markets for MCFC. As mentioned previously, FCE has demonstrated a 5-fold increase in stack power output since 1992, and a several-fold decrease in cost in terms of $/kWe over the same time period. A continuation of this cost reduction trajectory would lead to much broader commercial markets for MCFC.

3.15 REFERENCES

1. Farooque, M. FuelCell Energy, Inc. *Personal e-mail communication with Sujit Das*, Oak Ridge National Laboratory, Oak Ridge, TN 37932, Dec. 10 (2010).
2. Daly, J., and M. Farooque. *Effective sulfur control for fuel cells – FCE experience*, Proceedings of the 2010 ASME Eighth International Fuel Cell Science, Engineering, and Technology Conference, Jun. 14-16 (2010).
3. Remick, R., and D. Wheeler. *Molten carbonate and phosphoric acid fuel cells: overview and gap analysis*, Technical Report NREL/TP-560-49072, September (2010).
4. Lucas, T., and J. Doyon: Continuous method and apparatus for manufacture of uniform size flake or powder, US Patent 7,060,219 B2, Jun. 13 (2006).
5. Yuh, C., J. Colpetzer, K. Dickson, M. Farooque, and G. Xu. *Carbonate fuel cell materials*, J. of Materials Engineering and Performance, Vol. 15, p. 457 (2006).
6. Hoffman, J., C. Yuh, and A. Jopek. *Electrolyte and material challenges*, Handbook of Fuel Cells – Fundamentals, Technology, and Applications, John Wiley & Sons, Ltd. p. 921 (2003).
7. Katikaneni, S., and J. Daly. *Pre-processing assembly for pre-processing fuel feedstocks for use in a fuel cell system*, US Patent 7,871,450 B2, Jan. 18 (2011).
8. Katikaneni, S., and S. Parab. *High capacity sulfur adsorbent bed and gas desulfurization method*, US Patent 7,063,732 B2, Jun. 20 (2006).
9. Mugikura, Y., M. Yoshikawa, Y. Izaki, and T. Watanabe. The Second International Fuel Cell Conference, p. 169 (1996).
10. Yoshikawa, M., Y. Mugikura, T. Watanabe, T. Yagi, and Y. Fujita. The Eighth Fuel Cell Symposium Proceedings, Japan, p. 293 (2001).
11. Swarr, T., and W. Wnuck. *Method of preparing a dimensionally stable electrode for use in a MCFC*, US Patent 4,714,586, Dec. 22 (1987).
12. Doyon, J. *Fuel cell anode and fuel cell*, US Patent 5,558,948, Sep. 24 (1996).
13. Yuh, C., and J. Li. *Anode support for carbonate fuel cells*, US Patent 6,719,946 B2, Apr. 13 (2004).
14. Xu, G., and C. Yuh. *Cathode side hardware for carbonate fuel cells*, US Patent 7,914,946 B2, Mar. 29 (2011).
15. Ma, Z., C. Yuh, D. Kelley, M. Farooque, and W. Beesley. *Fuel cell plate structure having baffles in wet seal area*, US Patent 7,740,988 B2, Jun. 22 (2010).
16. Bregoli, L., and M. Pearson. *Electrolyte paste for molten carbonate fuel cells*, US Patent 5,468,573, Nov. 21 (1995).
17. Blanchet, S., J. Doyon, and L. Novacco. *Corrugated current collector for direct internal reforming fuel cells*, US Patent 6,492,045 B1, Dec. 10 (2002).
18. Correa, S., T. Lucas, and L. Novacco. *Fuel cell assembly and method of making same*, US Patent US 2008/0280180 A1, Nov. 13 (2008).
19. Li, J., C. Yuh, T. Lucas, and M. Primerano. *Bipolar separator plate with improved wet seals*, US Patent 6,372,374 B1, Apr. 16 (2002).
20. Hyun, S., H. Cho, and J. Lee. *Manufacturing method of high pure alpha-$LiAlO_2$*, US Patent US 2010/0233073 A1, Sep. 16 (2010).
21. Huang, C., and C. Yuh. *Electrolyte matrix for molten carbonate fuel cells*, US Patent 5,869,203, Feb. 9 (1999).
22. Ma, Z., R. Venkataraman, and L. Novacco. H*igh performance internal reforming unit for*

high temperature fuel cells, US Patent 7,431,746 B2, Oct. 7 (2008).
23. Blanchet, S. *Fuel cell stack compressive loading system*, US Patent 6,797,425, Sep. 28 (2004).
24. Arneson, K., F. Ernst, Jr., A. Durante, and G. Chenot. *Assembly for and method of housing an object such as fuel cell balance of plant equipment, for transport to and storage at user location*, US Patent 7,556,472 B2, Jul. 7 (2009).
25. Lucas, T., and M. Farooque. *Private meetings with Sujit Das, Wei Zhang, Joshua Warren, Surya Saripalli*, Oak Ridge National Laboratory, Oak Ridge, TN 37932, (2010 and 2011).
26. Johnsen, R., C. Yuh, and M. Farooque. *Carbonate fuel cell and components thereof for in-situ delayed addition of carbonate electrolyte*, US Patent 7,939,219 B2, May 10 (2011).
27. Farooque, M. *Direct FuelCell Opportunities*, MCFC and PAFC R&D Workshop sponsored by U.S. Department of Energy, Office of Energy Efficiency and Renewable Energy, Fuel Cell Technologies Program, http://www1.eere.energy.gov/hydrogenandfuelcells/pdfs/mcfc_pafc_workshop_farooque.pdf (2009).

4. SOLID OXIDE FUEL CELLS

4.1 BASIC OPERATION

Of the three fuel cell types examined in this study, solid oxide fuel cells (SOFC) can be regarded as the least mature with respect to commercial development due to several technological hurdles that have limited their acceptance in the marketplace. Nevertheless, considerable research and development has been devoted to advancing this technology which offers many desirable characteristics such as high electrical efficiency, cogeneration opportunities, fuel flexibility with the prospect of internal reforming, and the absence of the electrolyte management issues attendant to fuel cells using liquid phase electrolytes such as PAFC and MCFC. Fundamental work in the 1940s by Baur and Preis[1] which demonstrated that stabilized zirconias (ZrO_2) could conduct oxide ions (O^{-2}) forms the core of modern SOFC technology. Since then, SOFC technology has been advanced by numerous industrial and academia developers spanning the globe including Forschungszentrum Julich, Siemens Westinghouse, Rolls Royce, Versa Power, and Bloom Energy to name only a few.

Solid oxide fuel cells typically use natural gas as a raw fuel feedstock from which a hydrogen rich fuel stream is derived through either external or internal reforming. In Figure 4-1, the basic operation of an internally reforming SOFC is illustrated.

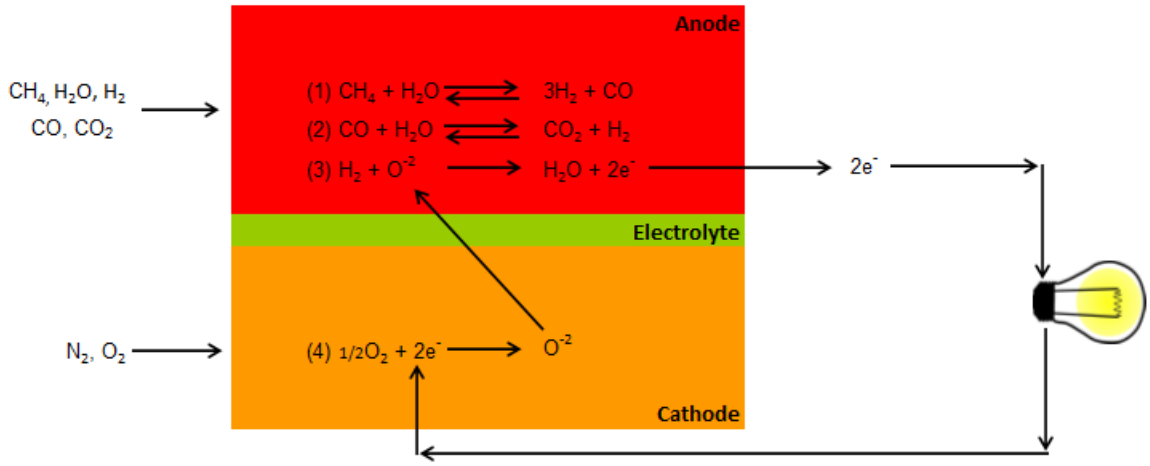

Figure 4-1. Basic Operation of a Solid Oxide Fuel Cell

A prereformer (not shown) converts a natural gas stream into a mixture of primarily methane, water, diatomic hydrogen, carbon monoxide, and carbon dioxide. This mixture is shown to enter the anode in Figure 4-1 from the top left. Anodes are comprised of a catalytic material that catalyzes the reforming reaction, reaction (1), where methane and water react to form diatomic hydrogen and carbon monoxide. In turn, carbon monoxide is shown to react with another molecule of water in the water-gas shift reaction, reaction (2), to produce carbon dioxide and an additional molecule of diatomic hydrogen. In reaction (3), the fuel cell electrochemical reaction, diatomic hydrogen reacts with an oxide ion to form water with two electrons liberated. The electrolyte layer is nonconductive to electrons, forcing the two liberated electrons through an

external circuit where they pass through an electrical load and perform work before being returned to the cathode. In the cathode, the two electrons are joined with an oxygen atom to form an oxide ion which is conducted through the electrolyte to participate in another cycle of reaction (3). Alternatively, a solid oxide fuel cell may use external reforming in which case the fuel stream initially entering the anode will still consist of the same species indicated in Figure 4-1, but at very different ratios. Specifically, the concentration of methane will be very low implying very little occurrence of reaction (1). Reactions (2, 3, and 4) prevail. Whether to employ internal or external reforming is a complex decision with many benefits and tradeoffs that will be explored in a subsequent section.

4.2 CELL, STACK, AND SYSTEM DESIGN ASSUMPTIONS

Although their technologies are sure to continue evolving, PAFC and MCFC design and operation parameters have entered a relatively settled state as these fuel cell systems have comfortably advanced into the commercial production phase for the power ratings examined in this study. SOFC technology, however, remains largely in the development phase with the exception of Bloom Energy's recent 2008 entry into the marketplace with a 100 kWe system. As might be expected for any product in the technology development phase, the SOFC landscape is replete with competing design and operating alternatives. A summary of the major alternatives will be given in the following paragraphs before leading into the design selected for the present study.

One of the most common characteristic used for categorizing SOFC types is cell geometry. In the broadest sense, cell geometry types are either tubular or planar. The most common tubular design was pioneered by Siemens Westinghouse and uses cathodes, electrolytes, and anodes arranged as concentric cylinders. Figure 4-2 is a simplified illustration of the tubular concept. Air flows through a hollow tube center whose space is defined by the cathode layer while fuel flows over the tube's exterior, or anode layer. The tube is formed by extruding the cathode, sintering the cathode, and then applying the electrolyte and anode with a gas phase deposition technique such as electrochemical vapor deposition (EVD). The primary advantage of the tubular design over alternative designs is the ease with which the anode and cathode gas compartments can be sealed to preclude fuel and oxidant mixing. However the tubular design has several disadvantages including low volumetric power density, long current paths for electrons, and high cost manufacturing processes and materials.

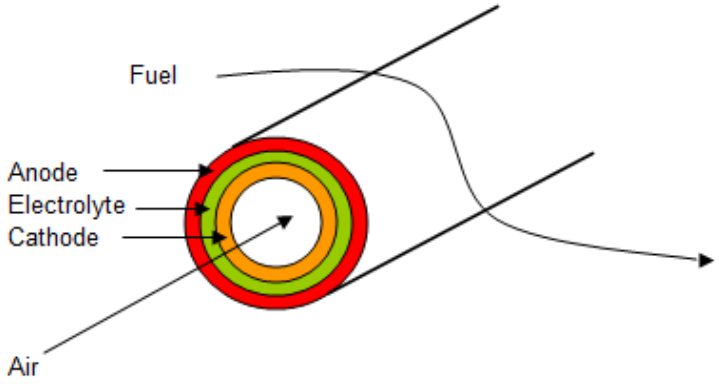

Figure 4-2. Tubular SOFC

Particularly expensive are the EVD process and the ceramic interconnects used in the Siemens Westinghouse design. The relatively high cost of tubular SOFC has prompted developers to severely curtail efforts to further develop this design. However, one American company, Accumentrics, is actively developing a tubular design similar to the Siemens Westinghouse design, but for systems in the 10 kWe or less range. Accumentrics uses faster and lower cost manufacturing processes such as pressing instead of extruding tubes, and slip casting and plasma spraying instead of EVD for layer deposition.[2]

Another cell design, called "segmented-in-series," incorporates aspects of both tubular and planar designs and is being actively developed by Rolls Royce for their 1 MWe, electrical only system. This design uses rectangular, flat supports having numerous, fuel-conveying, parallel tubes as depicted in Figure 4-3.

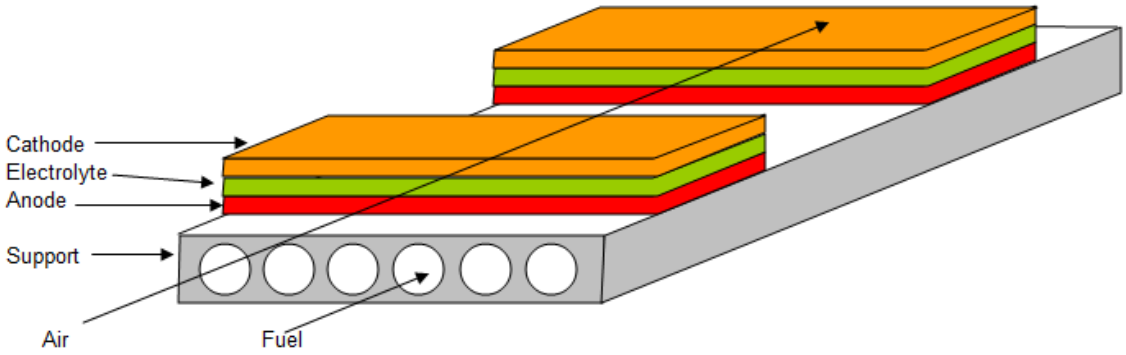

Figure 4-3. Segment-in-series SOFC

Rolls Royce uses an in-house screen printing process for the deposition of anode, electrolyte, and cathode layers onto outsourced support structures.[3] Interconnects (not shown) connect the segments (i.e. the fuel cells) in series to attain a practical voltage. Moreover, the assemblies shown in Figure 4-3 are housed in a vessel supplied with pressurized oxidant to which the cathodes are exposed. Pressurization is well known to improve maximum possible electrical efficiency as demonstrated by the Nernst equation. The segmented-in-series design has advantages of both tubular and planar designs. Specifically, the segment-in-series design allows relatively easy sealing as with tubular designs, but with the shorter current paths of planar designs. Also, the use of a flat, planar support allows low cost manufacturing processes such as screen printing for the deposition of electrode and electrolyte layers. However, the extruded support structure also represents a significant cost for these systems.

The majority of SOFC development in recent years has been focused on cells having a planar geometry. The planar design may be circular or rectangular as indicated in Figure 4-4, but much more frequently the rectangular geometry is adopted with square being the preferred rectangular shape.

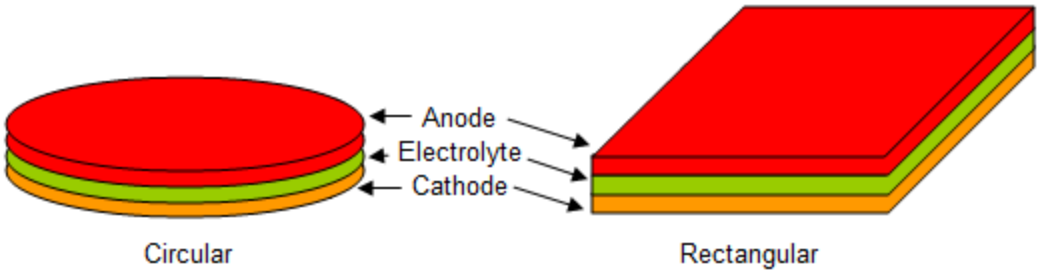

Figure 4-4. Planar SOFC, Circular and Rectangular

Various reasons exist for why rectangular is preferred over circular, one of which is that modern cell manufacturing frequently uses tape casting where a liquid slurry of cell material is cast continuously and dried into a rectangular shaped tape analogous to an unrolled paper roll. Rectangular shaped cells can thus be easily cut from the rectangular tape with little wasted tape, whereas, cutting circular cells from the rectangular shape would necessarily create significant scrap. Rectangular cells are also more compatible with screen printing processes, another low cost manufacturing technique frequently used in the production of solid oxide fuel cells. Due to the prevalence of rectangular designs in modern SOFC development, emphasis will be placed on this geometry throughout this report.

Cells may be further categorized by how they are supported, that is, how mechanical strength is provided so that cells do not easily break. For instance, a typical rectangular cell may have planform dimensions of 10 x 10 cm^2, but have an entire thickness (anode, plus electrolyte, plus cathode) that is less than 1.0 mm. Usually, the cell is supported by one of the ceramic layers (anode, electrolyte, or cathode) by manufacturing that layer sufficiently thick to provide mechanical support. Alternatively, but less common, cells may be supported by a porous metallic substrate onto which the ceramic layers are deposited in a green state and then subsequently sintered. Such a design is restricted to the use of ceramics whose sintering temperatures are sufficiently low to be tolerated by the metallic substrate. Additionally, metallic supported designs are often further complicated by both corrosion of the metallic substrate and a coefficient of thermal expansion (CTE) mismatch between it and the ceramic layers which it supports. The metallic substrate design does, however, lend itself to relatively easy sealing such as with welding. Also, this design minimizes the quantity of expensive ceramics used as there is no requirement to manufacture one of the ceramic layers sufficiently thick to provide mechanical support. In the United Kingdom, CeresPower is actively developing, and as of February 2011, field testing a metallic supported, combined heat and power SOFC appropriately sized for meeting the energy requirements of a single residential home.[5]

More frequently, planar cells are supported by one of the ceramic layers rather than with a metallic substrate. Cathode supported planar cells, while technically feasible, are the least common design and are not discussed further.

Electrolyte supported cells use a relatively thick electrolyte layer, a design choice that comes with performance tradeoffs. The capacity for an electrolyte layer to conduct ions is a function of the material type used, the cell operating temperature, and the thickness of the electrolyte layer.

One source indicates at least 19 materials which have been examined as electrolytes for SOFC.[6] Among these 19 materials, one is regarded as the traditional SOFC electrolyte, YSZ. YSZ, standing for yttria stabilized zirconia, is a zirconia (ZrO_2) based material doped with yttrium oxide (Y_2O_3). Doping zirconia with a certain mole percentage of yttrium oxide results in a crystal structure less likely to undergo temperature dependent morphological changes than would be observed in zirconia alone. In this way, yttrium oxide "stabilizes" zirconia. Frequently, the mole percentage of yttrium oxide is written as a number preceding YSZ. The most common doping percentage is 8%, leading to the name 8YSZ, the most commonly used electrolyte in SOFC technology. 8YSZ, like most materials used as SOFC electrolytes, shows increasing ionic conductivity with increasing cell operating temperature. Thus, without considering other factors, it is clearly desirable to operate the fuel cell at higher temperatures. Furthermore, ionic conductivity increases as electrolyte layers become thinner, implying thin electrolytes are preferred. The consequence, then, of using an electrolyte supported design is reduced ionic conductivity, and hence cell power, due to a relatively thick electrolyte. Operating the fuel cell at higher temperatures can offset the reduction in ionic conductivity which accompanies the use of thick electrolytes. However, high operating temperatures limit material choices for other fuel cell system components to expensive, high temperature ceramics and/or metals, significantly increasing the cost of the fuel cell system. Specifically, cell interconnects must be made of expensive ceramics when an electrolyte supported design also dictates high operating temperatures in order to attain a practical ionic conductivity.

Alternatively, a lower overall system cost may be achieved if cell operating temperatures are reduced sufficiently (less than 800^{o}C) to enable the use of lower cost materials. When low operating temperatures are employed to take advantage of lower cost material options, the electrolyte layer must be sufficiently thin to attain a practical ionic conductivity. "How thin" an electrolyte layer must be varies according to material type as different materials have different ionic conductivities. The traditional SOFC material 8YSZ, for instance, requires a layer thickness of 10 μm or less to attain a practical ionic conductivity when systems are designed for less than 800^{o}C operating temperatures in order to take advantage of lower cost materials. As can be appreciated from the preceding example, the pursuit of an overall lower fuel cell system cost has generally shifted emphasis away from electrolyte supported designs.

The most commonly used design in modern SOFC technology with respect to mechanical supporting and geometry uses an anode supported, rectangular cell having planform dimensions in the range of 10 x 10 to 25 x 25 cm^2,[4] giving rise to the baseline planform cell geometry used in the present study and depicted in Figure 4-5 below. Seals are assumed to require 12% of total cell area similar to a recent 25 x 25 cm^2 cell manufactured by Versa Power.[9]

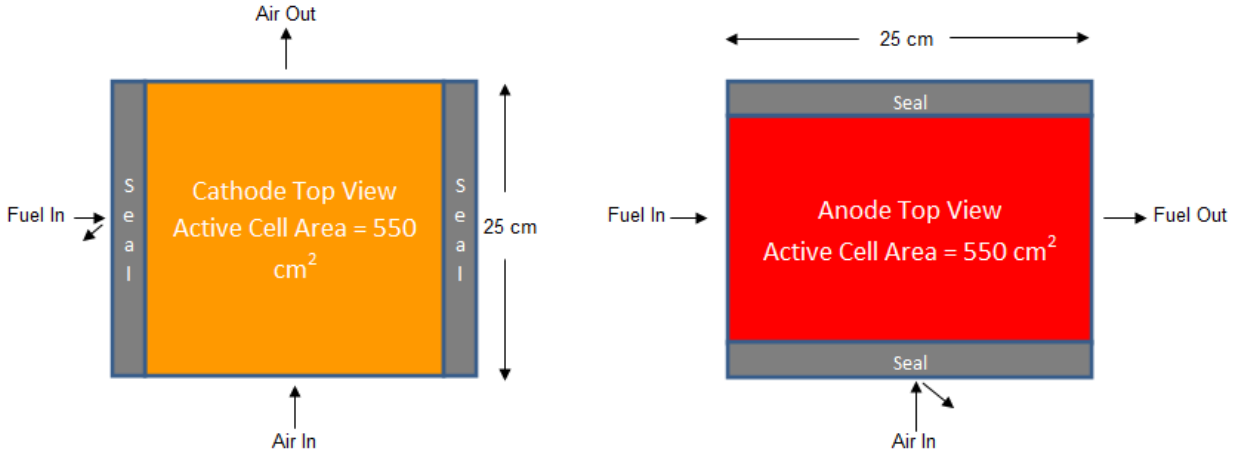

Figure 4-5. SOFC Planform Cell Geometry

The thickness of the anode support layer is typically in the range of 500 to 1500 microns with the required support thickness increasing as cell planform dimensions increase. The cost-benefit relationship for scaling up the planform dimensions of SOFC cells was examined by Thijssen.[7] Using larger cells has the benefit of reducing the part count of repeat units such as cells and interconnects as fewer cells are required to achieve a given stack power. Also, the cell area is better utilized as a larger proportion of cell area can be devoted to power generation rather than sealing. The use of fewer cells also leads to a simplification of manifolding. In these respects, larger cells can potentially reduce system costs, especially for systems in the power range examined in the present study. However, larger cells require the use of greater quantities of expensive ceramics as the supporting layers must necessarily be manufactured with a greater thickness to provide adequate mechanical support to the brittle ceramic cells. Manufacturing yield would also be expected to decrease with an increase in cell planform dimensions as the probability of a defect increases with cell area. Thermomechanical stresses likewise are magnified as cells become larger, potentially leading to decreased performance and/or failure. Thijssen indicates that scale-up of cell planform dimensions from the industry standard 100 cm^2 to the range of 750-1000 cm^2 can result in a 10-20% reduction in overall cost for large (2 MWe) SOFC systems.

Primary among the list of reasons for operating SOFCs at reduced temperatures is that doing so permits the use of lower cost metallic as opposed to ceramic interconnects, having costs on the order of $6.67/kWe and $137.50/kWe, respectively, per Surdoval et al.[8] Moreover, ceramic based interconnects are unsuitable for operating temperatures lower than 800^oC due to low electronic conductivity. Metallic interconnects, however, show excellent electronic conductivity at this, and even lower temperatures. In addition, metallic interconnects can be manufactured with lower cost techniques such as forming stamping, machining, welding, and brazing, resulting in a part that is substantially cheaper than one made of ceramics. In addition to having good electronic conductivity, interconnects are required to have good corrosion resistance, to have strength in high temperature environments, and to be CTE matched with adjacent components, i.e. separator plates and electrodes. Alumina forming alloys have excellent corrosion resistance but very poor electrical conductivity (ideal for MCFC wet seals but not for SOFC interconnects) and are thus not pursued. Chromia forming alloys such as ferritic stainless steels have emerged as one of the most suitable materials for use as metallic interconnects, but not without serious

limitations. These materials corrode in SOFC environments with the corrosion products causing electrical resistance. Additionally, chromium vapors arising from the chromium constituent in the interconnect material are known to poison cathodes. Coatings are usually applied to the cathode side of interconnects to retard the rates of corrosion and chromium volatilization. The development of satisfactory interconnects, and coatings for the same, is regarded as one of the most important R&D challenges for achieving a long stack life in SOFC. As such, interconnects, coating materials, and techniques for applying the coatings are considered in greater detail in a subsequent section.

As a true reflection of a product in the technological development phase, the SOFC landscape is replete with options for the cell ceramic layers with respect to material types, layer thicknesses, number of layers, particle sizes, porosities, etc. For instance, in addition to the 19 electrolyte material types mentioned previously, Wincewicz also lists 18 anode material types and 28 cathode material types,[6] implying 9,576 theoretical combinations based on this list alone if incompatibilities are not considered. While certain materials and combinations of materials have emerged as the preferred, the aforementioned serves to convey the complexity of simply selecting a baseline material set for modeling purposes. Numerous options likewise exist for contact layer and interconnect designs. Design aspects of the model's baseline cell structure (shown in Figure 4-6) were selected to be representative of a variety of sources,[10,11,12]

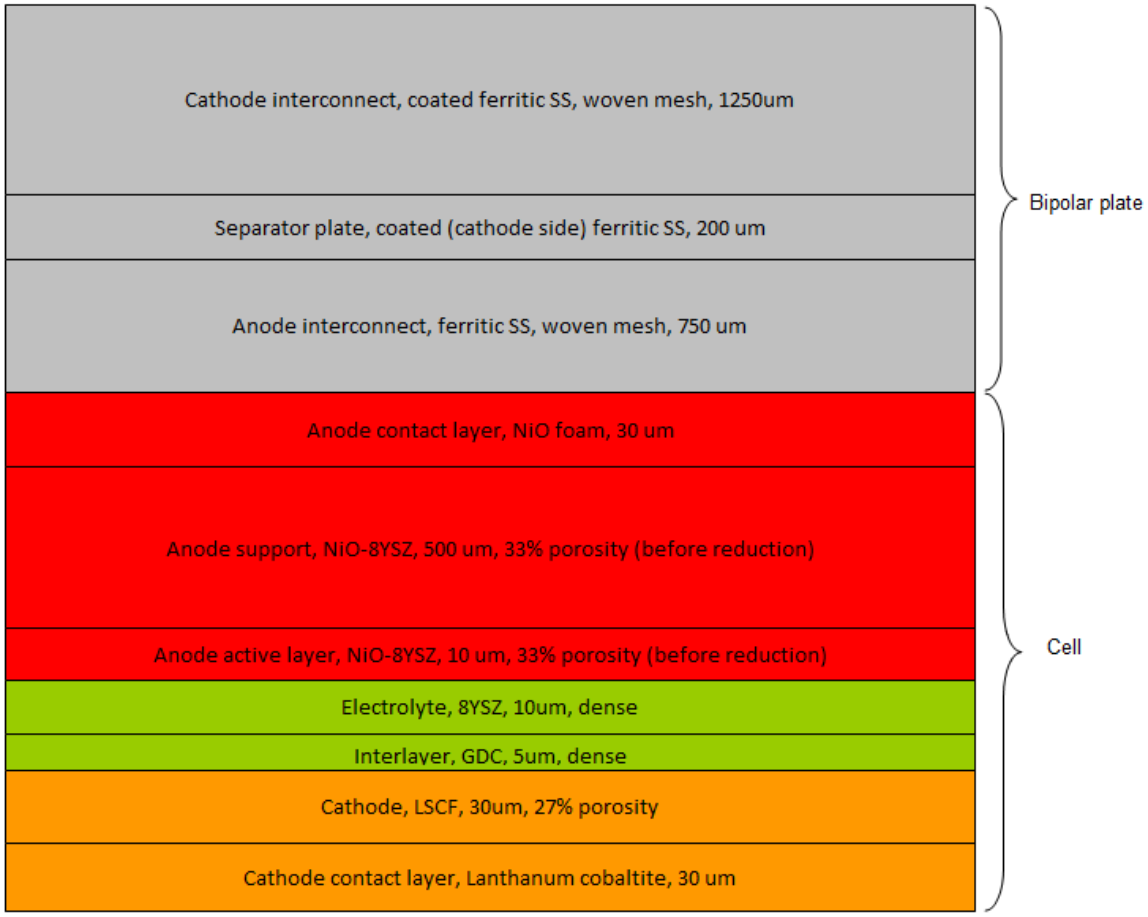

Figure 4-6. SOFC Cell Structure

A 625 cm^2 cell is supported by a 500 μm thick NiO-8YSZ anode support with 33% porosity before the in-situ reduction of NiO to Ni. The 10 μm anode active layer likewise consists of NiO-8YSZ, but of a higher surface area (i.e. smaller particle size) than the support. A dense, 10 μm 8YSZ electrolyte layer is protected from a 27% porous, 30 μm LSCF (lanthanum strontium cobalt ferrite) cathode by a dense, 5 μm GDC (gadolinia doped ceria) interlayer. 30 μm thick contact layers of Ni foam and lanthanum cobaltite are added to reduce the electrical resistance between the electrodes and their respective interconnects. The anode and cathode interconnects are assumed to be woven mesh, ferritic stainless steels which sandwich a solid separator plate of a similar material type. Cathode side hardware is assumed to be treated with a contact and vapor barrier coating. The above configuration results in a pitch of approximately 9 cells per inch. SOFC developers are actively pursuing stacks having approximately 100 cells each, with multiple stacks in turn aggregated into stack towers or modules.[9] It has been reported that under practical, commercially relevant conditions, SOFC stacks achieve a power density that is usually in the range of 0.3-0.5 W/cm^2.[13] Stacks are assumed to be internally manifolded for both fuel and oxidant using a "picture frame" cell holder design similar to those readily available in the patent literature[11,12] and illustrated in Figure 4-7.

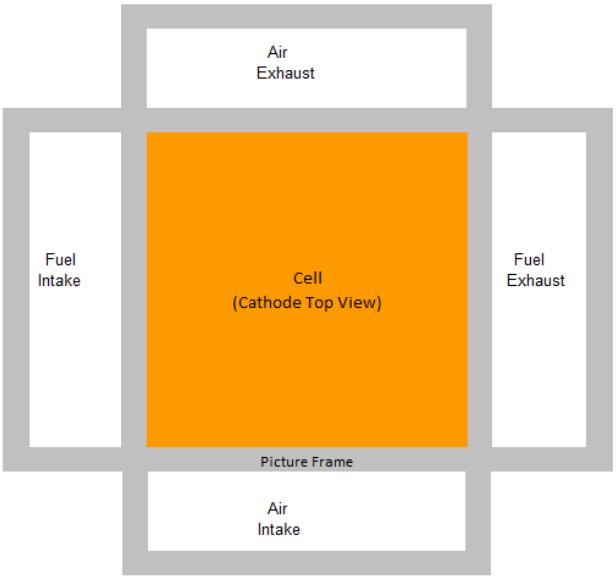

Figure 4-7. SOFC Picture Frame Cell Holder

In the present study it was desired to model a combined heat and power SOFC operating in the range of 100-400 kWe. However, unlike for PAFC and MCFC, a commercially available SOFC product meeting these specifications is not presently available. Such a system was, however, successfully demonstrated by Siemens Westinghouse in the late 1990s when their 100 kWe combined heat and power unit accumulated over 16,000 hours of operation. Presently, Bloom Energy offers a 100 kWe, electrical only SOFC, named Bloom Box®, which it began offering in 2008. Approximately 120 units have been installed as of an April 15, 2011 company press release,[14] One of these units is deployed at the headquarters of Electric Power Board (EPB) in Chattanooga, TN and was demonstrated for ORNL staff by EPB personnel. Combined heat and power applications are not actively pursued by Bloom Energy as they assert such applications are

economical only in the few instances where the customer has a constant and non-fluctuating CHP load.[15]

As such, for modeling purposes, a combined heat and power SOFC design was conceptualized based upon state of the art and likely near-term future technologies. The baseline cell, stack, and power assumptions for the model are summarized in Figure 4-8. A power density of 0.4 W/cm^2 is achieved with a current density of 0.571 A/cm^2 and 0.7 volts per cell in stacks of 114 cells each. Four stacks are aggregated into a single stack module, and, in turn, four stack modules are integrated with BOP components into a system producing 401 kW gross DC at beginning of life. This direct current is inverted with an efficiency of 96% into 385 kW gross AC. Parasitic loads are assumed to require 6% of beginning of life gross AC, leaving 362 kW net AC at zero hours.

Table 4-1. SOFC Cell, Stack, and Power Assumptions

Cell area	25 cm X 25 cm = 625cm^2
Percent of cell area used for sealing	12%
Active cell area	625 cm^2 x 0.88 = 550 cm^2
Current density	0.571 A/cm^2
Voltage	0.700 V
Power density	0.400 W/cm^2
Single cell power	220 W
Gross System DC at 0hr	$\frac{220\ W}{cell} \times \frac{114\ cells}{stack} \times \frac{4\ stacks}{stack\ module} \times \frac{4\ stack\ modules}{system} = \frac{401\ kW}{system}$
Losses:	
Inverter efficiency 96%	401 kW DC x 0.96 = 385 kW AC
Parasitic Losses 6%	385 kW x 0.94 = 362 kW net AC at 0 hr
Electrical efficiency (LHV natural gas)	55%
Thermal efficiency	35% → 0.79 MMBtu/hr
Total system efficiency	90%

Among the most attractive qualities of solid oxide fuel cells is the prospect of internal reforming. Internal reforming is attractive from both an efficiency and cost perspective. A theoretical efficiency gain is realized as the endothermic reforming reaction diminishes the stack cooling duty of the cathode blower (translation, parasitic loads subtract a smaller percentage from gross AC). Furthermore, significant capital cost savings can be realized from internal reforming due to a smaller cathode blower requirement, and the elimination of an external reformer with its associated steam boiler, water pump, and piping.

Sufficiently high temperatures and the creation of water in the anode compartment by the fuel cell electrochemical reaction (reaction 3 in Figure 4-1) provide the necessary ingredients for internal reforming. However, well known technological challenges have complicated the realization of reliable, internal reforming SOFCs. Chief among these challenges are the thermomechanical stresses resulting from the large temperature gradient across cells from the

point of fuel intake to the point of fuel exhaust. The reforming reaction has very fast kinetics under SOFC conditions, resulting in extensive cooling of the anode edge adjacent to the fuel intake. Thermomechanical stresses accrue as a result of this temperature gradient and result in cell damage and eventual cell failure. Optimization of anode microstructure is required before 100% internal reforming becomes a reality. To address this need, the use of a nonuniform distribution of nickel throughout anode layers is being studied as a means for creating an anode environment where the reforming reaction is more evenly dispersed across the cell. A recent patent assigned to Bloom Energy describes a process whereby the distribution of nickel in an anode is controlled by screen printing multiple layers of anode material with each layer having differing types and ratios of materials, resulting in a stratified or layered control of the distribution of nickel.[16] As an alternative to the screen printing process, this patent describes an inkjet printing process which gives the manufacturer a continuous, three dimensional control of the nickel distribution. Inkjet printing is a developing technology being investigated for the above-mentioned and other SOFC manufacturing applications, including segmented-in-series cells[17] and for the printing of extremely thin (<10 μm) electrolyte layers on anode supported planar cells.[18] Additional development is needed before inkjet printing is a practical manufacturing alternative.

A compromise between external reforming and 100% internal reforming is called prereforming. A prereformer is a catalyzed reforming vessel external to the stack that converts a percentage of the natural gas feedstock into hydrogen before it is introduced into the anode. In addition, higher hydrocarbons are converted to methane in order to reduce the likelihood of carbon deposition on the anode. Frequently, steam laden anode exhaust is recycled to the prereformer to provide the heat and steam necessary for the reforming reaction. A conflicting tradeoff exists with anode recycling. A sufficient quantity of exhaust should be recycled to preclude carbon deposition. Simultaneously, it is advantageous to minimize the quantity of exhaust recycled as the exhaust becomes a diluent to the hydrogen fuel, penalizing efficiency. Typical anode gas recycle percentages are in the range of 60-65%, giving a steam to carbon ratio of about 2:1. At these percentages of anode gas recycle, a sufficient quantity of steam can be harvested to eliminate the need for an external boiler for primary steam generation. The Bloom Box®, for example, requires water as a customer supplied input only for system startups.[19] Recent exemplary designs in the patent literature which use prereforming and anode gas recycle are given by Ahmed[20] of Ceramics Fuel Cells Limited and McElroy et al.[21] of Bloom Energy.

For modeling purposes, an internally reforming SOFC using anode gas recycle and prereforming was conceptualized by ORNL and verified by Versa Power.[22] The mechanical balance of plant for the model SOFC is illustrated in Figure 4-8. Pipeline quality natural gas undergoes ambient temperature desulfurization using processes similar to those described for molten carbonate fuel cells in Section 3.2. The desulfurized natural gas stream is then heated by afterburner exhaust before it and a portion of the anode exhaust are introduced into the prereformer. Next, the fuel stream enters the fuel cell anodes where the reforming reactions are completed and the fuel cell electrochemical reaction takes place (reactions 1-3 in Figure 4-1). An oxidant stream, supplied by a blower, is first preheated by afterburner exhaust before being supplied to the cathodes as required for reactions (3) and (4). The portion of anode exhaust not recycled to the prereformer is combusted with cathode exhaust in an afterburner. The afterburner exhaust passes through heat exchangers to warm the incoming fuel and oxidant streams as previously mentioned.

Afterburner exhaust exiting the air preheater passes through a final heat exchanger to transfer heat to a customer supplied CHP load before being exhausted to the atmosphere.

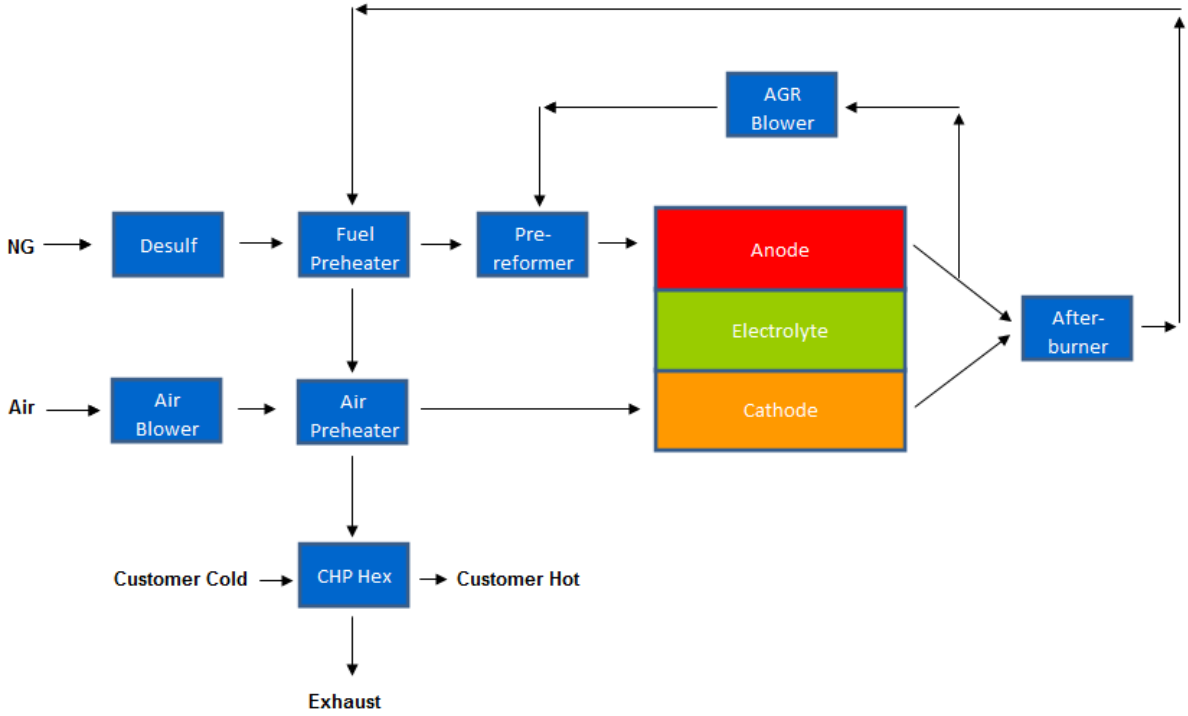

Figure 4-8. SOFC Mechanical Balance of Plant

4.3 HIGH LEVEL MANUFACTURING SYSTEM DESIGN

Figure 4-9 is a high level illustration of the manufacturing model assumed for this study. Anode slurry is prepared with milling and mixing equipment before being cast into a tape and dried. Anode supports are obtained by cutting the tape. Serial screen printings are used to apply the anode active layer and then the electrolyte layer before the ceramic body is sintered in air in a continuous belt tunnel kiln. Serial screen printings are then used to apply the interlayer and cathode before a second sintering step. Next, contact layers are screen printed and completed cells are integrated with outsourced stack hardware (picture frames, interconnects, separator plates, seals, spacers, end plates, and tie rods) to form completed stacks. Cathode side hardware is assumed to receive a protective coating prior to stack assembly. Completed stacks undergo leak and electrical testing at operational temperatures before being integrated with BOP components into a completed system. Completed systems are tested, an enclosure is placed over the system, and it is then loaded for shipping. All subsequent costs (shipping, installation, and commissioning) are outside the boundaries of the present study. In the following sections, the above described manufacturing steps are expanded and described in further detail.

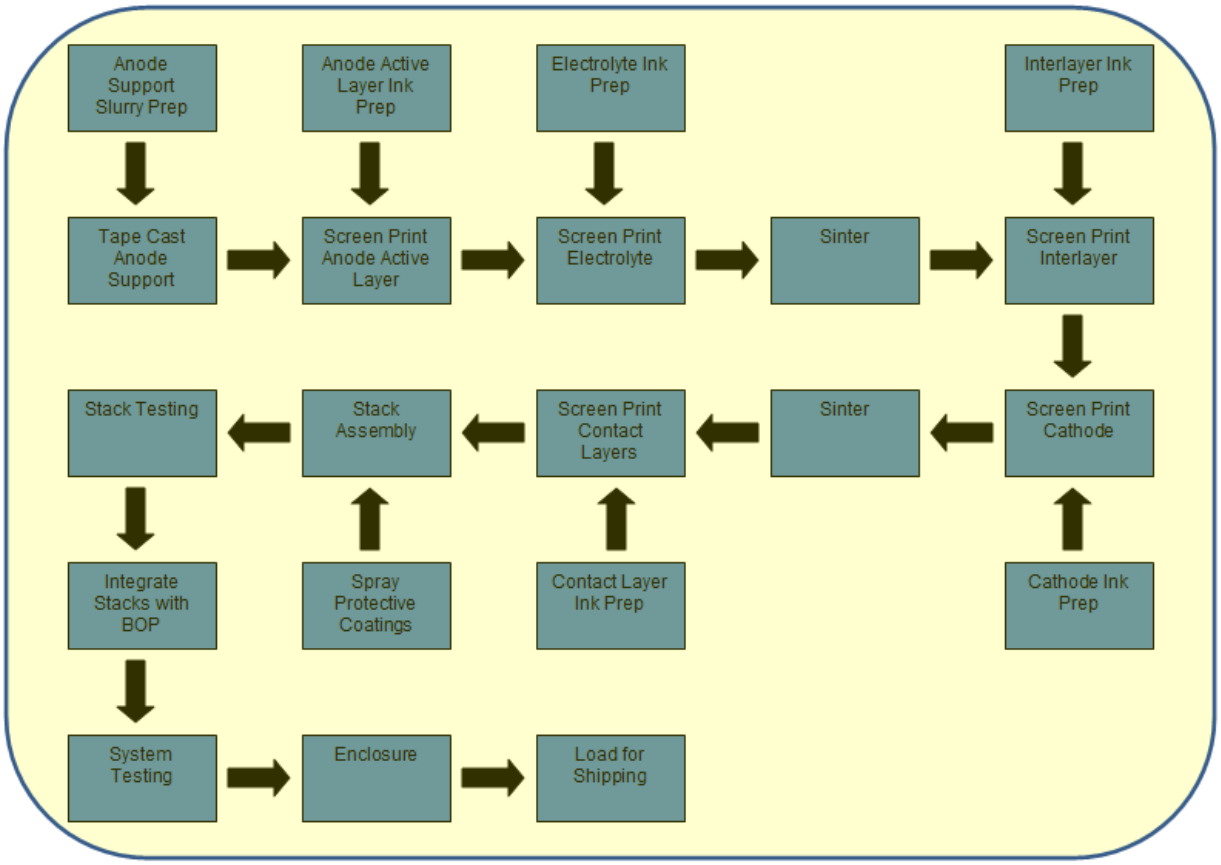

Figure 4-9. High Level SOFC Manufacturing Process Steps

4.4 ANODE SUPPORT MANUFACTURING

Tape casting and screen printing, two well-developed manufacturing processes borrowed from the electronics industry, form the core of state of the art, planar, solid oxide fuel cell manufacturing. Developed in the 1940s by Glenn Howatt,[23] tape casting has been used extensively in the electronics industry for the manufacture of capacitors. The tape casting principle is illustrated in Figure 4-10.

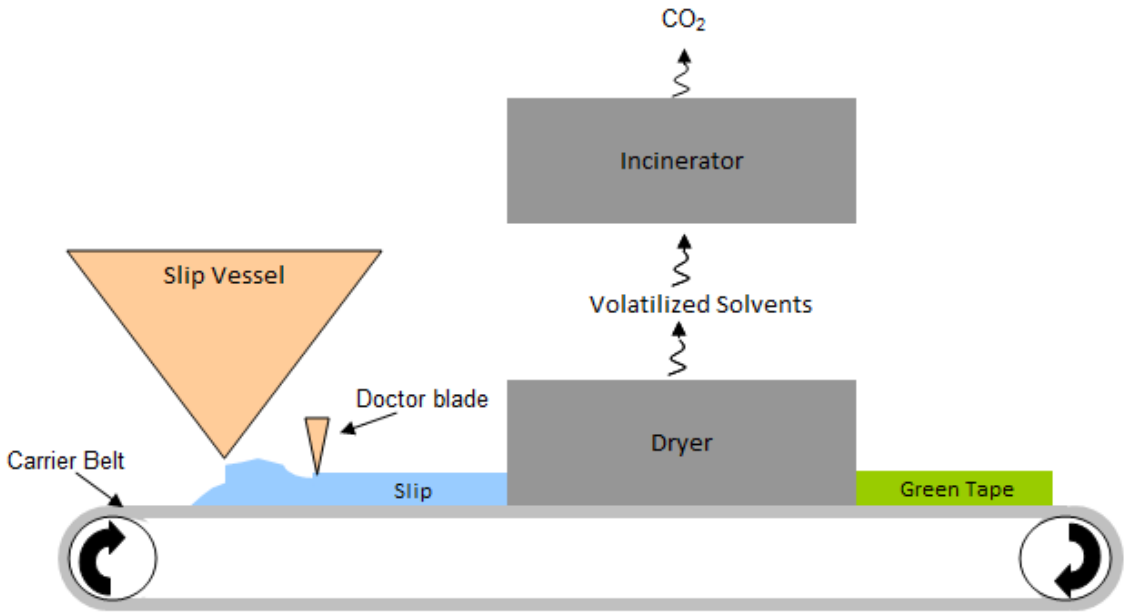

Figure 4-10. Tape Casting

Ceramic and metal powders are blended with solvents, binders, modifiers, and performers into a slurry (also called a slip). Slip is passed through a vessel with an orifice and deposited onto carrier paper transported by a continuously moving belt. The carrier belt transports the slip to a doctor blade whose positioning adjusts slip thickness. After slip thickness has been set to the desired level by the doctor blade, the carrier belt transports the liquid slip through a drying chamber where solvents are removed by heating and subsequently combusted with an incinerator. Binders hold together the now solid phase tape, from which supports are obtained by cutting or punching the green tape after separation from the carrier paper.

State of the art tape casters approach 100 ft in length with casting deck widths in excess of 40 in. Tape caster productivity is determined by slip drying rates. Drying rates, in turn, are determined by tape thickness, the length and temperature of the drying zone, and slip formulation. Environmentally friendly, aqueous slip formulations exist, but organic formulations are preferred from a productivity standpoint as drying proceeds more quickly. Incinerators or other ventilation engineering controls are required for organic based formulations. A typical casting speed for manufacturing SOFC anode supports with state of the art equipment is on the order of 12 linear inches per minute.

Slips are typically prepared with high energy mixing equipment such as high shear mixers or ball mills. A typical slip formulation is given by Song et al.:[24]

- 50/50 volume mixture of NiO and 8YSZ
- 35 wt% toluene and ethanol as solvent
- 10 vol% carbon black as pore former
- 1 wt% modifier
- 20 wt% binder

Particle size reduction of ceramic and nickel oxide powders by attrition milling or ball milling may precede slip preparation to achieve the fuel cell manufacturer's desired particle size. For modeling purposes, ceramic powder inputs are treated as direct materials purchased by the fuel cell manufacturer from a supplier. However, it should be noted that the processes (e.g. calcining) used for the manufacture of ceramic powders from their raw material inputs are important determinants of the manufacturing steps required of the fuel cell manufacturer, as well as the performance of the fuel cell itself. The model's anode support manufacturing process is shown in Figure 4-11.

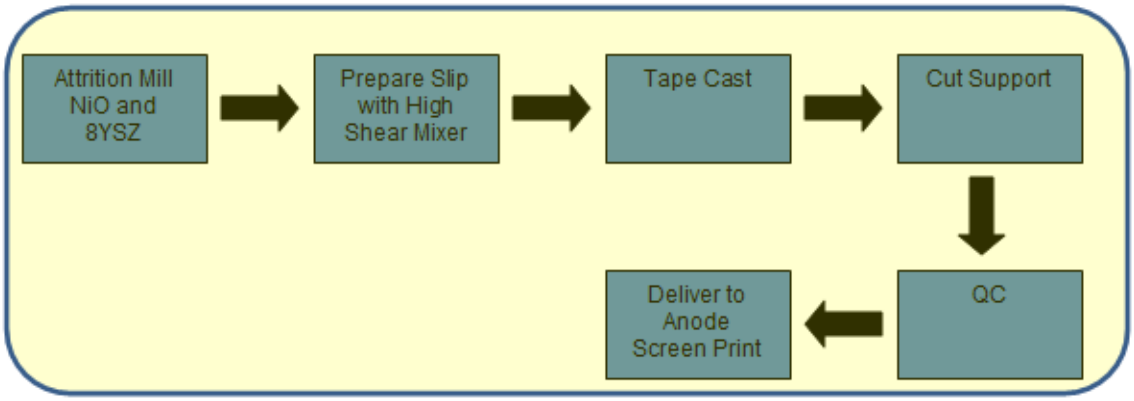

Figure 4-11. SOFC Anode Support Manufacturing Process

NiO and 8YSZ powders are assumed to be purchased from a supplier and size reduced with attrition milling by the fuel cell manufacturer. Slip is prepared with high shear mixing and cast into a tape. Supports are obtained from the tape with automated cutting or punching. Supports are visually inspected for defects, and weight and size measurements are obtained to enable a porosity calculation. Supports passing quality control inspection are delivered to the anode active layer manufacturing station.

4.5 CELL LAYER MANUFACTURING

Anode active layers (and all other ceramic layers) are assumed to be deposited with an automated screen printing process, a second manufacturing technique borrowed from the electronics industry. One central theme in the evolution of electronics is the desire to place ever increasing amounts of processing power in smaller spaces. To help achieve that goal, advanced electronics manufacturing uses an approach referred to as surface mount technology (SMT). SMT permits the use of both sides of a printed circuit board for the placement of electronics components such as integrated circuits, capacitors, resistors, etc. An electrically conductive solder is used to mechanically bind components to printed circuit boards and complete an electrical circuit between the board and component. In keeping with the trend to go ever smaller with electronic devices, modern integrated circuits may have hundreds of leads in a one inch square area that must be accurately attached to the printed circuit board.[25] Screen printer technology has evolved accordingly so that solder paste can be precisely and accurately deposited onto printed circuit boards in a pattern corresponding to this great number of

component leads. The thin, high resolution prints required in modern SMT are sufficiently similar to the prints required in SOFC manufacturing to make modern screen printers adaptable to the manufacturing of these fuel cells. However, SMT prints are generally thicker than the desired SOFC prints meaning further technology advances are needed to optimize screen printing for fuel cells.[26] Menzler et al. indicate 5 µm thick layers (post sintering) are the current minimum thickness achievable with modern screen printing technology.[4] Automatic conveyers, loaders, and unloaders for screen printers are readily available in the commercial marketplace to make this a low labor cost, low overall cost, highly automated, high productivity fuel cell manufacturing process.

Ceramic powders to be screen printed are normally suspended in an organic solvent to create a paste-like ink with rheological properties suited for screen printing. Specifically, the ink should flow when shear forces are applied by the screen printer squeegee so that ink flows into the mesh screen. When the shear forces are removed, the ink should assume a more rigid, paste-like state with sufficient structural integrity to retain the shape imparted to it by the screen once the screen is lifted. A simplified diagram of the screen printing process is shown in Figure 4-12 with the squeegee assumed to be moving from left to right.

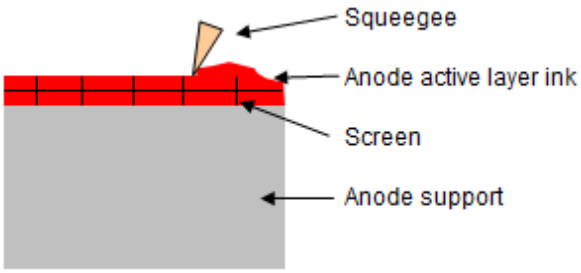

Figure 4-12. Screen Printing

Song et al. give a typical ink formulation which uses 60 wt% ceramic powders and 40wt% organic vehicle.[24] In turn, the organic vehicle is itself 96 wt% terpineol and 4 wt% ethyl cellulose. As in the electronics industry, 3-roll mills are frequently used for SOFC ink preparation.[27] The 3 roll mill principle is illustrated in Figure 4-13. Ink is processed by feeding into a roller system whose rotation brings the ink through a narrow gap between the leftmost roll and the center roll. Ink adheres to the center roll and passes through another narrow gap between it and the rightmost roll before being separated from the rightmost roll with a blade.

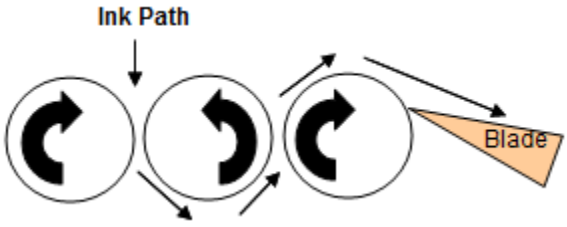

Figure 4-13. 3-roll Mill

The anode active layer screen print process assumed for modeling purposes is shown in Figure 4-14. Ink is prepared with a 3-roll mill and screen printed onto a previously weighed anode support. The cell is conveyed to a quality control station where the print is visually inspected and the support with ink layer is check weighed to determine the mass of ink added. Then, the cell is passed through a continuous dryer to dry the ink layer in preparation to receive the electrolyte print. Subsequent screen printing steps (electrolyte, interlayer, cathode, contact layers) are substantially equivalent to the one described here for the anode active layer with respect to process flow. As such, Figure 4-15 is representative of all subsequent screen printing steps.

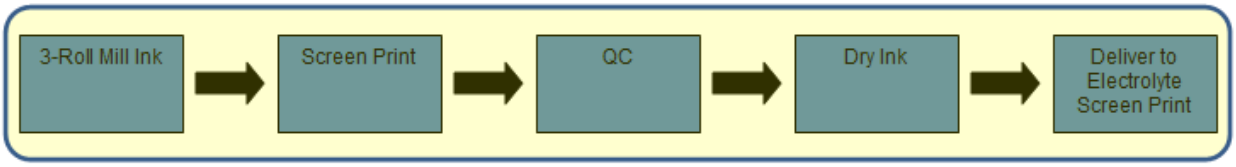

Figure 4-14. SOFC Anode Active Layer Manufacturing Process

4.6 SINTERING

Sintering is the process whereby powders are formed into a solid body by applying sufficient heat (and possibly pressure) such that the powders soften, flow and then consolidate into a solid body once heat and pressure are removed. Large energy, capital, floor space, and time requirements are associated with sintering in SOFC. One industry partner indicated that entire SOFC manufacturing systems are usually designed around sintering requirements.[28] Typical SOFC sintering steps use ambient atmosphere resistance furnaces with temperatures in excess of 1000^{o}C and cell residence times that may be in excess of 18 hours. Capital and floor space costs vary according to size and mode of operation. Furnaces may be stationary batch furnaces or continuous belt tunnel furnaces, with continuous furnaces usually preferred in high volume manufacturing scenarios. In both cases, stationary or continuous, capital costs and floor space requirements are significant.

Minimizing the number, duration, and temperature of sintering steps offers the potential for significant cost savings. To reduce the number of sintering steps, usual practice is to sinter the tape cast anode support, screen printed anode active layer, and screen printed electrolyte in a single firing step, called co-sintering. It is desired that the anode support and anode active layer remain porous post sintering to allow gas diffusion. Furthermore, it is desired that the anode active layer retain a small particle size (i.e. high surface area) post sintering so that an extensive triple phase boundary exists for the electrochemical reaction. Finally, it is desired that the electrolyte become fully dense post sintering to prevent gas exchange between the anode and cathode compartments. Achieving these disparate goals makes sintering a challenging process. Co-sintering has the additional challenges of CTE mismatches and possible chemical incompatibilities between layers.

Multiple parameters affect the quality of a sintered body, including maximum temperature, rate of temperature change, particle size, the use of pore formers, etc. The optimization of these

parameters to achieve a low cost, reliable, and high power density cell is a very active R&D topic with many examples available in the public literature.[24,29,30] Alternative sintering techniques are being examined, such as microwave sintering, that offer the potential of substantially reduced costs and processing times with finer microstructure giving an extensive triple phase boundary. [31,32]

As can be appreciated from Figure 4-6 and Figure 4-9, the model assumes a tape cast NiO-8YSZ anode support is screen printed with a NiO-8YSZ anode active layer and an 8YSZ electrolyte layer before being sintered in a continuous resistance furnace. The sintered half-cell is then screen printed with a GDC interlayer and an LSCF cathode before a second continuous sintering step. Typical sintering temperatures are on the order 1400^{o}C for NiO-8YSZ and 1050-1100^{o}C for LSCF.[4] Much effort has been directed at reducing the sintering temperature of GDC, with temperatures in the same range as the one mentioned above for LSCF having been reported.[33] While the model assumes two sintering steps, it is acknowledged that a third may be required where the interlayer is sintered alone, before the cathode sinter and after the electrolyte sinter, instead of co-sintered with the cathode. The model further assumes a quality control inspection after each sintering step that entails a visual examination and helium leak test. Cells passing quality control inspection are then screen printed with both anode and cathode contact layers to reduce electrical resistance between the electrodes and interconnects.

4.7 STACK AND SYSTEM ASSEMBLY

Stack assembly entails integrating cells with picture frames, interconnects, separator plates, seals, spacers, end plates, and tie rods. For modeling purposes, it is assumed that the fuel cell manufacturer produces cells in-house, but outsources the manufacture of the remaining above-mentioned items. Before the assembly process is addressed, a discussion of the particular challenges related to protective coatings and seals will be given.

One of the biggest challenges in planar designs which use metallic interconnects is the difficulty of achieving reliable seals. Glass and glass-ceramics are the traditional materials of choice. While these type seals are commercially available, most are intended for low temperature applications and are CTE mismatched with SOFC components. CTE matching is crucial for seal reliability as glass-ceramic seals are brittle, non-compliant seals that easily fracture when thermomechanically stressed. One source indicates only a small group of high temperature glasses within the borate or phosphate-doped aluminosilicate families have shown CTE compatibility with the ferritic stainless steels commonly used for stack hardware.[34] However, even these seals can prove to be inadequate as devitrification is noted to occur within the first few hours of operation. As the glass crystallizes, it loses its initial CTE compatibility and becomes susceptible to failure with any subsequent thermal cycling or shutdown/startups. The use of glass seals is further compounded as detrimental chemical interactions between seals and other stack components (cells, interconnects) are known to occur.

Compressive sealing with compliant gasket materials has also been examined. Compressive seals are an improvement over glass seals in one respect, i.e. they are free of the CTE mismatch challenges associated with glass seals. Compressive seals may be mica based or metallic. Mica

seals are compatible with the high temperatures of SOFC, but require large compressive loads due to the through-seal porosity and surface irregularity of mica sheets. However, even with large compressive loads, mica seals are unable to attain true hermeticity. Furthermore, mica seals may leach minerals which poison the catalyst. Nickel and copper are among the metallic materials which have been examined for compressive seals. Such seals have proven inadequate due to poor oxidation resistance. In 2010, Menzler et al. note that to the best of their knowledge no stack has been successfully operated which uses compressive sealing.[4]

Seal improvement is an active R&D topic. An example strategy for potentially improving glass seals entails the use of composite seals having a glass component and a metal or metal oxide component.[35] Another example for improving glass seals uses a glass-ceramic seal whose composition may be 10% or less glass and 90% or more crystalline to limit the amount of glass to crystalline phase transition,[36] which, as explained previously, is an important seal failure mode. Improved compressive seal designs are also being examined. Brule et al. describe a sealing mechanism incorporating aspects of both glass-ceramic designs and compressive design.[34] A "plastically deformable ceramic green tape reinforced by ceramic fiber with high ceramic powder loading" is formed with a tape casting procedure. A gasket is obtained from the green tape by cutting a pattern corresponding to stack hardware, and a seal is formed when a compressive load applied to the stack deforms the gasket between the two interfaces where the gasket is disposed. Felt materials (metallic, ceramic) have also been examined as improved compressive seals.[37] The compliant and compressible felt is made gas impervious through a number of methods including impregnation with another material, metal foil layers, etc. Seal designs using brazing have also been examined, but have not yet demonstrated reliability in practical applications.[4]

Another large challenge in planar designs which use metallic interconnects is the interconnect itself. One requirement of an interconnect is that it be CTE matched with other fuel cell components. Ferritic stainless steels having a Cr content of approximately 20% have proven to be sufficiently CTE compatible with YSZ or ceria based cells when operated in the temperature range of 600-800^{o}C. However, these stainless steels develop thermally grown oxide (TGO) scales (corrosion products) on the cathode side hardware, particularly aluminum oxides and silicon oxides, which are poor electrical conductors. Chromium TGO scales also develop; however, these are good electrical conductors. Unfortunately, these chromium oxide scales continue to grow over time, exhibiting increased electrical resistance and spallation with extended fuel cell operation. Perhaps equally important is that these chromium oxide scales can react in the cathode environment to form a Cr vapor that diffuses to and poisons the cathode. It was found that some chromium oxides, such as $(Cr,Mn)_3O_4$, exhibit significantly lower rates of Cr vaporization than other chromium oxide species, such as Cr_2O_3.[37] Several ferritic stainless steels (e.g. Croffer 22 APU) have been developed especially for SOFC applications having carefully tailored compositions, leading to the preferred chromium oxide scales while minimizing the formation of the electrically resistive aluminum- and silicon-based scales. Coatings are typically applied to cathode side hardware to enhance/preserve electrical conductivity and minimize Cr volatilization. Manganese cobalt oxide coatings and perovskite coatings are common. Recent analysis by Seabaugh et al. comparing various coating processes indicates an average cost of approximately $2 per 625 cm^2 part at a production volume of 400 MWe per year.[38]

For modeling purposes it has been assumed that seals are state of the art glass ceramic materials. Interconnects, separator plates, and picture frames are assumed to be SOFC- specific ferritic stainless steels. A manganese cobalt oxide coating is assumed for cathode side hardware. It is further assumed that stack assembly will be manual with the potential of automation only in high production volume scenarios. As can be appreciated in Figure 4-10, stack testing follows stack assembly. The final processing steps assumed in the model include stack integration with BOP components, system wide testing, placing an enclosure over the system, and loading the completed system for shipping.

4.8 MODEL RESULTS

Annual production volumes of 5, 20, 50, and 500 MWe/yr are shown in Figure 4-15 to have manufacturing costs of $1907, $1242, $1073, and $970/kWe, respectively.

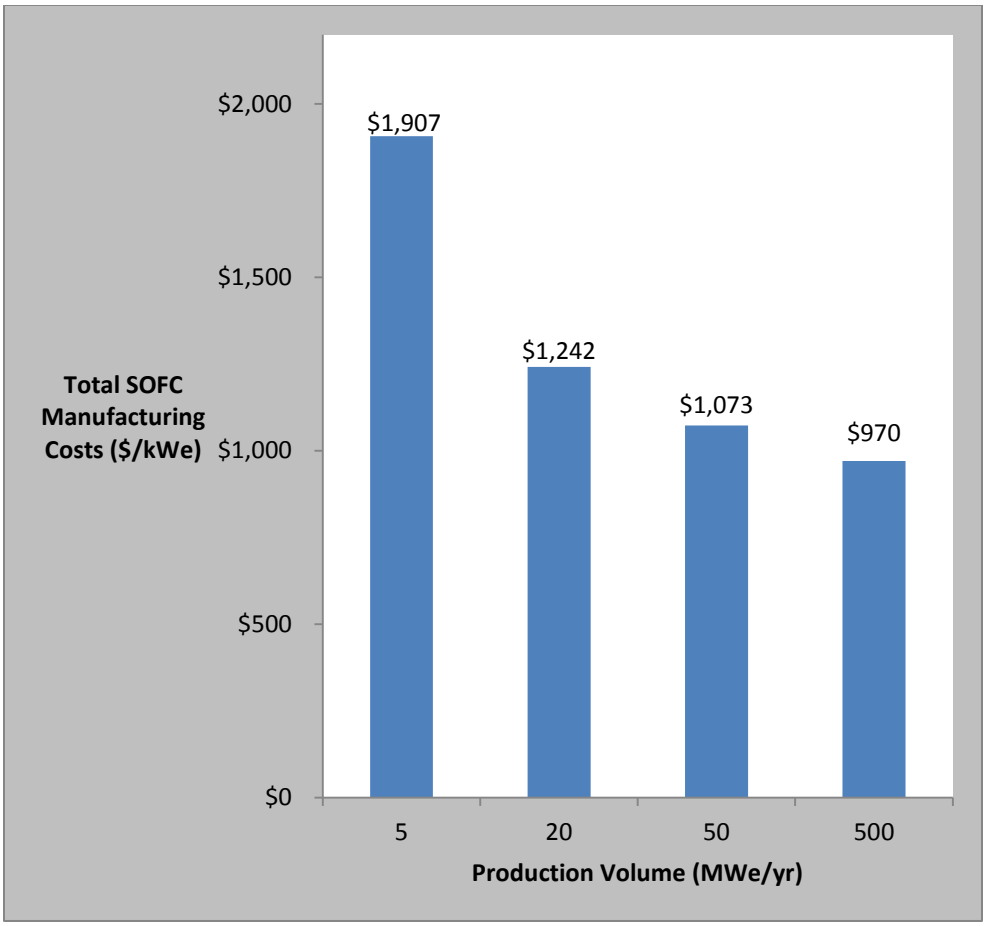

Figure 4-15. Total SOFC Manufacturing Costs for Varying Production Volumes

As with PAFC and MCFC, the total manufacturing cost curve follows a hyperbolic pattern, reaching a limiting value of approximately $970/kWe for production volumes in excess of several hundred MWe/yr. The baseline production volume of 20 MWe/yr (i.e. roughly equivalent to the actual current production volumes for the US manufacturers of PAFC and MCFC) is estimated to have a manufacturing cost of $1242/kWe as stated previously. This represents a 35% reduction from the low volume scenario of 5 MWe/yr, where manufacturing costs are estimated to be $1907/kWe. A 22% reduction in cost appears achievable just by increasing production volume from 20 to 500 MWe/yr, even if manufacturing technology is assumed unchanged (i.e. production lines are replicated in parallel) and no learning curve is experienced. As production volume increases from 5 to 500 MWe/yr, cost reductions accrue from:

- reduced contribution of fixed costs (capital and floor space) to total system cost on a per unit basis

- reduced indirect labor requirement (modeled as a decreasing percentage of direct labor as production volume increases).
- volume discounts on materials and components purchased from suppliers (developed in consultation with suppliers, industry partners, and economy of scale factors)

In order to highlight how costs are distributed and where they are concentrated, total manufacturing costs were disaggregated into seven cost components - labor, energy, floor space, capital, cell materials, stack components, and BOP components and subsystems. Definitions and assumptions pertaining to labor, energy, floor space, and capital costs are detailed in section 1.2. The remaining three cost components – cell materials, stack components, and BOP components and subsystems - represent those items which are purchased from suppliers by the SOFC manufacturer. Utilizing capital, floor space, energy, and labor resources, the SOFC developer manufactures and assembles these purchased items into a fuel cell system. Figure 4-16, below, is an elaboration of Figure 4-15 in that total manufacturing cost has now been disaggregated into the seven cost components mentioned above.

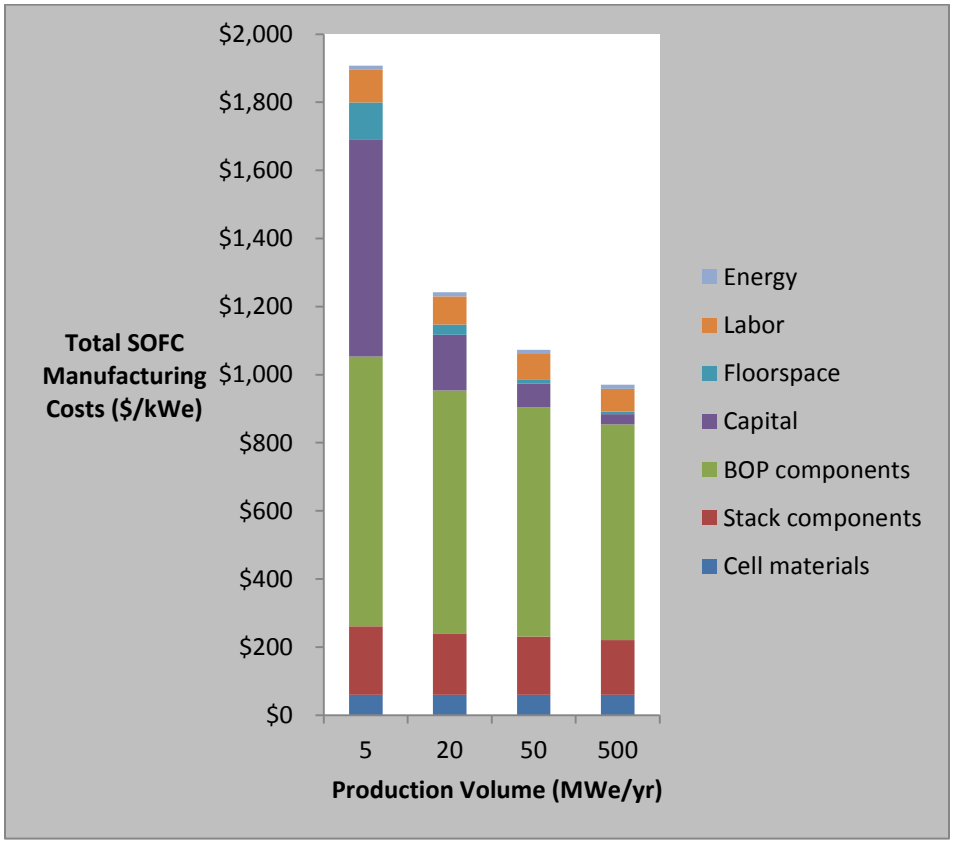

Figure 4-16. Total SOFC Manufacturing Costs and Cost Components for Varying Production Volumes

It may be readily observed in Figure 4-16 that items purchased from suppliers (cell materials, stack components, and BOP components and subsystems) collectively comprise the largest manufacturing costs incurred by the SOFC manufacturer. Figure 4-17, below, shows that

purchased materials and components, when taken in aggregate, are estimated to constitute 55% to 88% of total manufacturing cost. Purchasing costs for BOP components and subsystems represent more than 50% of total manufacturing cost for three of the four production volumes examined. The fixed costs of capital and floor space are noted to decrease in cost proportion from 39% to 4% with increasing production volume as underutilized sintering and tape casting capacity comes online. Labor and energy costs remain relatively constant in proportion at about 6% and 1%, respectively. SOFC labor costs as compared with PAFC and MCFC are estimated to be generally lower in proportion due to the high automation potential of tape casting and screen printing.

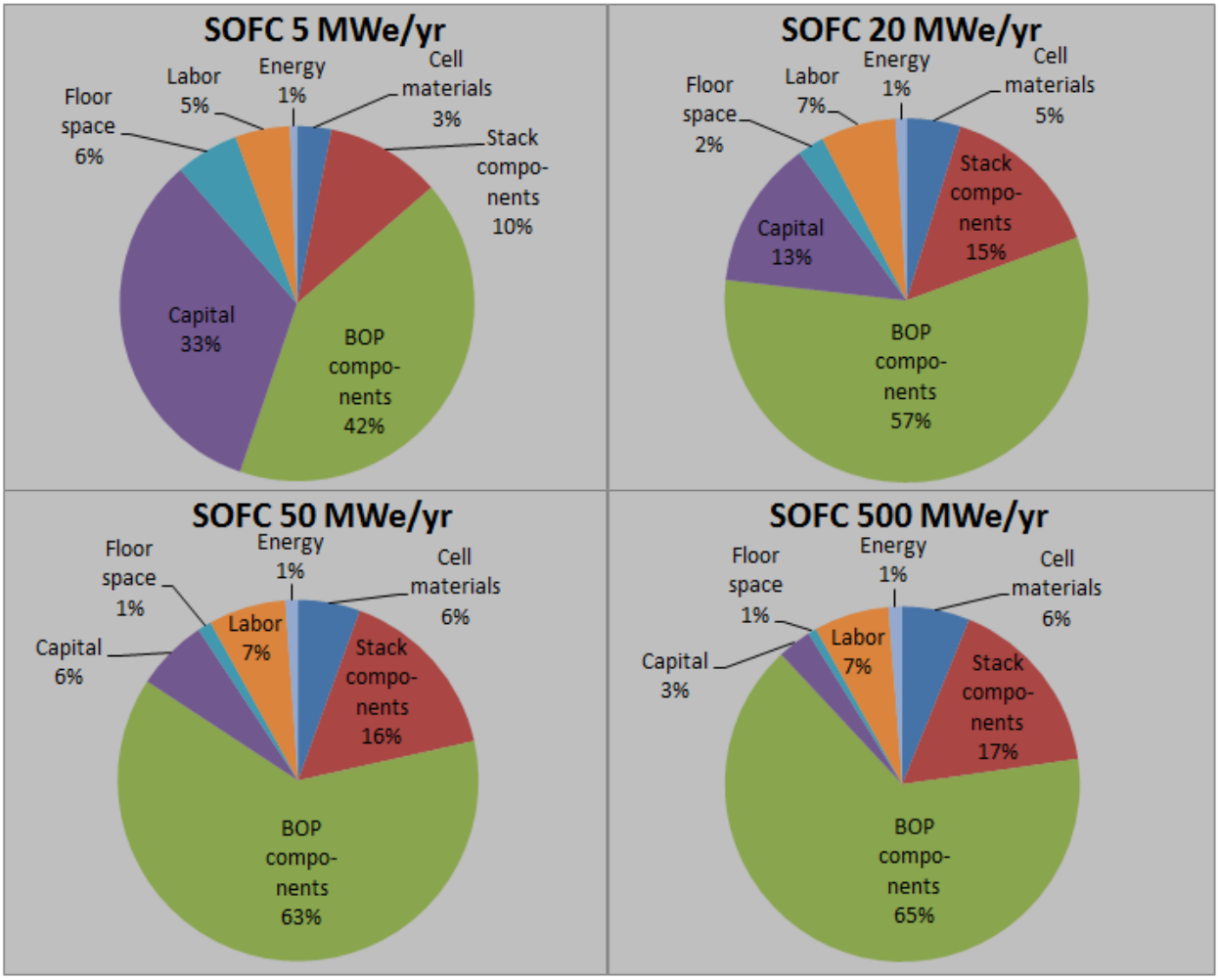

Figure 4-17. Total SOFC Manufacturing Cost Distribution for Varying Production Volumes

Because materials and components purchased from suppliers are estimated to constitute approximately three-fourths of total manufacturing costs, these components are examined in further detail in the following paragraphs. Major purchased items are listed in Table 4-2, and categorized as either cell, stack, or BOP.

Table 4-2. Major SOFC Cell Materials, Stack Components, and BOP Components and Subsystems Purchased from Suppliers

SOFC PURCHASED MATERIALS, COMPONENTS, AND SUBSYSTEMS		
CELL	STACK	BOP
NiO	Picture frame	Air preheater
8YSZ	Anode flow field	Fuel preheater
Toluene	Cathode flow field	Waste heat recovery
Ethanol	Separator plate	Prereformer
Carbon black	Spacers	Desulfurizer
Anode support slurry modifier	Anode seals	Afterburner
Anode support slurry binder	Cathode seals	Blowers
Terpineol	Stack end plates	Inverter and power conditioning
Ethyl cellulose	Tie rods	Instruments and controls
GDC		Piping
LSCF		Insulation
Lanthanum cobaltite		Enclosure
		Bus bars, wiring, dielectrics

Major cell materials identified in Table 4-2 include NiO and 8YSZ, one or both of which is the primary constituent of anode supports, anodes, electrolytes, and anode contact layers. Toluene, ethanol, modifier, and binder are incorporated into anode support tape casting slurries. Carbon black is employed as a poreformer in all ceramic cell layers except the electrolyte and interlayer. Terpineol and ethyl cellulose are incorporated into screen printing inks. The model cell adopted for the present study also uses a GDC interlayer and a LSCF cathode. Lanthanum cobaltite is used for the cathode contact layer.

Major stack components are also identified in Table 4-2. A picture frame is used to hold ceramic cells and provide pathways for conducting gases into and out of stacks. Anode and cathode flow fields, along with separator plates, provide electrical interconnection and gas conduction to cells. Seals and spacers provide proper spacing between cell and stack components, as well as gas compartmentalization. Stack end plates and tie rods are the final stack components listed in Table 4-2.

Major balance of plant components and subsystems purchased from suppliers are also listed in Table 4-2. Heat exchangers include an air preheater, fuel preheater, and a waste heat recovery heat exchanger for CHP applications. A desulfurizer and prereformer process fuel before its introduction into stacks. Depleted fuel exiting stacks is combusted with cathode exhaust in an afterburner. A cathode blower provides oxidant to cathodes while an anode gas recycle blower returns a portion of anode exhaust to the prereformer. Electrical balance of plant components and subsystems include the inverter and power conditioning subsystem; instruments and controls; and bus bars, wiring, and dielectrics. Piping, insulation, and an enclosure for the fuel cell system are the final BOP components and subsystems listed in Table 4-2.

Figure 4-18 is a Pareto chart showing the estimated costs of all purchased items listed in Table 4-2 for the baseline manufacturing volume of 20 MWe/yr. An item's bar color – blue, red, or green – indicates whether it is a cell material, stack component, or BOP component, respectively.

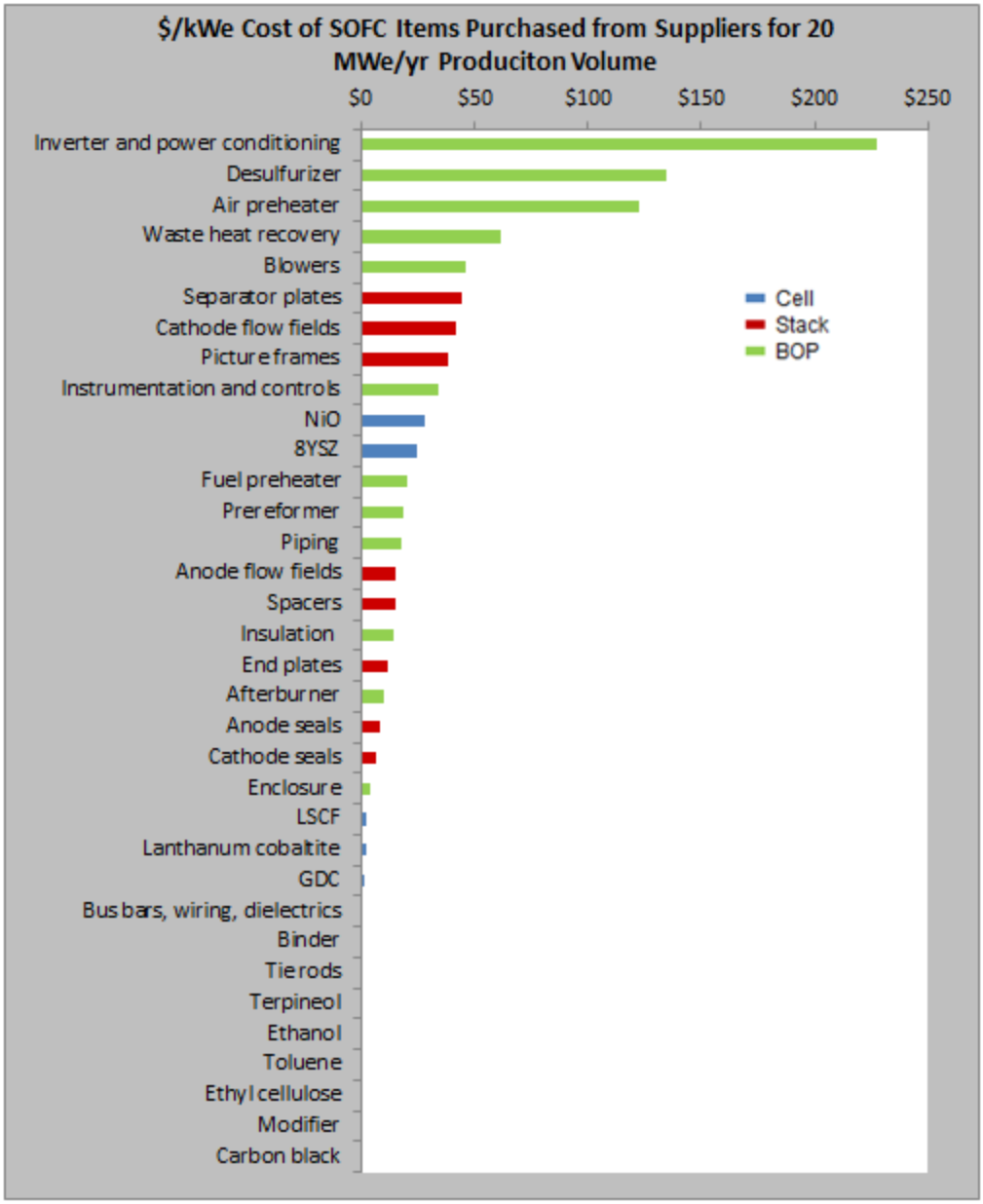

Figure 4-18. SOFC Pareto Chart of Cost of Items Purchased from Suppliers for 20 MWe/yr Production Volume

All of the top five highest cost purchased items are BOP components and subsystems, led by the inverter and power conditioning subsystem and followed by the adsorbent based desulfurizer system. The air preheater and waste heat recovery heat exchanger costs are high due to the large surface areas required for these components. A substantial stack cooling duty placed on the cathode blower and stringent high temperature requirements placed on the anode gas recycle blower contribute to the high cost of this category. The top five highest cost purchased items are followed by three stack components – separator plates, cathode flow fields, and picture frames. Cathode flow fields and the cathode side of the separator plate are modeled as having been treated with a coating of manganese cobalt spinel, contributing to their relative high costs.

NiO and 8YSZ are the most significant cell materials purchased from suppliers as these materials comprise the bulk of the thick anode support. The remaining cell materials are relatively insignificant in terms of cost as the layers which they constitute are extremely thin. The cost of the rare earth metals commonly used in SOFC technology - yttrium, lanthanum, gadolinium, samarium, cerium, and scandium – have gathered increasing attention due to their recent history market price behavior. While highly transparent commodity exchanges exist for setting the market prices of platinum and nickel (important for PAFC and MCFC, respectively), the market prices of rare earth metals are currently set through private trade. Furthermore, over 90% of the world's rare earth metal production currently occurs in just one county, China. Increasing demand for rare earth metals, inefficient marketplaces, and restrictive production quotas in China have contributed to a ten to twenty fold increase in rare earth metal prices from pre-2007 levels. These factors obviously complicate the determination of an accurate materials cost for cell manufacturing. However, because ceramic cell layers are manufactured extremely thin, and rare earth metals are frequently added only as a dopant to another material (e.g. zirconia doped with 8 mol percent yttrium), the total mass of rare earth metals in solid oxide fuel cells is insufficient for these elements to be significant contributors to overall system cost. The Pareto analysis in Figure 4-20 generally corroborates Thijssen's observation that the recent large increases in the market prices of rare earth metals has not added significantly to SOFC cost.[39]

Figure 4-19 lists all manufacturing steps examined in this study, and the costs incurred at each of those steps for the baseline production volume of 20 MWe/yr. Steps are grouped and classified according to component or task. For example, the anode manufacturing process was described with ten steps, beginning with attrition milling of anode support material and concluding with the drying of anode active layer ink after screen printing. These ten steps are grouped under the heading "Anode" in Figure 4-19. Steps are listed in a sequence which reflects the chronology of the actual manufacturing process, with first steps occurring at the top of the graph and final steps at the bottom. The relatively large contribution of items purchased from suppliers (cell materials, stack components, and BOP components) to total manufacturing cost is clearly reemphasized in this graph.

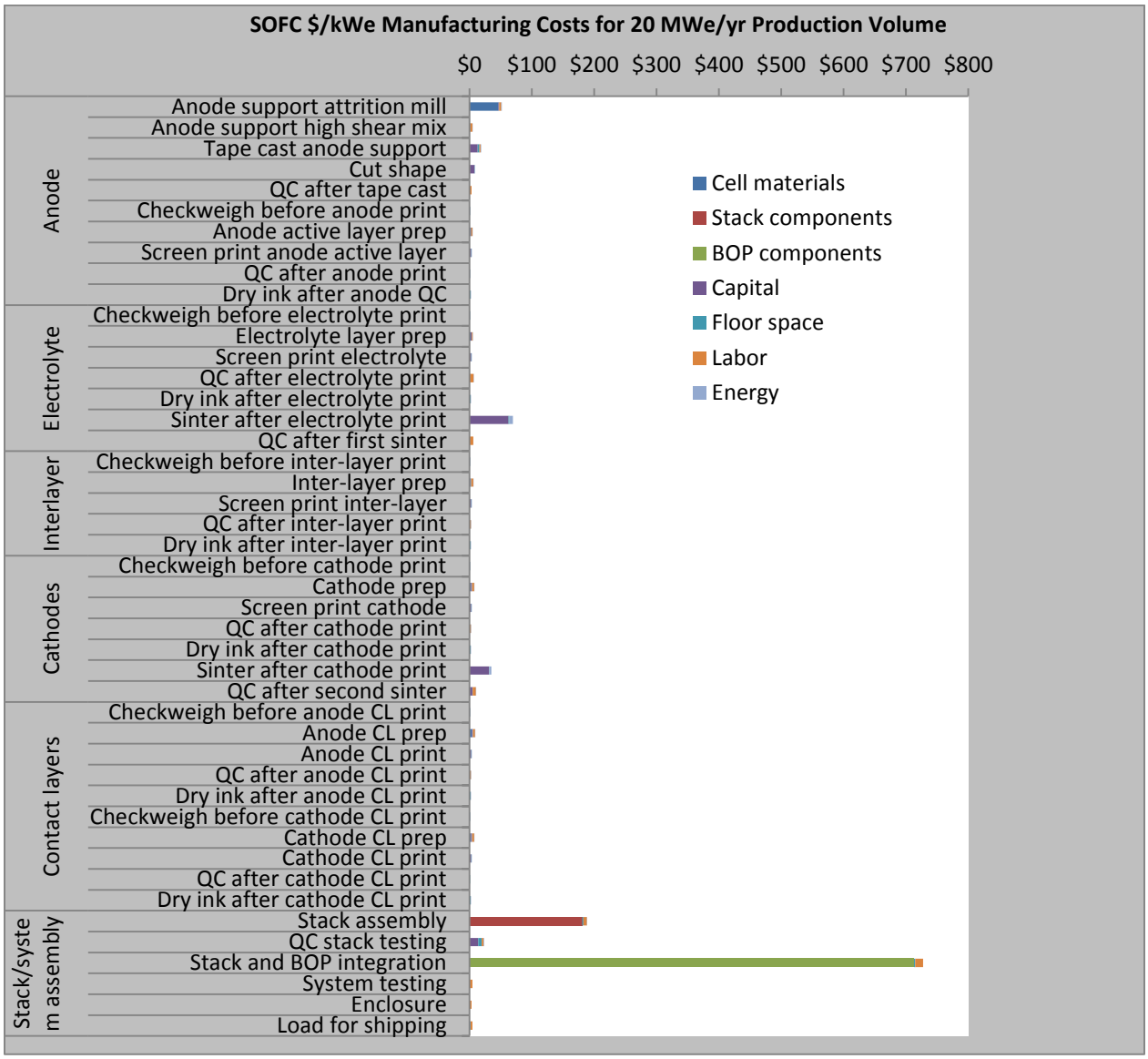

Figure 4-19. Total SOFC Manufacturing Cost Disaggregated by Process Steps and Cost Components for 20 MWe/yr Production Volume

As discussed previously, materials and components purchased from suppliers are estimated to constitute roughly 75% of total manufacturing costs, implying the remaining cost components (i.e. capital floor space, energy, and labor) are estimated to collectively represent roughly 25% of total costs. To better describe these components, Figure 4-20 lists all costs other than purchased material and components costs for each step of the manufacturing process. Figure 4-20 is completely analogous to Figure 4-19, with the exception that purchased item costs have been excluded, and the x-axis adjusted, to improve the graphical resolution of the remaining cost components.

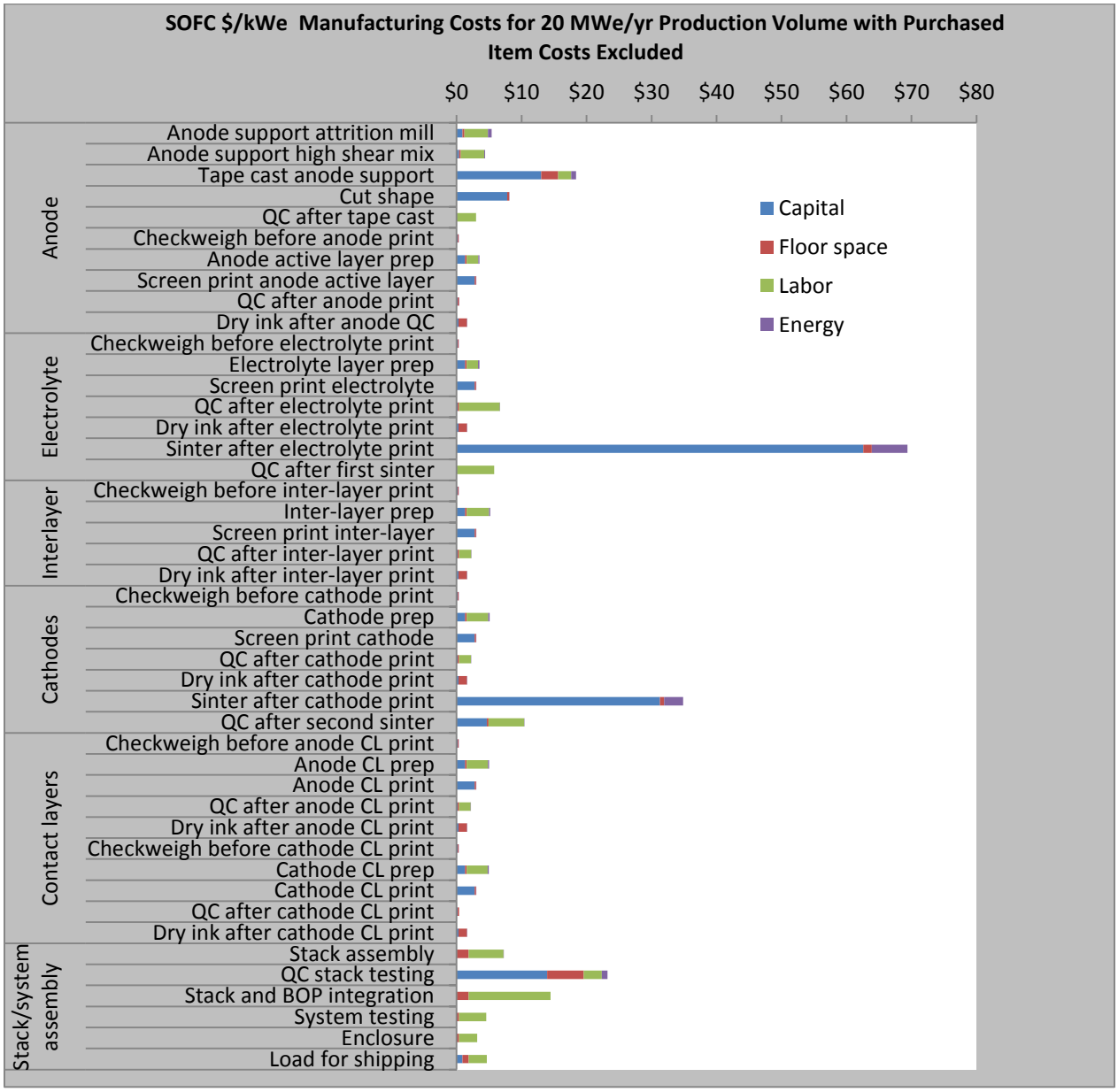

Figure 4-20. Total SOFC Manufacturing Cost Disaggregated by Process Steps and Cost Components for 20 MWe/yr Production Volume with Purchased Item Costs Excluded

The highest cost steps when purchased items are excluded from consideration are the two sintering steps, followed by stack quality control testing and then anode support tape casting. In particular, for the baseline production volume of 20 MWe/yr, these 4 most expensive steps are driven by capital costs. Cell manufacturing, which uses tape casting, screen printing, and continuous sintering furnaces, has the highest level of automation in the fuel cell system manufacturing process. The highest labor costs can be seen in the quality control steps, and stack and system assembly steps as these are primarily manual operations. The two sintering steps also incur the largest energy costs, while stack quality control testing incurs the largest floor space cost.

Several of the larger labor, capital, floor space, and energy costs identified in Figure 4-20 are significant contributors to total manufacturing cost. Figure 4-21, similar to Figure 4-18, is a Pareto chart which compares, not only purchased item costs, but all cost component categories for the baseline production volume of 20 MWe/yr.

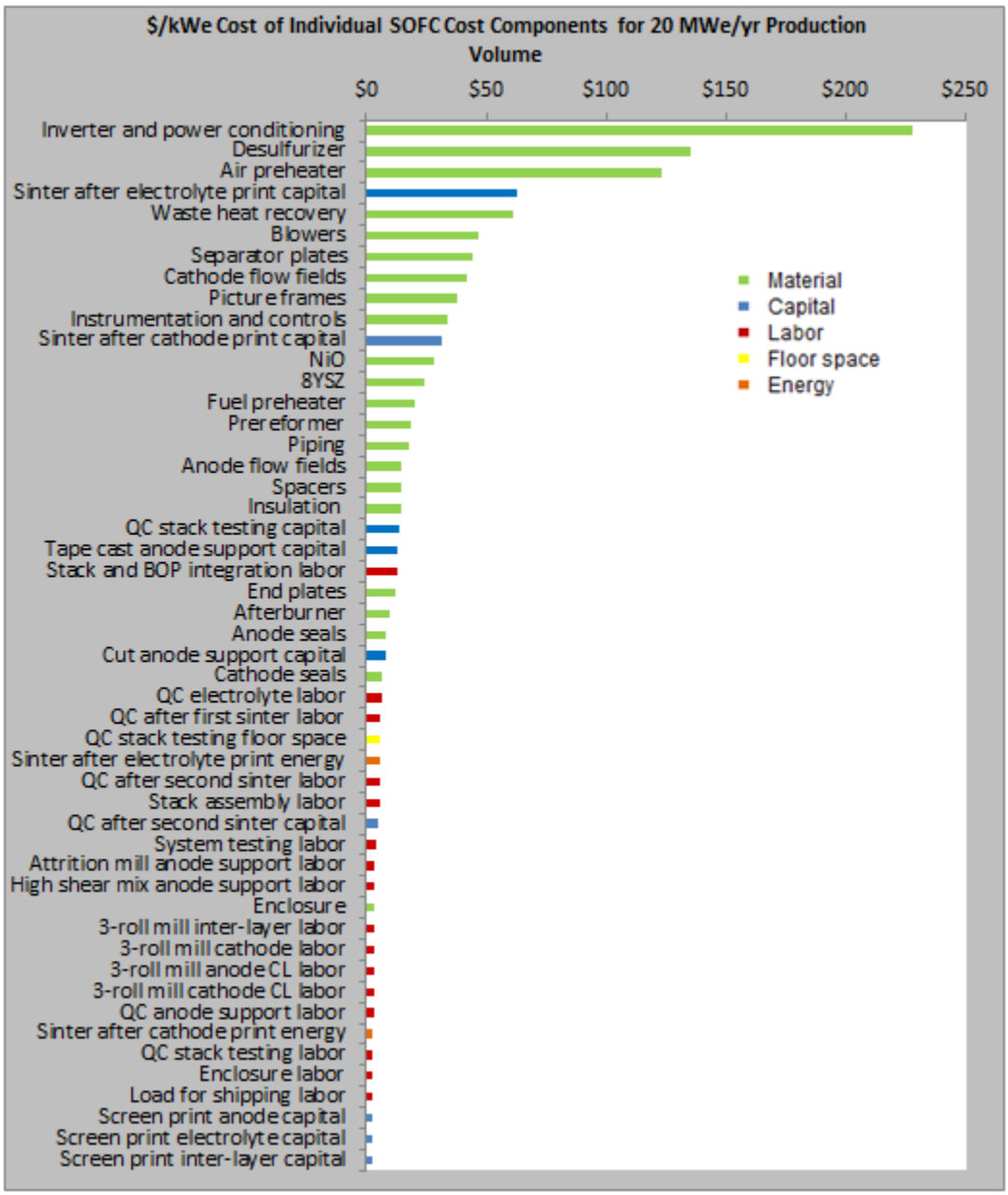

Figure 4-21. SOFC Pareto Chart for All Cost Components for 20 MWe/yr Production Volume

The top fifty highest cost components are listed using the indicated color code (note that the three purchased item cost categories – cell materials, stack components, and BOP components – have been assigned the same color, green). While 214 individual cost components were identified, it is well worth noting that the top fifty most expensive constitute over 94% of total

manufacturing cost. The top half of the chart is dominated by the costs of items purchased from suppliers including BOP components and subsystems, stack components, and the major materials which comprise the thick anode support (NiO and 8YSZ). Four of the top five are BOP components or subsystem, including the inverter, desulfurizer, air preheater, and waste heat recovery heat exchanger. Also among the top five is the capital cost attributable to the first sintering step. The capital costs for the second sintering step, stack testing, and tape casting are also significant capital costs appearing it the top half of the chart. The highest labor cost identified is attributable to stack and BOP integration, appearing in the 22nd rank. The lower half of the chart shows a more diverse mixture of cost component categories. Two energy cost components are registered in the top fifty, namely the energy costs associated with the two sintering steps. The floor space cost attributable to quality control stack testing is the only one of this cost component category to be listed in the top fifty.

Figure 4-22, below, is an elaboration of Figure 4-15 in that total manufacturing cost is disaggregated into cell, stack, and BOP costs. With reference to Figure 4-19, cell costs are defined as all costs (material, capital, labor, energy, and floor space) associated with the steps under the Anode, Electrolyte, Inter-layer, Cathode, and Contact layer categories. Stack costs have been defined as all costs associated with the Stack assembly and QC stack testing steps under the Stack/System assembly category. The last four steps listed in the graph are defined as the BOP costs.

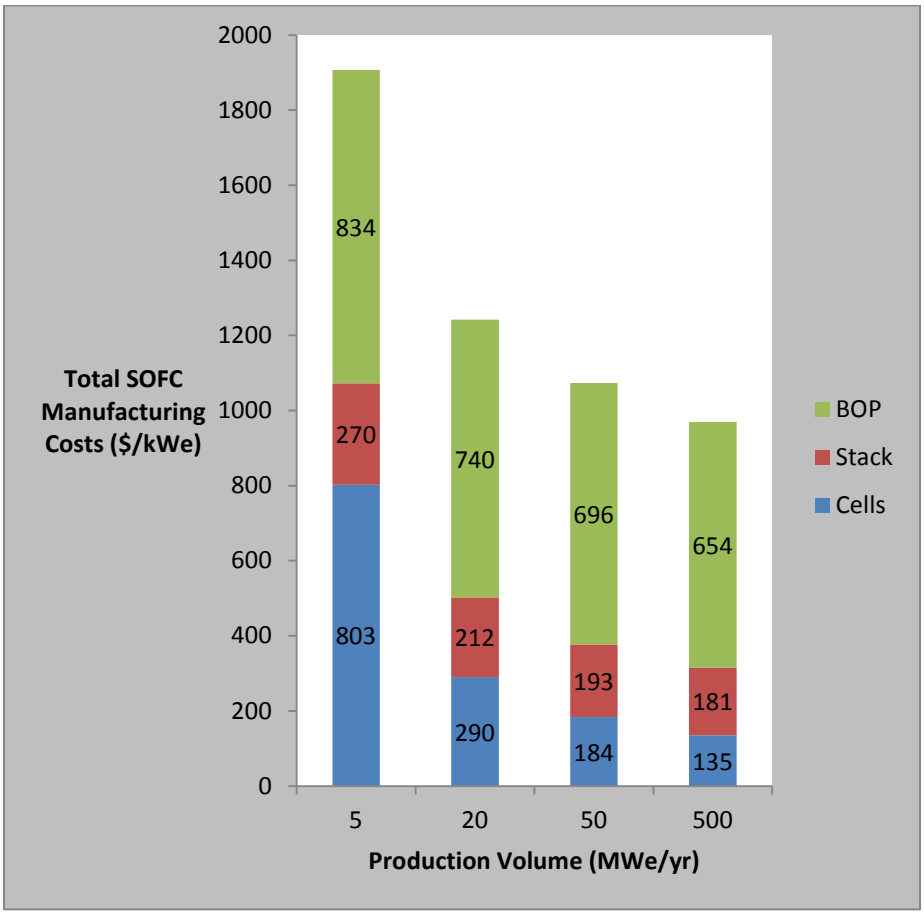

Figure 4-22. SOFC Manufacturing Costs Disaggregated by Cell, Stack, and BOP for Varying Production Volumes

All three cost categories are noted to decline with increasing production volume. Cell costs in particular decline sharply as underutilized cell manufacturing capital is increasingly utilized, spreading fixed capital costs over more units of production. The distribution of cell, stack, and BOP costs is further explained with Figure 4-23. For the three highest production volumes examined, costs are roughly distributed as two-thirds BOP, one-sixth stacks, and one-sixth cells.

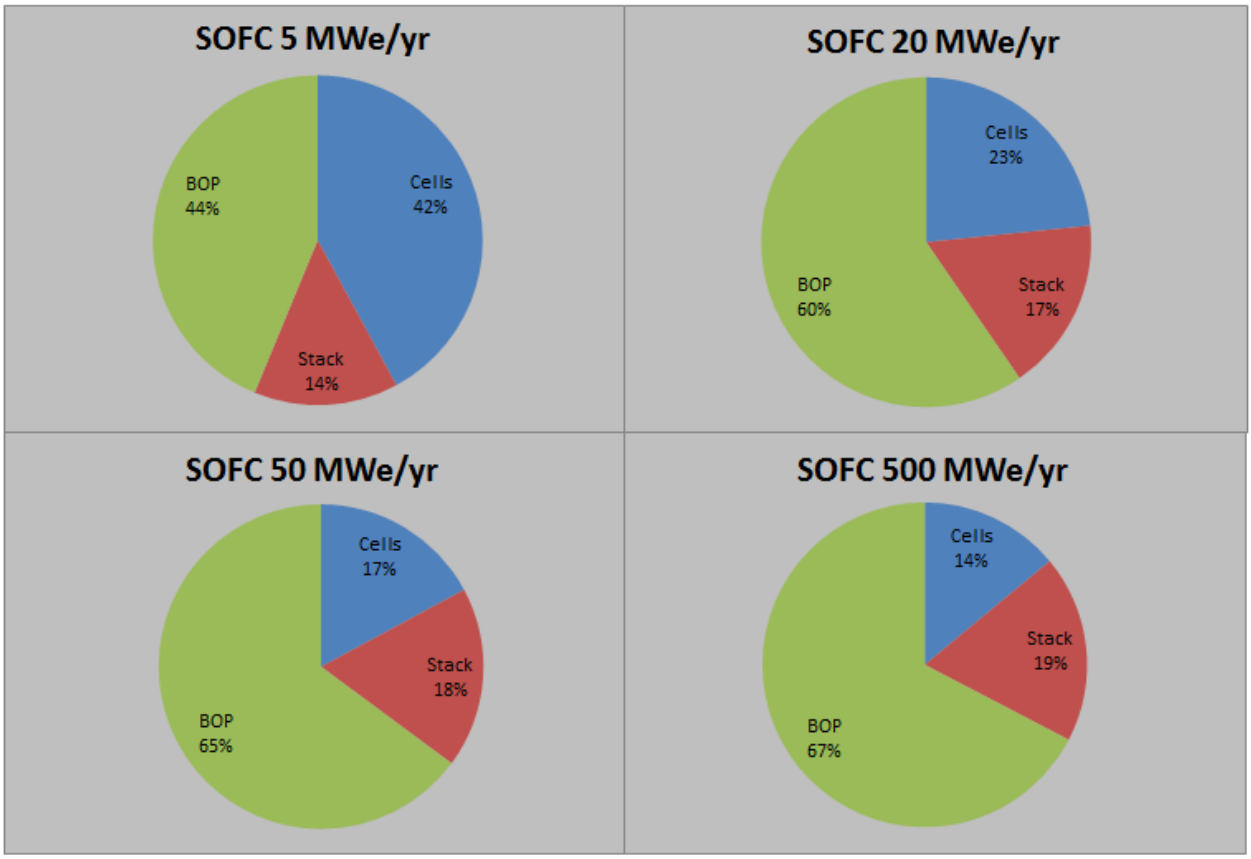

Figure 4-23. SOFC Cell, Stack, and BOP Cost Distribution for Varying Annual Production Volumes

Monte Carlo simulation was conducted to assess the impact of stochastic and uncertain inputs on cost estimation. For the baseline production volume of 20 MWe/yr, total manufacturing cost is estimated to be between $1213 and $1321/kWe with 90% confidence after 10,000 trials as shown in Figure 4-24. The cost distribution is unimodal and bell-shaped, with slight skewing to the right.

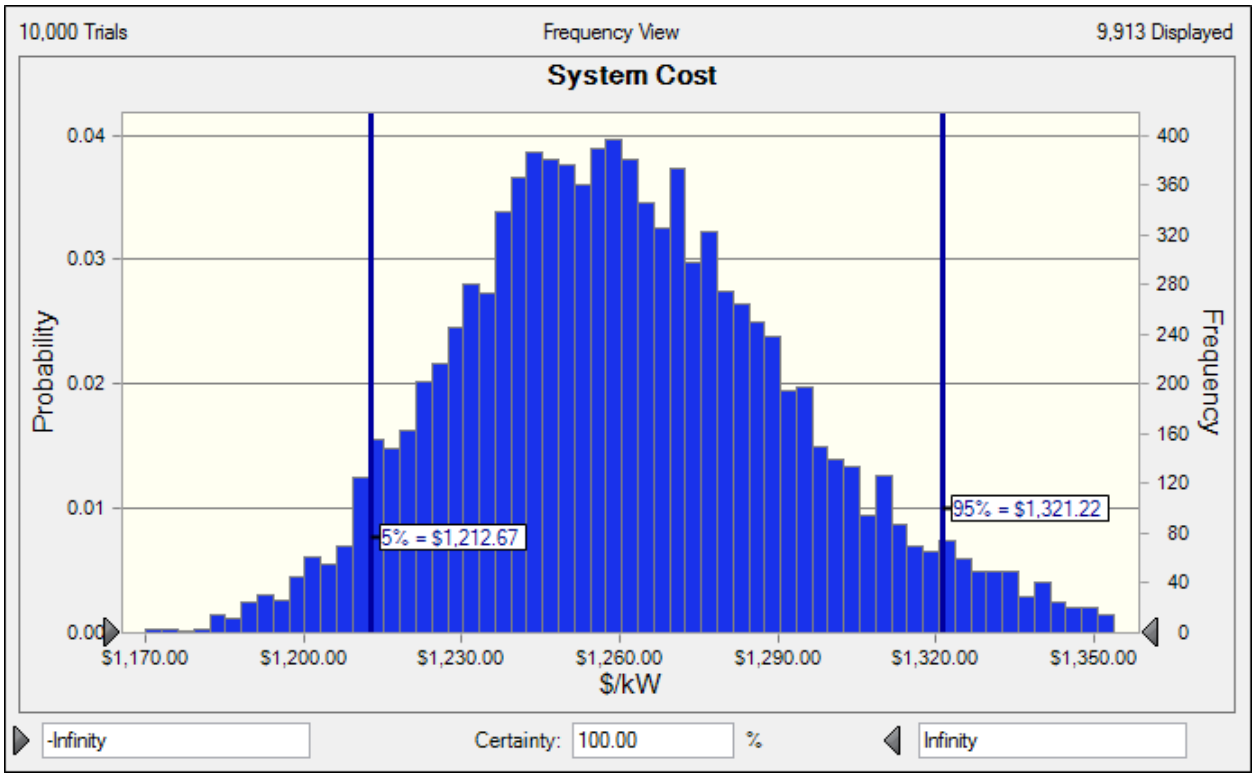

Figure 4-24. Monte Carlo Simulation of Total SOFC Manufacturing Cost for 20 MWe/yr Production Volume

Sensitivity analysis, shown in Figure 4-25, reveals that power density represents over 70% of the variability in this model. Power density was modeled as N(0.4, 0.0009) W/cm^2, implying the randomly selected power density has over a 99% probability of being on the interval (0.3, 0.5) W/cm^2. Power density, capital recovery rate, and the market price of YSZ constitute nearly 90% of model variance. Aggressive price assumptions were selected for YSZ (and other rare earth containing SOFC compounds, e.g. LSCF) to capture the possibility of continued large increases in rare earth prices. Among these rare earth containing compounds, only YSZ had an appreciable impact on model variance due to the relatively large quantity of YSZ used in anode supports. Sensitivity analysis assumptions are presented in Table 4-3.

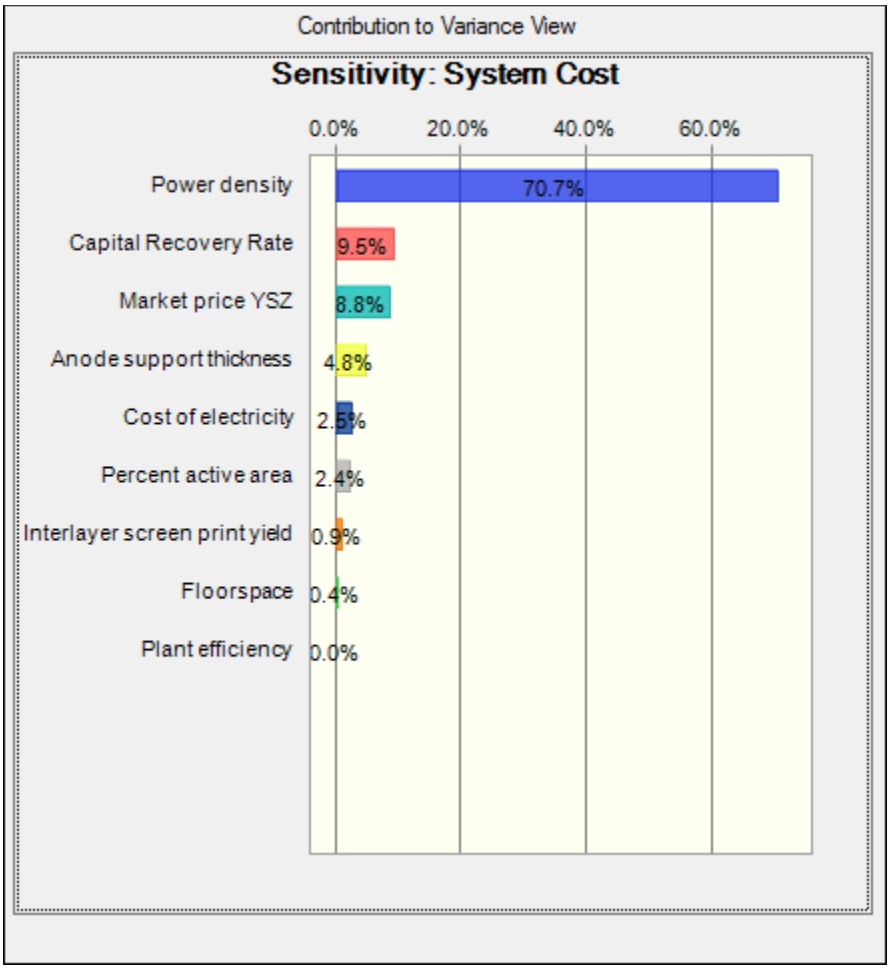

Figure 4-25. Sensitivity Analysis for Total SOFC Manufacturing Cost for 20 MWe/yr Production Volume

Table 4-3. Sensitivity Analysis Assumptions for Total SOFC Manufacturing Cost for 20 MWe/yr Production Volume

Variable	Distribution Family	Parameters	Units
Power density	Normal	mean = 0.4, sd = .03	W/cm^2
Capital recovery rate	Triangular	min = 8, most likely = 12, max = 18	%
Market price YSZ	Triangular	min = 40, most likely = 60, max = 150	$/kg
Anode support thickness	Triangular	min = 400, most likely = 500, max = 700	µm
Cost of electricity	Lognormal	mean = .08, sd = .04	$/kWh
Percent active area	Triangular	min = 85, most likely = 88, max = 91	%
Interlayer screen print yield	Uniform	min = 88, max = 97	%
Floorspace	Triangular	min = 12, most likely = 22, max = 24	$/ft^2$
Plant efficiency	Triangular	min = 75, most likely = 80, max = 85	%

4.9 OPPORTUNITIES

Model results generally corroborate other SOFC cost studies conducted over the last decade by showing that, under high volume scenarios, SOFC systems may be manufactured for less than $1000/kWe.[7] While this cost would be competitive with conventional energy conversion systems in the sub-megawatt distributed generation space (e.g. microturbines and reciprocating engines), advances in SOFC technology are needed to improve stack reliability such that a commercially acceptable five year stack is attainable. Manufacturing related cost reduction opportunities identified in this study include:

- Volume production – For modeling purposes, a baseline production volume of 20 MWe/yr was selected because of its equivalence with PAFC and MCFC model assumptions. However, it is acknowledged that no actual manufacturer of SOFC CHP systems is operating at an equivalent production volume. A 22% reduction in manufacturing cost from $1242/kWe to $970/kWe appears achievable just by increasing production volume from the model baseline to 500 MWe/yr, even if manufacturing technology is assumed unchanged (i.e. production lines are replicated in parallel) and no learning curve is experienced.

- BOP components and subsystems – Approximately two-thirds of total manufacturing costs are the purchase and assembly costs attributable to balance of plant. Among the highest cost BOP components and subsystems are the inverter and power conditioning subsystem, the desulfurizer, and the air preheat and waste heat recovery heat exchangers.

- Stack repeat components – Stainless steel interconnects, separator plates, and picture frames may be manufactured with either machining or powder metallurgy techniques. In either case, the processes used to manufacture these components contribute significantly to their cost. Cathode side stainless steel components are typically treated with high cost coatings to preserve electrical conductivity and slow the rate of cathode poisoning by chromia vapors. Other repeat components such as seals and spacers also contribute significantly to cost.

- Sintering – Sintering is the bottleneck of cell manufacturing. Sintering is a slow, carefully controlled process which is capital, maintenance, floor space, and energy intensive. Reducing the duration and/or number of sintering steps can lead to significant cost savings. High production volume is needed so that sintering capital cost is spread over many units of production. Alternatives to traditional resistance furnaces, such as microwave sintering furnaces are being examined and merit further examination.

- Screen printing – Screen printers that have been optimized for the electronics industry have been adopted by the SOFC industry. While screen printer manufacturers are taking notice of the use of their products by SOFC manufacturers,[26] by in large, screen printer specifications are dictating cell parameters rather than cell requirements guiding screen

printer specifications.[3] Such is typical of a low volume industry such as SOFC manufacturing. SOFC developers need screen printers optimized for printing the thin layers desired in a cell. Moreover, screen printers are needed which are optimized for SOFC ink rheology rather than solder paste rheology. However, screen printer manufacturers need a large volume commitment from SOFC manufacturers to devote significant resources to optimizing screen printers for SOFC. An alternative to screen printing is inkjet printing which allows 3-dimensional control of cell microstructure. 3-dimensional control of microstructure is a key ingredient for enabling truly robust internal reforming.

- Automation – Cell manufacturing uses automated equipment readily available in the marketplace (attrition mills, high shear mixers, tape casters, screen printers, continuous resistance furnaces). However, stack and system assembly, as well as visual quality control steps, are manual and labor intensive. High production volume is needed to justify the capital expenditure to automate these processes.

- Seals and interconnects – Sealing and interconnect challenges are arguably the largest factors inhibiting the mass commercialization of SOFC systems, as model results suggest that these systems can be manufactured at competitive costs. A suitable sealing material which is gas tight, chemically non-reactive, and can withstand thermal cycling without embrittlement is needed. Similarly, an interconnect material which remains a good electrical conductor over time without poisoning cathodes will be required. While perhaps best classified as material challenges, the above mentioned seal and interconnect opportunities have manufacturing implications (e.g. protective coatings applied to cathode side stainless steel hardware).

The results of this cost model suggest that a manufacturing cost of less than $1000/kWe may be attainable in high production volume scenarios. This cost would likely make solid oxide fuel cells cost competitive with traditional sources of stationary power. However, the technological challenges of seal and interconnect failure must be resolved before widespread commercial acceptance of solid oxide fuel cells can be expected.

4.10 REFERENCES

1. Baur, E., and H. Preis. Zeitung für Elektrochemie, 1937. 43: p. 727 - 732.
2. Bessette, N., and J. Rawson, Accumentrics, Inc. *Private meeting with Joshua Warren, Wei Zhang, and Sujit Das*, Oak Ridge National Laboratory, Oak Ridge, TN 37932, Aug. 4 (2010).
3. Birmingham, D., Rolls Royce, Inc. *Private meeting with Joshua Warren and Wei Zhang*, Oak Ridge National Laboratory, Oak Ridge, TN 37932, Jul. 16 (2010).
4. Menzler, N., F. Tietz, S. Uhlenbruck, H. Buchkremer, and D. Stover. *Materials and manufacturing technologies for solid oxide fuel cells*, J. of Material Sciences, Vol. 45, p. 3109 (2010).
5. CeresPower: http://www.cerespower.com/store/files/231-Field%20Trial%20commencement%20010211.pdf (2011).
6. Wincewicz, K., and J. Cooper. *Taxonomies of SOFC material and manufacturing alternatives*, J. of Power Sources, Vol. 140, p. 280 (2005).
7. Thijssen, J. *The impact of scale-up and production volume on SOFC manufacturing cost*, prepared for National Energy Technology Laboratory, Apr. 2 (2007).
8. Surdoval, W., S. Singhal, and G. McVay. Proceedings of the 7th International Symposium on Solid Oxide Fuel Cells, The Electrochemical Society, Pennington, NJ (2001).
9. Borglum, B. *Cell and Stack Developments at Versa Power Systems*, 10th Annual SECA Workshop, Pittsburgh, PN, Jul. 15 (2009).
10. Stover, D., H. Buchkremer, A. Mai, N. Menzler, and M. Zahid. *Processing and properties of advanced solid oxide fuel cells*, Materials Science Forum, Vols. 539-543, p. 1367 (2007).
11. Haltiner Jr., K., S. Mukerjee, L. Chick, K. Meinhardt, V. Sprenkle, K. Weil, and J. Kim. *Solid bonded interconnect system in a lightweight solid oxide fuel cell system*, US Patent 7,754,367 B2, Jul. 13 (2010).
12. Couse, S., and Z. Tang. *Solid oxide fuel cell stack with floating cells*, US Patent 7,553,579 B2, Jun. 30 (2009).
13. EG&G Technical Services, Inc. Fuel Cell Handbook (7th Edition), Nov. (2004).
14. Bloom Energy: http://c0688662.cdn.cloudfiles.rackspacecloud.com/downloads-pdf-release-bloom-CA-expansion-4-15-2011.pdf (2011).
15. Bloom Energy. http://www.bloomenergy.com/products/solid-oxide-fuel-cell/ (2010).
16. Armstrong, T., E. Batawi, and E. Petersen. *Internal reforming anode for solid oxide fuel cells*, US Patent 2011/0039183 A1, Feb. 17 (2011).
17. Faino, N., W. Rosensteel, B. Gorman, and N. Sullivan. *Progress toward inkjet deposition of segmented-in-series solid oxide fuel cell architectures*, 219th Electrochemical Society Meeting, Vol. 35, Iss. 1, p. 593, May 1 (2011).
18. Tomov, R., M. Krauz, J. Jewulski, S. Hopkins, J. Kluczowski, D. Glowacka, and B. Glowacki. *Direct ceramic inkjet printing of yttria-stabilized zirconia electrolyte layers for anode-supported solid oxide fuel cells* J. of Power Sources, Vol. 195, Iss. 21, p. 7160, Nov. 1 (2010).
19. Bloom Energy. http://c0688662.cdn.cloudfiles.rackspacecloud.com/downloads_pdf_Bloomenergy_DataSheet_ES-5000_1.pdf (2010).

20. Ahmed, K. *Fuel cell system*, US Patent 7,452,619 B2, Nov. 18 (2008).
21. McElroy, J., D. Weingaertner, S. Venkataraman, and S. Couse. *Operation of fuel cell systems with reduced carbon formation and leading edge damage*, US Patent 2010/0047637, Feb. 25 (2010).
22. Tang, Z. Versa Power Systems, Inc. *Private teleconferences with Joshua Warren, Wei Zhang, and Sujit Das*, Oak Ridge National Laboratory, Oak Ridge, TN 37932, Sep. (2010).
23. Howatt, G. *Continuous process for forming high dielectric ceramic plates*, US Patent 2,486,410, Nov.1 (1949).
24. Song, J., N. Sammes, S. Park, S. Boo, H. Kim, H. Moon, and S. Hyun. *Fabrication and characterization of anode-supported planar solid oxide fuel cell manufactured by a tape casting process*, J. of Fuel Cell Science and Technology, Vol. 5, p. 021003, May (2008).
25. Prasad, R. *Surface mount technology*, 2nd edition, Kluwer Academic Publishers, Norwell, MA (1997).
26. Brown, D. *Screen printing in the dawn of fuel cells*, SMT Magazine, Dec. 1 (2006).
27. Stover, D., H. Buchkremer, and J. Huijsmans. *MEA/cell preparation methods: Europe/USA*, Handbook of Fuel Cells – Fundamentals, Technology, and Applications, John Wiley & Sons, Ltd. p. 1015 (2003).
28. Day, M., S. Swartz, L. Thrun, and M. Seabaugh, Nextech Materials, Inc. *Private meeting with Joshua Warren, Wei Zhang, and Tom Zowadzinski*, Oak Ridge National Laboratory, Oak Ridge, TN 37932, Jul. 14 (2010).
29. Mori, M., and Z. Wang. *Sintering mechanisms of cobalt doped ceria and zirconia electrolytes in intermediate-temperature solid oxide fuel cells*, J. of Fuel Cell Science and Technology, Vol. 8, p. 011007, Feb. (2011).
30. Cologna, M., M. Sglavo, and M. Bertoldi. *Sintering and deformation of solid oxide fuel cells produced by sequential tape casting*, International J. of Applied Ceramic Technology, Vol. 7, p. 803, Nov. (2010).
31. Nguyen, D. *SOFC electrode sintering by microwave heating*, US Patent 2009/0110992, Apr. 30 (2009).
32. Jiao, Z., N. Shikazono, and N. Kasagi. *An ultra-fast fabrication technique for anode support solid oxide fuel cells by microwave*, J. of Power Sources, Vol. 196, p. 5940, accepted Feb. 17 (2011).
33. Reddy, K., and K. Kuran. *Sinterability, mechanical, microstructural, and electrical properties of gadolinium-doped ceria electrolyte for low temperature solid oxide fuel cells*, J. of Electroceramics, Vol. 15, p. 45 (2005).
34. Brule, R., X. Zhang, D. Chahal, and Z. Tang. *High temperature gas seals*, US Patent 7,799,419 B2, Sep. 21 (2010).
35. Lonnroth, N., A. Hauch, M. Mogensen, and M. Chen. *Composite glass seal for a solid oxide electrolyser cell stack*, US Patent 2011/0100805 A1, May 5 (2011).
36. Badding, M., S. Marjanovic, L. Pinckney, and D. St. Julien. *Glass-ceramic seals for use in solid oxide fuel cells*, US Patent 7,674,735 B2, Mar. 9 (2010).
37. Yang, Z., J. Hardy, M. Walker, G. Xia, S. Simner, and J. Stevenson. *Structure and conductivity of thermally grown scales on ferritic Fe-Cr-Mn steel for SOFC interconnect applications*, J. of Electrochemical Society, Vol. 151, p. A1825, (2004).
38. Seabaugh, M., M. Beachy, S. Ibanez, R. Kimbrell, M. Day, L. Thrun, and S. Swartz. *Manufacturing analysis of SOFC interconnect coating processes*, 11th Annual SECA

Workshop, Pittsburgh, PA, Jul. 28 (2010).
39. Thijssen, J. *Market impact of rare earth element use in solid oxide fuel cells*, prepared for National Energy Technology Laboratory, Oct. 18 (2010).

5. CONCLUSIONS

The manufacturing processes for three CHP fuel cell technologies (PAFC, MCFC, and SOFC) operating in the 100-400 kWe range were examined. Two fuel cell technologies, PAFC and MCFC, are represented by commercially available products while the third, SOFC, is still largely in the technology development phase. Manufacturing cost models were developed to be largely representative of commercially available PAFC and MCFC systems. A conceptual SOFC system was created for modeling purposes, having a design representative of state of the art and likely near term future technology. Many of the manufacturing opportunities identified in this study are fuel cell technology specific, and have been discussed at length in their respective sections. However, some manufacturing opportunities are common among the three fuel cell technologies, including:

- Volume production – Increased production volume reduces manufacturing cost by spreading capital, floor space, and indirect labor costs across more and more units of production. Volume related pricing discounts for items sourced from suppliers are also to be expected as production volume increases. Although not modeled in the present study, learning by doing also reduces costs over time as more efficient manufacturing techniques and product technology advances are identified. Early adopters and favorable tax treatment are essential for sustaining demand and creating cost reducing learning opportunities as fuel cells transition from niche markets to mass commercialization.

- Technology breakthroughs - Technology breakthroughs are needed in all three fuel cell classes to reduce first and/or lifecycle costs before wide commercial acceptance is realized. Reducing platinum loading, electrolyte loss, and fuel processing costs, as well as increasing power density are among the most important needs in PAFC. Advances needed in MCFC technology include increasing power density, as well as reducing electrolyte loss, cathode dissolution, and fuel processing first costs and O&M costs. First costs for SOFC systems may approach an acceptable level under high production volume scenarios; however, sealing and interconnect challenges must be resolved before a commercially acceptable stack lifetime is attained.

- Materials – Items sourced from suppliers constitute more than 50% of total manufacturing cost for all three technologies for the range of annual production volumes examined in this study (5-500 MWe/yr), emphasizing the need for well-developed supplier relationships for controlling costs. Standardization of components which may be in common among the fuel cell technologies (e.g. inverters, desulfurizers, etc.) would increase the fuel cell industry's leverage with suppliers.

- Automation - Cell manufacturing is relatively automated e.g. cloud tower and Gravure printing for PAFC, powder doctor and tape casting for MCFC, and tape casting and screen printing for SOFC. Conversely, stack and system assembly as well as many quality control steps are manual and labor intensive. Higher production volumes are

likely needed to justify the capital expenditure for the automation of these steps which would likely require custom equipment.

- Bottlenecks - Process bottlenecks are often heat treatment steps (sintering, carbonization, graphitization) and stack conditioning and testing steps.

- Online sulfur detection – Online sulfur detection has been mentioned across the board by industry partners as essential for optimizing the utilization of the desulfurizer and avoiding catastrophic introduction of sulfur compounds into anodes. Low cost detection methods are needed.

- Heat exchangers – Heat exchangers have some of the highest costs incurred by fuel cell manufacturers. Low cost, durable heat exchangers which are robust to thermal cycling would improve fuel cell costs and reliability.

- Continuous mixing – All three fuel cell technologies employ batch process liquid phase material preparation (e.g tape cast slurries, Pt catalyst floccing, etc.). Continuous mixing methods may be preferable for several reasons. For example, skin losses of high cost materials such as Pt would be reduced with continuous mixing as compared with small batch processing. In addition, the desired chemical and physical characteristics of the solution, suspension, etc. being prepared may be more easily maintained with continuous mixing which avoids the shelf life issues of settling and reacting associated with large batch processing.

- Instruments and controls – State of the art fuel cell systems may have ten to twenty year lifespans. Instrument and control systems with similar life expectancies are needed.

- Net shape insulation – High temperature sections of fuel cell systems such as stacks, reformers, etc. must be properly insulated using high cost materials. Net shape insulation manufacturing may reduce costs by minimizing cutting waste.

The considerable resources which have been devoted to fuel cell technology development in the last half century have succeeded in introducing commercial products to limited niche markets. Among these fuel cell products are stationary combined heat and power systems such as those examined in the present study. These systems, however, are presently too expensive on both a first and lifecycle cost basis for wide commercial acceptance. It has been the goal of the present cost modeling effort to highlight those manufacturing inputs where R&D resources have the greatest potential for effecting significant cost reductions, and in turn broadening market opportunities for these fuel cell systems.